2014

Electrical Conductivity Imaging via Boundary Value Problems for the 1-Laplacian

Johann Veras
University of Central Florida

ELECTRICAL CONDUCTIVITY IMAGING VIA BOUNDARY VALUE PROBLEMS FOR THE 1-LAPLACIAN

by

JOHANN VERAS
B.S. University of Central Florida, 2009
M.S. University of Central Florida, 2011

A dissertation submitted in partial fulfilment of the requirements
for the degree of Doctor of Philosophy
in the Department of Mathematics
in the College of Sciences
at the University of Central Florida
Orlando, FL

Summer Term
2014

Major Professor: Alexandru Tamasan

ABSTRACT

We study an inverse problem which seeks to image the internal conductivity map of a body by one measurement of boundary and interior data. In our study the interior data is the magnitude of the current density induced by electrodes. Access to interior measurements has been made possible since the work of M. Joy et al. in early 1990s and couples two physical principles: electromagnetics and magnetic resonance. In 2007 Nachman et al. has shown that it is possible to recover the conductivity from the magnitude of one current density field inside. The method now known as Current Density Impedance Imaging is based on solving boundary value problems for the 1-Laplacian in an appropriate Riemann metric space. We consider two types of methods: the ones based on level sets and a variational approach, which aim to solve specific boundary value problem associated with the 1-Laplacian. We will address the Cauchy and Dirichlet problems with full and partial data, and also the Complete Electrode Model (CEM). The latter model is known to describe most accurately the voltage potential distribution in a conductive body, while taking into account the transition of current from the electrode to the body. For the CEM the problem is non-unique. We characterize the non-uniqueness, and explain which additional measurements fix the solution. Multiple numerical schemes for each of the methods are implemented to demonstrate the computational feasibility.

ACKNOWLEDGMENTS

I am grateful to my wife Tracy, my parents Manuel and Milagros, my siblings Manuel, Pamela and Lauren, my nephew Emill and my niece Emelie for all their support, loving and understanding throughout the tough times I often encountered while finishing graduate school. Without their help this would not have been possible.

I am specially grateful to my advisor Dr. Tamasan for all the hard work, support and dedication towards my mathematical development throughout my career in graduate school. Also, I would like to thank him for his guidance not only in the educational aspect, but also in a personal one. Dr. Tamasan's teachings have helped me a great deal in my new career in the industrial world.

I would like to thank all the staff, including professors, of the math department at UCF for all their help, support and guidance.

TABLE OF CONTENTS

LIST OF FIGURES

CHAPTER 1: INTRODUCTION TO CDII

1.1 Introduction

In this thesis we are concerned with the determination of the electrical conductivity inside a body in a noninvasive manner using outside measurements of the voltage and/or current, and the induced interior magnitude of the current density. Electrical conductivity is a measure of a body's ability to conduct electrical charges. A quantitative display of the conductivity distribution inside a body produces more than a tomographic picture of its interior. Currently there are many medical imaging methods such as X-ray computed tomography (CT) scanners, Magnetic Resonance Imaging (MRI), ultrasound scanners, Optical Tomography (OT) and Electrical Impedance Tomography (EIT) to mention a few. Each method images a particular set of physical properties of the body. For example, an MRI or a CT scan on a body can image the density of its tissues while OT images its optical attenuation properties. Depending on the application of the method each has its advantages and disadvantages. The medical imaging method considered here, Current Density Impedance Imaging (CDII) [41], images the electrical conductivity properties of a body. The advantage of using CDII over other methods is seen when imaging breast tumors at its early stages. This type of tumor may have similar density as the surrounding healthy tissues, but largely differ in the electrical conductivity properties. Thus, making CDII a more attractive breast tumor detection method over ultrasound.

Originally motivated by oil explorations the problem of conductivity imaging, also known as Electrical Impedance Tomography (EIT), seeks to recover the conductivity of a body from multiple boundary measurements of voltages and corresponding currents. The problem has roots in the works of Langer (1930) and Tikhonov (1943), with the most general mathematical question formulated by Calderón in 1980. A renewed interest in EIT stemmed from its application to medical

imaging in the works of Barber and Brown (1984, 1986), and Isaacson (1986). Subsequently, the interest in the mathematical side of the problem exploded and important mathematical advances were generated in works of Kohn and Vogelius (1984, 1985), Sylvester and Uhlmann (1987), Nachman (1988, 1996), Astala-Paivarinta (2006), Kenig et al. (2008), which satisfactorily settled the original question (in three dimensions, the answer for a rough coefficient is still unknown). The evolution and development of EIT can be traced in the series of surveys by Cheney et al. (1999), Borcea (2002, 2003), and Uhlmann (2009). With all the great mathematical advances obtained in EIT, by now it is well understood that the boundary data has exponentially low sensitivity to the variation of the conductivity inside, yielding images of low resolution, e.g. Cheney and Isaacson (1991). The reason lies in the severely ill-posedness of the problem. As shown in Alessandrini (1988) the stability is merely of logarithmic-type and cannot be improved in general, see Mandache (2001). The recent work in Isakov (2008) seeks to distinguish some particular cases of increased stability. This severely ill-posedness is intrinsic to any inverse boundary value problem in diffusion models such as, for example, the mathematical model in Optical Tomography, e.g., Arridge (1999).

CDII belongs to a new class of Inverse Problems which seek to significantly improve both the quantitative accuracy and the resolution of traditional inverse boundary value problems by using data that can be determined in the interior of the object. These have been dubbed *hybrid, dual*, or *coupled physics methods* as they employ a combination of two different kinds of physical measurements. Typically one method provides good resolution but the observed property has poor contrast, while the other method seek a property with good contrast, but the method has poor resolution. For instance, in Magnetic Resonance Elastography (MRE) one is to image a high contrast (in malignant vs. benign) elastic property (stiffness) of the tissue by observing the propagation of waves (a lower resolution technique) with a magnetic resonance imaging machine (a higher resolution technique), see McLaughlin et al. (2004, 2006, 2007) for a mathematical study of the method, and Muthupillai

et al. (1995) for original engineering work. Another rich example is the Thermo/Opto-Acoustic Tomography in which an integral (spherical) transform of the thermal/optical absorbtion (a high contrast) property of the tissue is observed by sound transducers placed at the boundary of a body. Originated in the engineering work of Kruger et al. (1995, 1999), this method generated such a strong interest that an abundance of results appeared in relatively short time: in its mathematical aspects we refer to Finch et al. (2004), Finch and Rakesh (2007, 2009), Agranovski et al. (2009), Kuchment and Kunyansky (2008, 2010), Nguyen (2009), Xu and Wang (2005, 2006), Stefanov and Uhlmann (2009,2010), and Bal and Uhlmann (2010). These methods hold high promise in practical applications as described in Wang (2007, 2010). Yet another example of a hybrid imaging method is Acousto-Optic/Electric Tomography (AOT/AET) which aims to image electrical conductivity/optical property of tissue by modification/modulation: an application of the ultrasound waves locally modify the tissue's desired property (i.e. conductivity/optical absorbtion) and measure the effect at the boundary. This effect was first observed experimentally by Lavandier et al. (2000). The waves can focus at a specific location in the interior (this can be done at the computational level, see Kuchment and Kunyansky, 2010), and thus one knows where the boundary effect comes from. AOT/AET is an extremely active area of current mathematical research including results of Ammari et al. (2008, 2009), Gebauer and Scherzer (2008), Kunyansky and Kuchment (2010), Bal and Schotland (2010), Bal (2011).

1.2 Current Density Imaging

The internal data used by CDII is the magnitude of the current density. Currently, such measurements can be obtained using MRI. New techniques seek to employ acoustic measurements [26]. The method of imaging the current density using MRI was developed in the early 1990 in the University of Toronto by Mike Joy and his team [44]. The body positioned in the MRI scanner

is induced with a low frequency polarized current I_+ which produces a phase change in the static magnetic resonance signal M (that is the magnetic resonance signal emitted in the absence of a current). Let $\vec{B} = (B_x, B_y, B_z)$ be the induced magnetic field with the z component B_z aligned with the static magnetic field. Then, the altered magnetic resonance image is proportional to the static magnetic field and it is given by

$$M_+(x, y, z) = M(x, y, z)e^{i\gamma B_z(x,y,z)T+i\varphi_0},$$

where γ is the known gyro-magnetic ratio, φ_0 is the phase due to the static magnetic field (see the appendix in [41]) and T is the duration of the current. A current I_- with opposite polarization for the same duration T is induced to generate a corresponding magnetic resonance signal

$$M_- = M(x, y, z)e^{-i\gamma B_z(x,y,z)T+i\varphi_0}.$$

By taking the ratio of the two magnetic resonance signals and using the principal value complex logarithm one can obtain the z component of $\vec{B}$, i.e.

$$B_z(x, y, z) = \frac{1}{2\gamma T} \log\left(\frac{M_+(x, y, z)}{M_-(x, y, z)}\right).$$

Using three rotations of the body one can obtain all the necessary components of the magnetic field. Then using Ampere's law $\vec{J} = \frac{1}{\mu_0}\nabla \times \vec{B}$, where μ_0 is the magnetic constant, one can compute the magnitude of the current density, $\left|\vec{J}\right|$. For more details on imaging of the current density see [44].

1.3 CDII as an Inverse Boundary Value Problem

In CDII we seek the unknown conductivity map of a body. The known data are the magnitude of the current density of the body induced by low frequency electrical currents injected on the boundary, and a combination of boundary data.

The physical model for CDII combines Maxwell's equations with magnetic resonance measurements as follows. Let $E(x,t) = \mathbb{R}e(\vec{E}(x,\nu)e^{i\nu t})$ denote the time-harmonic electric field, $H(x,t) = \mathbb{R}e(\vec{H}(x,\nu)e^{i\nu t})$ be the time harmonic magnetic field, and $J = \mathbb{R}e(\vec{J}(x,\nu)e^{i\nu t})$ be the time harmonic current density field $J = \mathbb{R}e(\vec{J}(x,\nu)e^{i\nu t})$. In the (quasi)-static case of $\nu \simeq 0$ these vector fields are related by the Maxwell system $\nabla \times \vec{H} = \sigma\vec{E}$ and $\nabla \times \vec{E} = 0$, where the coefficient σ defines the electric conductivity of the body, a quantity we propose to recover. The last equation defines the electric potential (scalar) field u by $\vec{E} = -\nabla u$. The relation between the current density $\vec{J}$ and the conductivity σ given by the Ohm's law $\vec{J} = -\sigma\vec{E}$. From its definition as a curl, $\vec{J}$ is divergence free so that, in combination with Ohm's law, one obtains the conductivity equation

$$\nabla \cdot \sigma\nabla u = 0. \tag{1.1}$$

Let $\Omega \subset \mathbb{R}^d, d \geq 2$, be the conductive body with an unknown conductivity map described by the positive function σ which is assumed to be essentially bounded away from infinity and from 0. Mathematically, Ω is an open connected set with a Lipschitz boundary $\partial\Omega$. Let $|J| \in L^2(\Omega)$ be the magnitude of the current density, and let $u \in H^1(\Omega)$ be the induced voltage potential. Then, using Ohm's law and taking the magnitude of the current density we get that

$$\sigma = \frac{|J|}{|\nabla u|}. \tag{1.2}$$

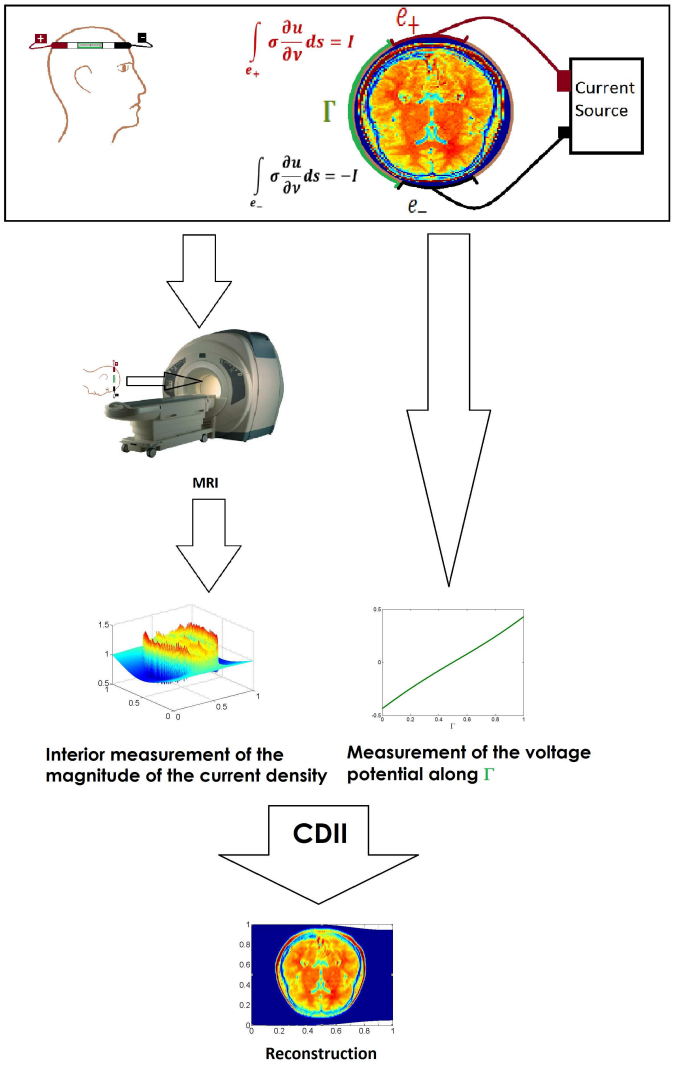

Figure 1.1: The cartoon above depicts the imaging process in CDII using Cauchy data. From top to bottom: the conductive body undergoes an MRI scan to obtain the magnitude of the current density and the boundary data (in this case the Cauchy data), then by solving (1.3) one obtains the voltage potential, and finally using (1.2) the conductivity is computed.

Throughout this thesis we assume the absence of electrical sources or sinks in Ω. Therefore, by the conservation law of electrical charges (1.1) and using (1.2) we get the following singular,

quasilinear, degenerate elliptic partial differential equation

$$\nabla \cdot \frac{|J|}{|\nabla u|} \nabla u = 0. \tag{1.3}$$

The PDE in (1.3) was first derived in [24]. For a complete survey on CDII see the 2011 article by A. Tamasan, et. al, [41]. There are two known approaches for computing the voltage potential in Ω: using the level set method and the variational approach. Then, the conductivity map is obtained via equation (1.2).

1.3.1 The Level Set Reconstruction Method

The level set method only applies to two dimensional conductive bodies. The equipotential lines of the voltage potential are reconstructed in Ω by solving a system of ordinary differential equations. Then the conductivity is imaged by using (1.2). This approach was first considered in [40]. In further chapters the terms ”level set method” and ”characteristics method” are interchanged. The difference between the two methods is that the ”level set method” reconstructs the equipotential lines of the voltage potential (see the next proposition) and the ”characteristic method” recovers the characteristics curves of (1.3) which turn out to be the same as the equipotential lines.

In order to reconstruct the voltage potential using the level set method a non-vanishing current density is necessary. This condition is achieved in the case where the voltage potential is generated by applying an almost two-to-one voltage on the boundary. Proofs of the last statement are shown in theorem A.0.3 and in [2].

Definition 1.3.1. *A function defined on a connected curve is almost two-to-one if the set of local maxima is either one point or one connected arc.*

The results stated in this subsection motivate the characteristics method reconstruction with Cauchy

data in chapter 2 and with Dirichlet data in chapter 3.

In a planar conductive body with an induced voltage potential the equipotential curves are geodesics. In the level set method it is assumed that a voltage potential exists, that is there exist a conductivity σ and an induced voltage potential $u \in H^1(\Omega)$ which satisfy the energy conservation law (1.1) in the weak sense, that is

$$\int_\Omega \nabla\phi \cdot (\sigma \nabla u)\, dx = 0, \quad \forall \phi \in C_0^\infty(\Omega).$$

We say that this type of voltage potential, u, is σ-harmonic.

Proposition 1.3.2 ([40]). *Let $\Omega \subset \mathbb{R}^2$ be a simply connected domain with a $C^{3,\delta}$ boundary. Let $\sigma \in C^{1,\delta}(\Omega)$, and let $u \in C^{2,\delta}(\Omega)$ be σ-harmonic, with $|\nabla u| > 0$ in Ω and $0 < \delta < 1$. Then the level sets of u are geodesics for the metric $g = |J|^2 I$, where $|J| = |\sigma \nabla u|$. In particular, if $\gamma : (0,1) \mapsto \Omega$, $\gamma(t) = (x(t), y(t))$ is any local parametrization of such a level curve, then it satisfies the geodesic system*

$$\begin{aligned} \ddot{x} &= -\dot{x}^2 \frac{|J|_x}{|J|}(x,y) - 2\dot{x}\dot{y}\frac{|J|_y}{|J|}(x,y) + \dot{y}^2 \frac{|J|_x}{|J|}(x,y), \\ \ddot{y} &= \dot{x}^2 \frac{|J|_y}{|J|}(x,y) - 2\dot{x}\dot{y}\frac{|J|_x}{|J|}(x,y) - \dot{y}^2 \frac{|J|_y}{|J|}(x,y), \end{aligned} \tag{1.4}$$

where the dot denotes $\frac{d}{dt}$.

In general a boundary value problem with two endpoints data coupled with the system of equations in (1.4) does not have a unique solution.

Theorem 1.3.3. *Let the unknown voltage potential u be σ-harmonic with $u|_{\partial\Omega} = f \in C^{2,\delta}(\delta\Omega)$ with f almost two-to-one. Let $|J| \in C^{1,\delta}(\Omega)$ be the measured magnitude of the current density for which $|J| = |\sigma \nabla u|$, and let $(x_0, y_0), (x_1, y_1) \in \partial\Omega$ be such that $f(x_0, y_0) = f(x_1, y_1)$. Then, the*

system (1.4), subject to the boundary conditions

$$(x(0), y(0)) = (x_0, y_0), \quad (x(1), y(1)) = (x_1, y_1),$$

has a unique solution $\gamma : [0,1] \mapsto \Omega, \gamma(t) = (x(t), y(t))$. *Moreover, the map* $u : \Omega \mapsto \mathbb{R}$ *is constant along* γ, *that is*

$$(u \circ \gamma)(t) = \lambda, \quad t \in [0,1].$$

One advantage of using level set methods is imaging the conductivity in a sub-domain of the body using only partial data. The figure 3.8 illustrates an example of the conductivity reconstructed on a sub-domain. The following result corresponds to imaging the conductivity with only partial Cauchy data.

Theorem 1.3.4 ([41]). *Let* $\Omega \subset \mathbb{R}^2$ *be a simply connected, bounded domain with a piecewise* C^1-*smooth boundary and* $\Gamma \subset \partial\Omega$. *Given* $f \in C^2(\Gamma), g \in C^1(\Gamma)$ *and* $|J| \in C^1(\overline{\Omega}) \cap C^2(\Omega)$, *then there exists a uniquely defined subregion* $\tilde{\Omega} \subset \Omega$ *and a unique pair* $(\sigma, u) \in C^2(\tilde{\Omega}) \times C^2(\tilde{\Omega})$ *such that* u *is* σ*-harmonic and* $|\sigma \nabla u| = |J|$ *in* $\tilde{\Omega}$, *and* $u|_\Gamma = f$ *and* $\delta_\nu u|_\Gamma = g$. *Moreover, if* f *is almost two-to-one and* Γ *is a maximal arc of monotony, then the above holds with* $\tilde{\Omega} = \Omega$.

For the reconstruction of the conductivity in a sub-domain with only partial Dirichlet data we state the following uniqueness result.

Theorem 1.3.5 ([40]). *Let* $\Omega \subset \mathbb{R}^2$ *be a simply connected domain with* $C^{2,\delta}$*-boundary,* $0 < \delta < 1$. *For* $i = 1, 2$ *let* $\sigma_i \in C^{2,\delta}(\Omega)$, u_i *be* σ_i*-harmonic with* $u_i|_{\delta\Omega} \in C^{2,\delta}(\partial\Omega)$ *almost two-to-one, and* $|J_i| = |\sigma_i \nabla u_i|$. *For* $\alpha < \beta$ *let*

$$\Omega_{\alpha,\beta} := \left\{ x \in \overline{\Omega} : \alpha < u_1 < \beta \right\}, \quad \textit{and} \quad \Gamma_{\alpha,\beta} := \Omega_{\alpha,\beta} \cap \partial\Omega.$$

1. Assume $u_1|_{\partial}\Gamma = u_2|_{\partial}\Gamma$ *and* $|J_1| = |J_2|$ *in the interior of* Ω*. Then*

$$u_1 = u_2 \text{ in } \Omega_{\alpha,\beta} \quad \text{and} \quad \sigma_1 = \sigma_2 in \Omega_{\alpha,\beta}.$$

2. Assume $u_1|_{\partial}\Gamma = u_2|_{\partial}\Gamma$ *and* $|J_1| = |J_2|$ *in the interior of* $\Omega_{\alpha,\beta}$*. Then*

$$\left\{x \in \overline{\Omega} : \alpha < u_1 < \beta\right\} = \Omega_{\alpha,\beta},$$
$$u_1 = u_2 \text{ in } \Omega_{\alpha,\beta} \quad \text{and}$$
$$\sigma_1 = \sigma_2 \text{ in } \Omega_{\alpha,\beta}.$$

In practical applications the voltage potential distribution in a body is induced by the injected currents on the boundary. The level set method or the characteristics method assumes the existence a voltage distribution in this body to generate the values of it along the equipotential lines. Then, the conductivity is imaged using the reconstructed values of the voltage potential. This method is sensitive to the irregularity of the measured data. Notice that in the equations such as (1.4, 2.12) and (3.5) the data $|J|$ is differentiated which decreases the accuracy of the numerical results. In the next two chapters we implement special methods of differentiation to differentiate the measured data. In the variational approach this is not an issue.

1.3.2 The Variational Approach

Due to the elliptic degeneracy and to the presence of singularities, the Dirichlet problem associated to the 1-Laplacian equation (1.3) may have many solutions, see [45]. However, in the variational approach, a relevant solution may be obtained by minimizing a functional associated with the conductivity equation (1.1).

The solutions of (3.1) subject to Dirichlet boundary conditions may not have a unique solution. Uniqueness is determined for the set of $|J|$'s for which there is a positive bounded conductivity σ and a σ-harmonic u such that $|J| = \sigma|\nabla u|$. Given that the boundary data $f \in H^{1/2}(\partial\Omega)$, we call the pair $(f, |J|)$ *admissible*. The following example taken from [45] for $|J| \equiv 1$ has an infinite number of solutions. Let $D = \{(x, y) \in \mathbb{R}^2 : x^2 + y^2 = 1\}$ be a unit circle. Consider the problem

$$\begin{aligned} \nabla \cdot \frac{\nabla u(x,y)}{|\nabla u(x,y)|} &= 0, \quad (x,y) \in D, \\ u(x,y) &= x^2 - y^2, \quad (x,y) \in \partial D. \end{aligned}$$

An infinite set of solutions u^λ dependent on the parameter $\lambda \in [-1, 1]$ is

$$u^\lambda(x,y) := \begin{cases} 2x^2 - 1, & \text{if } |x| \geq \sqrt{\frac{1+\lambda}{2}}, \quad |y| \leq \sqrt{\frac{1-\lambda}{2}}, \\ \lambda, & \text{if } |x| \leq \sqrt{\frac{1+\lambda}{2}}, \quad |y| \leq \sqrt{\frac{1-\lambda}{2}}, \\ 1 - 2y^2, & \text{if } |x| \leq \sqrt{\frac{1+\lambda}{2}}, \quad |y| \geq \sqrt{\frac{1-\lambda}{2}} \end{cases} .$$

The following is an important result for uniqueness in the variational approach with Dirichlet boundary conditions.

Let $(f, |J|)$ be an admissible pair. Define the functional F for functions $v \in H^1(\Omega)$ with $v|_{\partial\Omega} = f$ as

$$F[v] := \int_\Omega |J(x)||\nabla v| \, dx.$$

The Euler-Lagrange equation of F is the degenerate equation (1.3). From the set of solutions u^λ the only solution which minimizes the functional F is u^0 over the space of bounded variations, see [45] for details.

Let u be σ-harmonic and the minimizer of F with the admissible pair $(f, |J|)$. Observe,

$$\begin{aligned} F[v] &= \int_\Omega |J||\nabla v| \, dx = \int_\Omega |\sigma \nabla u||\nabla v| \, dx \\ &\geq \int_\Omega \sigma \nabla u \cdot \nabla v \, dx = \int_{\partial\Omega} \sigma \frac{\partial u}{\partial \nu} v \, ds, \end{aligned}$$

where ν is the outward unit normal. The lower bound is achieved when $v \equiv u$. This motivates the following theorem.

Theorem 1.3.6 ([39]). *Let $\Omega \subset \mathbb{R}^n$ be a domain with connected $C^{1,\delta}$-boundary and let $(f, |J|) \in C^{1,\delta}(\partial\Omega) \times C^{\delta}(\overline{\Omega})$ be an admissible pair generated by some unknown C^{δ}-conductivity. Assume that $|J| > 0$ a.e. in Ω . Then the minimization problem*

$$\textit{argmin} \left\{ F[u] : v \in W^{1,1}_{+}(\Omega) \cap C(\overline{\Omega}), v|_{\partial\Omega} = f) \right\}$$

has a unique solution u. Moreover, $\sigma = \frac{|J|}{|\nabla u|}$ is the unique conductivity in $C^{\delta}(\overline{\Omega})$ for which $|J|$ is the magnitude of the current density which maintaining the voltage f on the boundary.

Various numerical schemes have been developed to obtain the unknown conductivity through the variational approach, see for instance [39, 50].

In collaboration with Dr. Tamasan, Dr. Timonov and Dr. Nachman, my contributions to CDII are developed in detail in the next three chapters. The work described in chapters 2 and 3 are taken from our published articles [52] and[54], respectively. The work presented in chapter 4 will be submitted in the future for publication.

In chapter 2, see [52], we consider the problem of reconstruction of a sufficiently smooth planar conductivity from the knowledge of the magnitude $|J|$ of one current density field inside the domain, and the corresponding voltage and current on a part of the boundary. Mathematically, we

are lead to the Cauchy problem for the the 1-Laplacian with partial data. Different from existing works, we show that the equipotential lines are characteristics in a first order quasilinear partial differential equation. The conductivity can be recovered in the region flown by the characteristics originating at parts of the boundary where the data is available.

In chapter 3, see [54], we consider the numerical solvability of the Dirichlet problem for the 1-Laplacian in a planar domain endowed with a metric conformal with the Euclidean one. Provided that a regular solution exists, we present a globally convergent method to find it. The global convergence allows to show a local stability in the Dirichlet problem for the 1-Laplacian nearby regular solutions.

In chapter 4, we consider the hybrid inverse problem of recovering an isotropic electrical conductivity from the interior knowledge of the magnitude of one current density field generated by injecting current through a set of electrodes. The mathematical model reduces to solving the 1-Laplacian with boundary conditions coming from the Complete Electrode Model. This problem has non-unique solutions. We use a variation approach to characterize this non-uniqueness, and show that additional measurements of the voltage potential along one curve joining the electrodes uniquely recover the conductivity. A nonlinear algorithm is proposed and implemented to illustrate the theoretical results.

In the appendices I include a series of theorems I developed during my studies in Graduate school. Some of the work there may be relevant to the work presented in chapter 3.

CHAPTER 2: CONDUCTIVITY IMAGING BY THE METHOD OF CHARACTERISTICS

2.1 Introduction

In this chapter we present a novel reconstruction method in Current Density based Impedance Imaging (CDII): Let $\Omega \subset \mathbf{R}^2$ be a simply connected, bounded domain with piecewise smooth boundary, and σ be a sufficiently smooth conductivity in Ω bounded away from zero and infinity. A current g with $\int_{\partial\Omega} g ds = 0$ is normally injected at the boundary. Up to an additive constant, the voltage potential u distributes according to the solution of the Neumann problem

$$\nabla \cdot \sigma \nabla u = 0, \qquad \sigma \partial_\nu u|_{\partial\Omega} = g, \tag{2.1}$$

where ν is the outer unit normal to the boundary. Recall that the current density field J is uniquely defined by Ohm's law $J = -\sigma \nabla u$, regardless of the constant. We assume that its magnitude $|J|$ is known in Ω (or some subregion).

For clarity, we convene that properties referring to a boundary arc concern only the interior points. Properties pertaining to its end points are to be specified separately. We assume that the voltage u is measured on a boundary arc Γ on which the non-stationary condition

$$|\partial_\tau (u|_\Gamma)| > 0 \tag{2.2}$$

holds, where τ is the unit tangent. At a corner point both sided tangential derivatives are to satisfy (2.2). At the end points $\partial_\tau u|_\Gamma$ (or one sided derivative if it is a corner point) may vanish.

The conductivity imaging model considered here is the Cauchy problem for the 1-Laplacian (in

the metric $|J|^2 ds$):

$$\nabla \cdot \frac{|J|}{|\nabla u|} \nabla u = 0, \quad u|_\Gamma = f, \quad \partial_\nu u|_\Gamma = g, \tag{2.3}$$

where ν is the outer unit normal to the boundary.

The work [23] is the first to employ the 1-Laplacian in conductivity imaging in conjunction with Neumann boundary conditions. As shown in there, the Neumann problem can have none to multiple solutions, to conclude that one current density field by itself, in general, cannot determine the conductivity inside. To remedy this, in [38] the Cauchy problem (2.3) is considered and sufficient conditions on the boundary voltage are found to recover the conductivity stably. Further work in [39] and [42] consider the Dirichlet problem for the 1-Laplacian to show that boundary voltage on the entire boundary together with $|J|$ inside uniquely determine σ (this is in any dimension $d \geq 2$). In two dimensions the result is extended to imaging from partial data [40].

A marked difference from the approach in [38] is that in here one first injects a current, rather than maintain a specific voltage. As in [23], the current g satisfies

$$g|_{\Gamma_+} > 0, g|_{\Gamma_-} < 0, \text{ and, } g|_{\partial\Omega \setminus \Gamma_\pm} = 0, \tag{2.4}$$

where $\Gamma_\pm$ are two connected arcs. This applied current pattern is important since it yields

$$\inf_{\overline{\Omega}} |\nabla u| > 0, \tag{2.5}$$

see [3, 4].

Throughout the chapter $C^{k,\alpha}(\Omega)$, $\alpha \in (0,1)$, denotes the space of differentiable functions with α-Hölder continuous k-th derivative, for some $0 < \alpha < 1$. If $\alpha = 1$ then the k-th derivative is

assumed Lipschitz. The conductivity reconstruction is based on the following local existence and uniqueness result.

Theorem 2.1.1. *Let $\Omega \subset \mathbf{R}^2$ be a domain with piecewise Lipschitz boundary, and Γ be a smooth boundary arc. Assume that $|J| \in C^{1,1}(\Omega \cup \Gamma)$ is positive in a neighborhood of Γ. Let $g \in C^1(\Gamma)$, and $f \in C^2(\Gamma)$ be such that*

$$|f_\tau| > 0, \quad \textit{inside} \quad \Gamma, \tag{2.6}$$

where f_τ denotes the tangential derivative. Then there is a neighborhood $\tilde{\Omega}$ of Γ, in which (2.3) has a unique solution $u \in C^1(\tilde{\Omega})$ with $|\nabla u| \neq 0$.

The conductivity is determined in $\tilde{\Omega}$ by

$$\sigma = |J|/|\nabla u|. \tag{2.7}$$

Different from the method in [38], we show that the voltage potential u is constant along the characteristics of the quasilinear first order partial differential equation determined by the interior data:

$$-(\sin\theta)\theta_x + (\cos\theta)\theta_y + (\ln|J|)_x \cos\theta + (\ln|J|)_y \sin\theta = 0. \tag{2.8}$$

Theorem 2.1.2. *Let $\Omega \subset \mathbf{R}^2$ be a simply connected domain with piecewise $C^{3,\alpha}$-smooth boundary, $\sigma \in C^{2,\alpha}(\Omega)$ be a smoothly varying conductivity with unknown values inside Ω but known boundary values. A current $g \in C^{1,\alpha}(\partial\Omega)$ satisfying (2.4) is applied at the boundary, and the voltage potential $u|_\Gamma$ is measured along a boundary arc Γ to satisfy (2.2). Assume that the magnitude of the current density field $|J|$ generated by the injected current is known in a subdomain $\tilde{\Omega} \subset \Omega$ with $\Gamma \cap \partial\tilde{\Omega} \neq \emptyset$. Then the conductivity can be uniquely recovered in the region spanned by the characteristics of (2.8) that originate on $\Gamma \cap \partial\tilde{\Omega}$ and stay within $\tilde{\Omega}$.*

As a direct consequence of the smooth dependence on the data (see, e.g., [48]) of solutions of

initial value problems for systems of ordinary differential equations (ODE's), we show that the method is conditionally stable in a compact subset of the region flown by the characteristics.

Theorem 2.1.3 (Conditional Stability)**.** *Let $\Omega \subset \mathbf{R}^2$ be a simply connected domain with piecewise $C^{3,\alpha}$-smooth boundary, and $\sigma \in C^{2,\alpha}(\Omega)$ be an unknown conductivity. Let u be the solution of (4.1) for some applied current g satisfying (2.4), Γ be an arc at the boundary such that (2.2) holds on $\overline{\Gamma}$, and $|J| := \sigma|\nabla u|$ be known in Ω. Assume that $\tilde{g} \in C^1(\partial\Omega)$, $\tilde{f} \in C^2(\Gamma)$, and $|\tilde{J}| \in C^{1,1}(\overline{\Omega})$ are "noisy data" such that*

$$\max\{\|\partial_\tau(u|_\Gamma) - \tilde{f}_\tau\|_{C^1(\Gamma)}, \|g - \tilde{g}\|_{C^1(\partial\Omega)}, \|\nabla \ln |J| - \nabla \ln |\tilde{J}| \,\|_{Lip(\overline{\Omega})}\} \leq \eta, \tag{2.9}$$

for some $\eta > 0$ small enough. Let $\tilde{u}$ be defined along the characteristics for the noisy data $\tilde{g}, \tilde{f}, |\tilde{J}|$ as in (2.17). Let K be a compact set in the intersection of the domains spanned by characteristics originating at $\overline{\Gamma}$ for the two sets of data. Then, at each point in K

$$\left| \sigma - \frac{|\tilde{J}|}{|\nabla \tilde{u}|} \right| \leq C\eta,$$

for some constant $C > 0$, which depends on $\|\nabla \ln |J|\|_{Lip(\overline{\Omega})}$, $\|g\|_{C^1(\Gamma)}$, $\|f|_\Gamma\|_{C^2(\Gamma)}$, and the compact subset K.

The reconstruction methods described in the proof of the theorems above are implemented in Section 2.3. Complete and incomplete interior data results are presented. The algorithms are based on the numerical solutions of the Cauchy problem for the characteristic system and the spline interpolation.

2.2 The Method of Reconstruction

In this section we prove Theorems 2.1.1, 2.1.2, and 2.1.3.

Proof of Theorem 2.1.1: We first assume existence and address the local uniqueness question. Let $u_i \in C^1(\Omega_i \cup \Gamma)$, $i = 1, 2$, be two solutions of (2.3) defined nearby Γ such that $|\nabla u_i| > 0$. Let $s \mapsto (x_0(s), y_0(s))$ be the Euclidean arc-length parametrization of Γ. The assumption (2.2) yields

$$f_\tau(x_0(s), y_0(s)) := \langle x_0'(s), y_0'(s) \rangle \cdot \nabla u_i(x_0(s), y_0(s)) \neq 0, \quad i = 1, 2. \tag{2.10}$$

Since $|\nabla u_i| \neq 0$ in $\Omega_1 \cap \Omega_2$, which is a simple connected neighborhood of Γ, the argument functions $\theta_i = \arg(\nabla u_i)$ are $C^1(\Omega_1 \cap \Omega_2)$-smoothly defined for $i = 1, 2$. Since u_i are solutions of the 1-Laplacian in (2.3), it is easy to see that they satisfy the first order PDE (2.8).

To simplify notation in what follows we let

$$\theta_0(s) := \arg(f_\tau \partial_\tau + g\partial_\nu)|_{(x_0(s), y_0(s))}, \tag{2.11}$$

where $\{\partial_\tau, \partial_\nu\}$ is the positively oriented orthonormal frame of the unit tangent and normal vector on Γ.

Now let $t \mapsto (x_i(t, s), y_i(t, s))$ be the (Euclidean arc-length) parametrization of the equipotential maps $u_i(x_i(t, s), y_i(t, s)) = f(s)$, $i = 1, 2$. Then the map $t \mapsto (x_i(t, s), y_i(t, s), \theta_i(t, s))$ solves the corresponding characteristic system

$$\begin{cases} \frac{dx}{dt} = -\sin\theta \\ \frac{dy}{dt} = \cos\theta \\ \frac{d\theta}{dt} = -(\ln|J|)_x \cos\theta - (\ln|J|)_y \sin\theta, \end{cases} \tag{2.12}$$

subject to the initial conditions

$$x(0,s) = x_0(s), \quad y(0,s) = y_0(s), \quad \theta(0,s) = \theta_0(s), \tag{2.13}$$

where θ_0 defined in (2.11).

Uniqueness in the initial values problem for ODE implies that $(x_1(t,s), y_1(t,s)) = (x_2(t,s), y_2(t,s))$ whenever $(x_i(t,s), y_i(t,s)) \in \Omega_1 \cap \Omega_2$. Therefore u_1 and u_2 are constant on each other level sets. Since they also coincide at $t = 0$, they coincide in the region spanned by the family of curves $t \mapsto (x_1(t,s), y_1(t,s))$, $0 < s < Length(\Gamma)$.

The necessary and sufficient condition for an arbitrary curve $\gamma : s \mapsto (x_0(s), y_0(s))$ to be non-characteristic for (2.8) is for the determinant

$$\begin{vmatrix} -\sin\theta_0(s) & x_0'(s) \\ \cos\theta_0(s) & y_0'(s) \end{vmatrix} \neq 0. \tag{2.14}$$

By the hypothesis (2.10), the curve Γ is non-characteristic for the equation (2.8), and the pair (s,t) defines local coordinates near Γ, which yield that $u_1 = u_2$ in an open neighborhood of Γ. A monodromy argument extends the region of uniqueness to a maximal, simply connected set, see also (2.16).

To prove the local existence for solutions to the Cauchy problem (2.3) consider the problem (2.12) subject to the initial conditions

$$x(0,s) = x_0(s), \quad y(0,s) = y_0(s), \quad \theta(0,s) = \theta_0(s), \tag{2.15}$$

where $s \mapsto (x_0(s), y_0(s))$ is the arc-length parametrization of Γ, and $\theta_0(s)$ is defined in (2.11).

The hypothesis $f_\tau > 0$ at Γ together with the smoothness assumptions on the boundary data yields a C^1-smoothly defined argument map $\arg(f_\tau \partial_\tau + g\partial_\nu)$ along Γ. Since the right hand side of (2.12) is Lipschitz, for each s there exists a unique solution $t \mapsto (x(t,s), y(t,s), \theta(t,s))$ with t in some interval $[0, \beta(s))$. Moreover, since the initial conditions are C^1-smooth in parameter s, the solutions are also C^1 in the parameter s (they are already $C^{1,1}$ in t), see [48]. Define the sub-domain

$$\Omega_0 := \{(x(t,s), y(t,s)) \in \tilde{\Omega} : s \in (0, length(\Gamma)), t \in (0, \beta(s))\}, \tag{2.16}$$

the function u in Ω_0 by

$$u(x(t,s), y(t,s)) := f(x_0(s), y_0(s)), \tag{2.17}$$

and the discriminant

$$\Delta(t,s) := \begin{vmatrix} -\sin\theta(t,s) & x_s(t,s) \\ \cos\theta(t,s) & y_s(t,s) \end{vmatrix} = \begin{vmatrix} x_t(t,s) & x_s(t,s) \\ y_t(t,s) & y_s(t,s) \end{vmatrix}. \tag{2.18}$$

Since Γ is non-characteristic at every point, the equation (2.14) yields $\Delta(0,s) \neq 0$, for all $s \in (0, Length(\Gamma))$. Continuity of Δ implies that

$$\Delta(t,s) \neq 0, \quad \text{in} \quad \{(s,t) : \ s \in (0, length(\Gamma)), \ t \in [0, \tilde{\beta}(s))\},$$

for some $\tilde{\beta}(s) \leq \beta(s)$. Let us define

$$\Omega_1 := \{(x(s,t), y(t,s)) \in \Omega_0 : \ \Delta(t,s) \neq 0\}. \tag{2.19}$$

By differentiating in t and s (2.17) we get that

$$\nabla u(x(s,t), y(s,t)) = -\frac{f_\tau(x_0(s), y_0(s))}{\Delta(t,s)} \langle \cos\theta(t,s), \sin\theta(t,s) \rangle. \tag{2.20}$$

In particular

$$\frac{\nabla u(x,y)}{|\nabla u(x,y)|} = \langle \cos\theta(x,y), \sin\theta(x,y) \rangle, \quad (x,y) \in \tilde{\Omega}.$$

Since θ solves (2.8) then u solves the 1-Laplacian in Ω_1. A rotation of coordinates gives that $\partial_\nu u = g$ at Γ. ■

Note that the formula (2.14) says that the tangent at the boundary must not to be perpendicular to the $\nabla u(\gamma(s))$, or that the tangent must be transversal to the equipotential line of u at the point $(x_0(s), y_0(s))$.

Proof of Theorem 2.1.2: Since u solves the Cauchy (2.3), it remains to show that our assumptions are sufficient to yield $\nabla \ln |J| \in Lip(\Omega)$. Indeed, since the boundary $\partial\Omega$ is piecewise $C^{2,\alpha}$, $\sigma \in C^{2,\alpha}(\Omega)$, and $g \in C^{1,\alpha}(\partial\Omega)$ by the elliptic regularity (see e.g. [18]) of solutions of (2.1) yields $u \in C^{3,\alpha}(\overline{\Omega})$. Consequently, we obtain $|J| \in C^{2,\alpha}(\overline{\Omega})$. Moreover, since σ is bounded away from zero, and no singularities present due to the choice of the applied current, we also obtain $\min_{\overline{\Omega}} |J| > 0$. Therefore $\nabla \ln |J| \in C^{1,\alpha}(\overline{\Omega}) \subset Lip(\Omega)$. ■

The absence of singular points as in (2.5) makes the result [38, Lemma 3.1] still valid: Each equipotential set is a smooth curve of finite length and with the two endpoints at the boundary. In particular each point inside lies on a unique equipotential line which reaches the boundary. If $|J|$ is known in the entire domain Ω, then (by the uniqueness of solution in the initial value problem for ODEs,) the method recovers the entire equipotential line originating at Γ.

Proof of Theorem 2.1.3: In the followings, we distinguish the quantities corresponding to the

"noisy data" $(\tilde{g}, \tilde{J}, \tilde{f})$, by using a tilde $(\tilde{\cdot})$ in their notation. For example $\tilde{\Delta}$ denotes the discriminant in (2.18) corresponding to the noisy data.

Note that $\tilde{g}$ need not satisfy the pattern in (2.4). Instead by choosing η in (2.9) such that

$$0 < \eta < \min\{\min_{\Gamma}(f_\tau), \min_{\overline{\Omega}} |\nabla \ln |J||\}$$

we obtain $\tilde{f}_\tau > 0$ on Γ, and $|\tilde{J}| > 0$ in $\overline{\Omega}$. In particular $\ln|\tilde{J}| \in C^{1,1}(\Omega)$, which suffices to solve locally the Cauchy problem (2.3) associated with $\tilde{g}$ on $\partial\Omega$, $\tilde{f} \in \Gamma$, and $|\tilde{J}|$ in Ω. More precisely, the initial problem (2.12) and (2.13) yields a solution $t \mapsto (\tilde{x}(t,s), \tilde{y}(t,s), \tilde{\theta}(t,s))$, for each $s \in (0, Length(\Gamma))$ and $t \in (0, \tilde{\beta}(s))$. Here $\tilde{\beta}(s)$ represents the Euclidean length of the characteristic originating at the point $(x_0(s), y_0(s)) \in \Gamma$.

We estimate the error at an arbitrary point $(x^*, y^*) \in K$. We refer to such a point in the coordinates defined by the characteristics of both problems:

$$(x^*, y^*) := (x(t,s), y(t,s)) = (\tilde{x}(\tilde{t}, \tilde{s}), \tilde{y}(\tilde{t}, \tilde{s})). \tag{2.21}$$

Moreover, we use the simplified notations

$$|J|(t,s) := |J|(x(t,s), y(t,s)), \quad |\tilde{J}|(\tilde{t}, \tilde{s}) := |\tilde{J}|(\tilde{x}(\tilde{t}, \tilde{s}), \tilde{y}(\tilde{t}, \tilde{s})),$$
$$|\nabla u|(t,s) := |\nabla u|(x(t,s), y(t,s)), \quad |\nabla \tilde{u}|(\tilde{t}, \tilde{s}) := |\nabla \tilde{u}|(\tilde{x}(\tilde{t}, \tilde{s}), \tilde{y}(\tilde{t}, \tilde{s})).$$

Using the definition in (2.7) and (2.20) we get

$$\left| \sigma(x^*, y^*) - \frac{|\tilde{J}|}{|\nabla \tilde{u}|}(x^*, y^*) \right| = \left| |J|(t,s) \frac{|\Delta(t,s)|}{|f_\tau(s)|} - |\tilde{J}|(\tilde{t}, \tilde{s}) \frac{|\tilde{\Delta}(\tilde{t}, \tilde{s})|}{|\tilde{f}_\tau(\tilde{s})|} \right|. \tag{2.22}$$

By triangle inequality the right hand side of (2.22) is bounded by

$$\frac{|J|}{|f_\tau|}\left|\Delta-\tilde{\Delta}\right|+\frac{|J||\tilde{\Delta}|}{|f_\tau\tilde{f}_\tau|}\left|\tilde{f}_\tau-f_\tau\right|+\frac{|\tilde{\Delta}|}{|\tilde{f}_\tau|}\left||J|-|\tilde{J}|\right|, \tag{2.23}$$

where for brevity we dropped the arguments, but they are still as in (2.22).

The right hand side of the ODE system (2.12) is Lipschitz continuous, while the initial conditions are C^1 in the parameter s. The classical results on initial value problems (via the equivalent Volterra integral formulation) for ODEs (see e.g., [48]) yield a Lipschitz-continuous dependance of the solutions on the data $(f_\tau, g, |J|)$, and thus of $(s,t)\mapsto\Delta(s,t)$ on the data $(f_\tau, g, |J|)$. Since $\Delta, \tilde{\Delta}$ are bounded on the compact set K, we get

$$\left|\Delta-\tilde{\Delta}\right|\leq C\eta,$$

for some constant C depending on $\|\nabla\ln|J|\|_{Lip(\overline{\Omega})}$, $\|g\|_{C^1(\Gamma)}$, $\|f|_\Gamma\|_{C^2(\Gamma)}$, and K. Since $f_\tau, \tilde{f}_\tau$ are bounded away from zero on $\overline{\Gamma}$, from (2.23), we conclude that the second term of (2.22) is also bounded by some multiple of η. ■

Since the constant depends on an a priori Lipschitz bound on σ, the Theorem 2.1.3 only shows conditional stability.

2.3 Numerical Results

In this section we present various numerical experiments with two different types of conductivities to demonstrate the computational capabilities of the reconstruction method above.

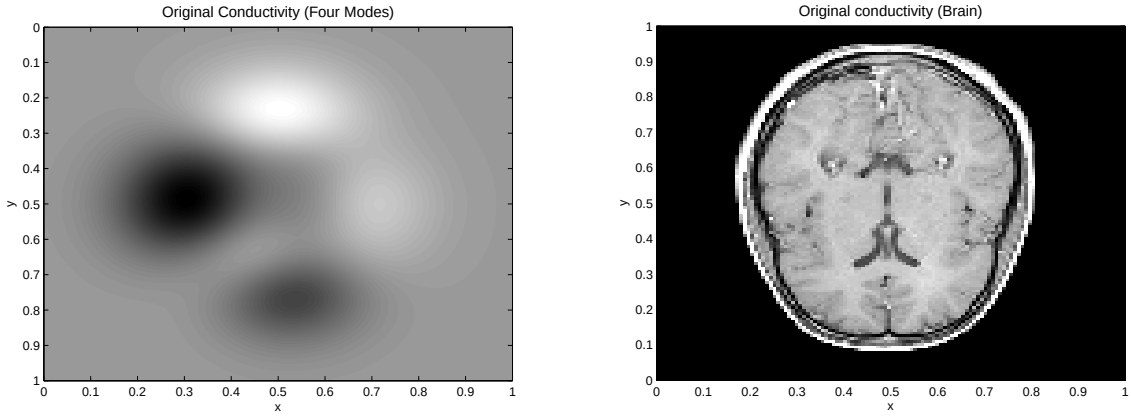

Figure 2.1: The original conductivity distribution map: the four modes (left) and the cross section of a human brain (right).

2.3.1 Data

The magnitude of the current density $|J|$ and the boundary voltage potential measurement f for the numerical experiments are obtained numerically.

We solve the Neumann problem (2.1) for two different conductivities by using the finite element method in MATLAB's PDE toolbox. The domain Ω is the unit box $[0,1] \times [0,1]$, and the boundary current $\tilde{g}(0,y) = \tilde{g}(1,y) = 0$, $\tilde{g}(x,1) = 1$, and $\tilde{g}(x,0) = -1$ is applied at the boundary. The first conductivity map is smoothly defined by the four modes function

$$\sigma(x,y) = 1 + 0.3 \cdot (A(x,y) - B(x,y) - C(x,y)), \tag{2.24}$$

where

$$A = 0.3 \cdot [1 - 3(2x-1)]^2 \cdot e^{-9\cdot(2x-1)^2-(6y-2)^2},$$
$$B = \left[\tfrac{3(2x-1)}{5} - 27\cdot(2x-1)^3 - [3\cdot(2y-1)]^5\right] \cdot e^{-\left[9\cdot(2x-1)^2+9\cdot(2y-1)^2\right]},$$
$$C = e^{-[3\cdot(2x-1)+1]^2-9\cdot(2y-1)^2};$$

see the left image in Figure 2.1. The second conductivity is a piecewise-smooth function given by a CT image of a human brain, shown in Figure 2.1 on the right. The values of the pixels of the CT image are scaled to model a conductivity distribution ranging from 1 to 1.8 S/m.

The gradient of the potential ∇u is computed via differentiation of interpolating fifth degree Lagrange polynomials. The interior data $|J| = \sigma|\nabla u|$ is computed in Ω and in the sub-domain $\Omega_1 = [0, 0.6] \times [0.25, 0.701]$ for each of the aforementioned voltage potentials. Finally, the boundary voltage potentials $u|_\Gamma = f$ and $u|_{\Gamma_1} = f_1$ are measured on the arcs $\Gamma = \{0\} \times [0, 1]$, and $\Gamma_1 = \{0\} \times [0.25, 0.701]$, respectively. See Figure 2.2 for the magnitude of the current density generated over Ω for the four modes and the brain.

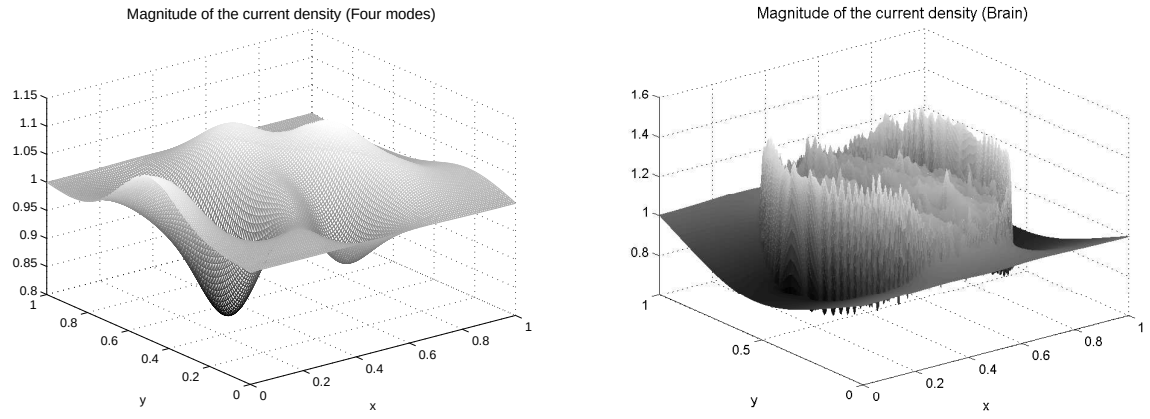

Figure 2.2: Magnitude of the current density of the four modes (left) and the cross section of a human brain (right) generated over the box $[0, 1] \times [0, 1]$.

2.3.2 Numerical Reconstruction of the Conductivity

Here we describe the steps to reconstruct a conductivity map in Ω using the method construed in section 2.2.

Step 1. Recall that in section 2.3.1 the injected current satisfies (2.4), hence $\theta = \frac{\pi}{2}$ on the line segment where the voltage potential is measured. Given $|J|$ in a box $[0, c] \times [a, b]$, we solve (2.12) using the adaptive Runge-Kutta-Fehlberg ODE solver for m characteristics subject to the initial conditions

$$x_j(0) = 0, y_j(0) = s_j, \theta_j(0) = \frac{\pi}{2}, \tag{2.25}$$

where $s_j = a + j\frac{b-a}{m-1}$, and $j = 1, 2, \ldots, m$.

The third equation in (2.12) contains the derivative of $\ln|J|$ in the direction of the unit vector $\eta = \langle \cos\theta, \sin\theta \rangle$:

$$\frac{d\theta}{dt} = -\partial_\eta \ln|J|.$$

In order to decrease the error made in differentiating $\ln|J|$ we use the center difference for the directional derivative:

$$\partial_\eta \ln|J|(x_j(t_{j_k}), y_j(t_{j_k})) = \frac{1}{2h}\left[\ln|J|(x^{j_k}_{j+h}, y^{j_k}_{j+h}) - \ln|J|(x^{j_k}_{j-h}, y^{j_k}_{j-h})\right],$$

where

$$\begin{aligned}
x^{j_k}_{j+h} &= x_j(t_{j_k}) + h \cdot \cos\theta_j(t_{j_k}), \\
x^{j_k}_{j-h} &= x_j(t_{j_k}) - h \cdot \cos\theta_j(t_{j_k}), \\
y^{j_k}_{j+h} &= y_j(t_{j_k}) + h \cdot \sin\theta_j(t_{j_k}), \\
y^{j_k}_{j-h} &= y_j(t_{j_k}) - h \cdot \sin\theta_j(t_{j_k}).
\end{aligned}$$

In all the numerical experiments the value of $\ln|J|$ (or $|J|$) at a point is interpolated by the bi-quintic piecewise Lagrange polynomials for points away from the boundary, and the bi-cubic or bi-linear interpolation for points near the boundary. For incomplete interior data, we extend $|J|$ outside the region $[0, c] \times [a, b]$ (where it is given) bi-linearly. The characteristic curves that exit this region are cut off. See, for example, the curve lying closest to the lower boundary in Figure 2.3.

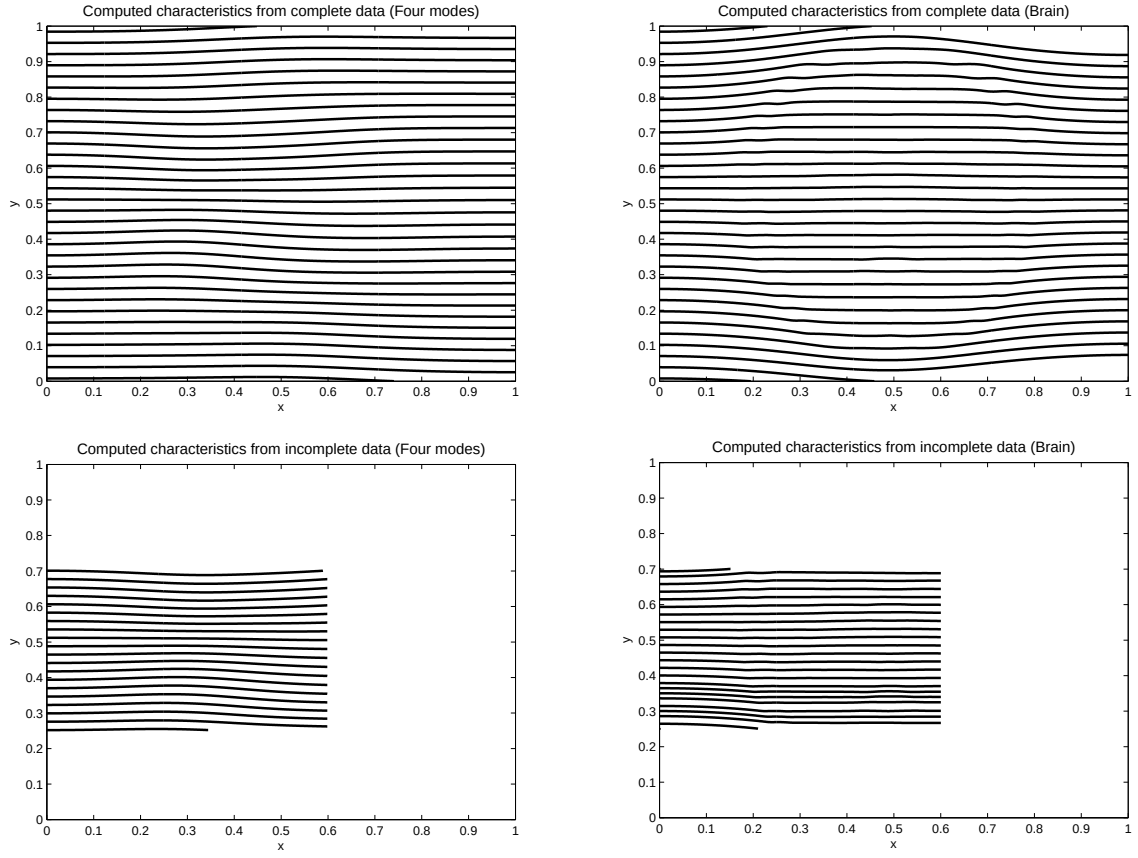

Figure 2.3: The top images show the characteristics of the four modes (left) and the brain (right) reconstructed from the interior data measured in $[0, 1] \times [0, 1]$. The bottom images show the characteristics for the four modes (left) and the brain (right) reconstructed from the interior data measured in $[0, 0.6] \times [0.25, 0.701]$.

Step 2. The characteristics are equipotential lines. The value of the potential along each charac-

teristic is determined by the measurement of the voltage potential at the boundary. Let

$$\gamma_j(t) = (x_j(t), y_j(t)),\ j \in \{1, 2, \ldots, m\}, t \in [0, \beta_j), \tag{2.26}$$

denote the equipotential line, which solves (2.12) subject to (2.25), and

$$\zeta_i(\xi) = (\hat{x}_i(\xi), \hat{y}_i(\xi)), \xi \in [0, \alpha_i),\ i \in \{1, 2, \ldots, n\}, \tag{2.27}$$

denote a smooth non-characteristic curve, which is transversal to each $\gamma_j, j = 1, 2, \ldots, m$. At the point of intersection we have

$$\begin{cases} 0 = u_x \frac{dx_j}{dt} + u_y \frac{dy_j}{dt}, \\ u_\xi = u_x \frac{d\hat{x}_i}{d\xi} + u_y \frac{d\hat{y}_i}{d\xi}, \end{cases}$$

and

$$\nabla u = \frac{u_\xi}{\frac{dy_j}{dt}\frac{d\hat{x}_i}{d\xi} - \frac{dx_j}{dt}\frac{d\hat{y}_i}{d\xi}} \left\langle \frac{dy_j}{dt}, -\frac{dx_j}{dt} \right\rangle. \tag{2.28}$$

The non-characteristic curves of (2.27) are obtained by one dimensional interpolation in between points lying on different characteristics, see the left illustration in Figure 2.4. The derivative u_ξ at the node where γ_j intersects ζ_i, is computed via the Lagrange polynomial interpolation along ζ_i.

In the particular case in which the characteristic curves are graphs, say $\left|\frac{dx_j}{dt}\right| > 0$, $j = 1, 2, \ldots, m$, a different method is employed to compute the gradient: the first component of each characteristic is regarded as the independent variable x and the other components can be expressed as functions $y_j = \phi_j(x)$ and $\theta_j = \psi_j(x)$, $j = 1, 2, \ldots, m$. Thus, letting $x^k = k\frac{c}{n-1}, k = 1, 2, \ldots, n$ we approximate the value of the functions $\{y_j = \phi_j(x)\}_{j=1}^m$ and $\{\theta_j = \psi_j(x)\}_{j=1}^m$ at equally spaced points via fifth degree piecewise Lagrange polynomials. For simplicity, we denote the interpolated point of the j^{th} characteristic at x^k by (x^k, y_j^k, θ_j^k). We construct a curve $\zeta_k(\xi) = (\hat{x}_k(\xi), \hat{y}_k(\xi))$ as in (2.27) by fixing k and selecting $(x^k, y_j^k)_{j=1}^m$ as the points for interpolation (see the right

illustration in Figure 2.4), so that $\frac{d\hat{x_k}}{d\xi} = 0$, $\frac{d\hat{y_k}}{d\xi} = 1$, and $u_\xi = u_y$. Using the first two equations in (2.12) and the curve ζ_k at the j^{th} point (x^k, y_j^k, θ_j^k), the formula (2.28) becomes

$$\nabla u = \frac{u_y}{\sin\theta_j^k} \left\langle \cos\theta_j^k, \sin\theta_j^k \right\rangle . \tag{2.29}$$

Note that since $y_j = \phi_j(x)$ for $j = 1, 2, \ldots, m$, then $0 < \theta < \pi$ for every $(x, \phi_j(x))$ in Ω, in particular $\sin\theta_j^k$ never vanishes.

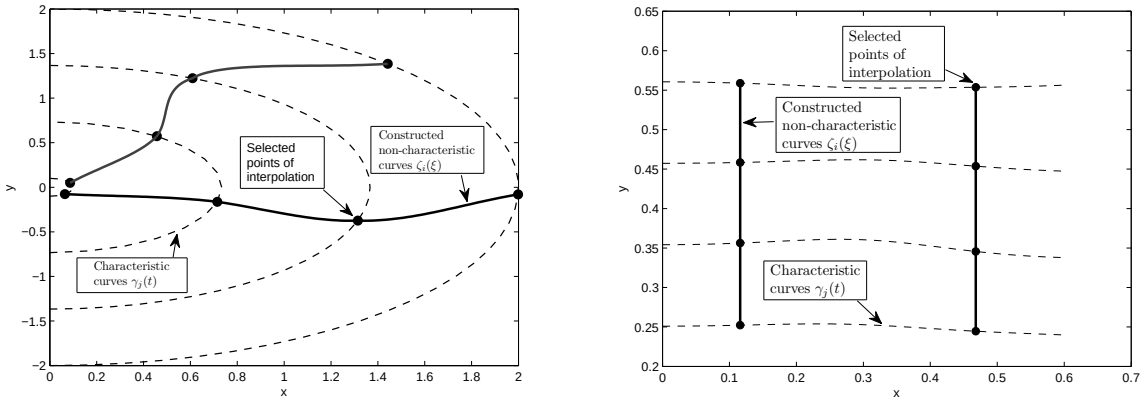

Figure 2.4: The left image illustrates an example of a set of constructed non-characteristic (solid line) curves as in (2.27) with selected points (solid dots) on the characteristic curves (dashed lines). The right image shows an example of a set of constructed non-characteristic curves (solid line) by selecting the points of interpolation (solid dots) on the characteristic curves (dashed lines) which can be described by functions. The reconstructed conductivities of the four modes and the brain, shown in Figure 3.8, were constructed on the characteristics computed as in step 1 of section 2.3.2 with non-characteristic and characteristic curves as in the the right image using (2.30).

Step 3. One recovers the conductivity by (2.28). In the specific case in which the equipotential curves are graphs the conductivity at (x^k, y_j^k) is also given by

$$\sigma(x^k, y_j^k) = \frac{|J|(x^k, y_j^k)}{u_y(x^k, y_j^k)} \sin\theta_j^k. \tag{2.30}$$

Note that in the case of graphs $u_y \neq 0$. The reconstructions in Figure 2.5 are done using formula

(2.30).

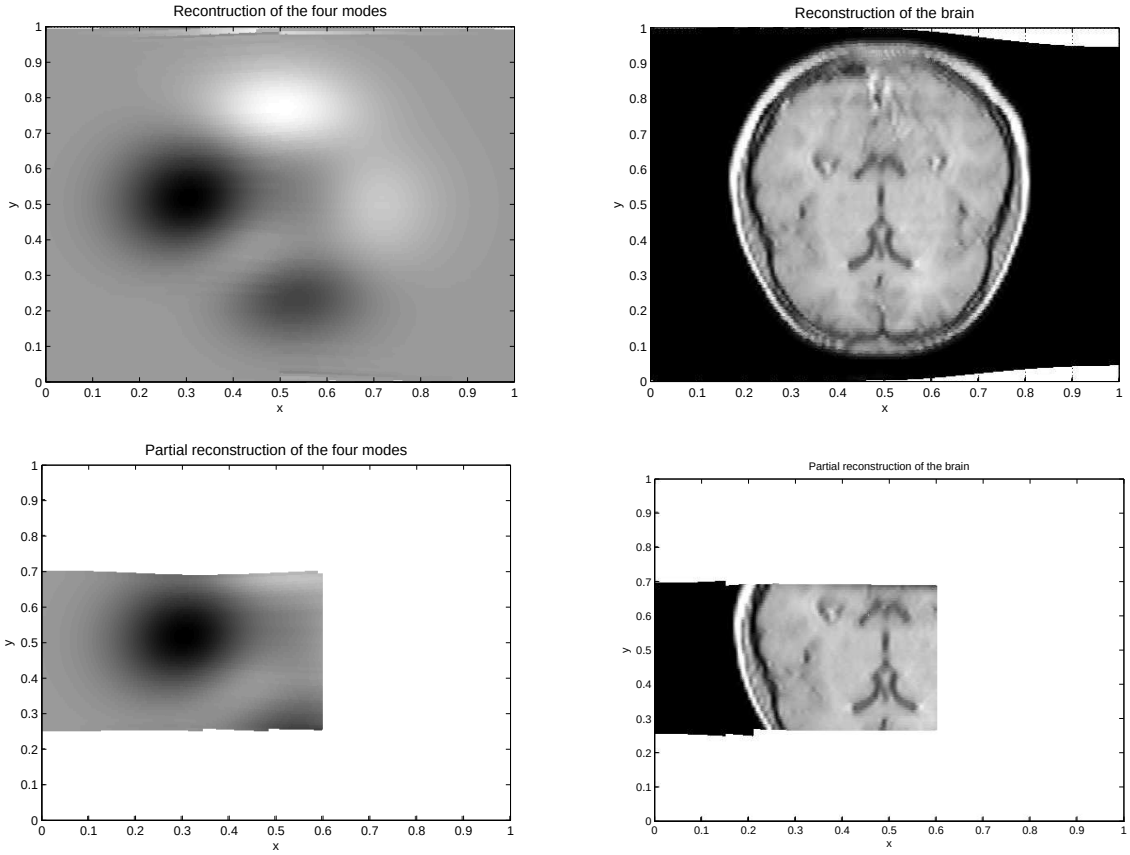

Figure 2.5: The top images show the reconstruction of the four modes (left) and the brain (right) reconstructed from the interior data measured in $[0,1]\times[0,1]$. The bottom images show the partial reconstruction of the four modes (left) and the brain (right) from the data measured in $[0,0.6]\times[0.25,0.701]$. The l_1 relative error for the reconstruction of the four modes and the brain from complete data are 0.18% and 1.37%, respectively.

The reconstruction method requires differentiation of the interior data, and the reconstructed potential. In the case of rough data, such as the brain experiment (see Figure 2.2), we use regularized differentiation, as explained below.

The interior data is convoluted with the two dimensional triangle function

$$T_{\epsilon_x,\epsilon_y}(x,y) = \begin{cases} \left(\frac{1-|x|}{\epsilon_x^2}\right)\cdot\left(\frac{1-|y|}{\epsilon_y^2}\right) & , \; if \; |x| \leq \epsilon_x \; and \; |y| \leq \epsilon_y \\ 0 & , \; otherwise \end{cases}$$

before differentiation by directional central difference. The reconstructed values of the potential are not available on a rectangular grid, which forces us to convolute u indirectly by

$$\int_{-\infty}^{\infty}\int_{-\infty}^{\infty} \Phi(\alpha,\beta) T_{\epsilon_x,\epsilon_y}(u-\alpha, x-\beta)\mathrm{d}\alpha\mathrm{d}\beta,$$

where $x \mapsto (x, \Phi(u_0, x))$ is the parametrization of the equipotential curve with voltage potential u_0.

We stress that in this chapter we only regularize the differentiation of the magnitude of the current density but not of the voltage potential generated numerically by solving (2.1). Moreover, in the case of smooth data, like in the four modes experiment, we did not use any regularization in the differentiation. The l_1-relative error

$$\frac{1}{mn}\sum_{j=1}^{m}\sum_{i=1}^{n}\frac{|\sigma-\tilde{\sigma}|}{\sigma}(x(t_{j_i}), y(t_{j_i}))$$

in the reconstruction of the brain from the complete interior data is 0.0137, and from incomplete interior data is 0.0149. The l_1-relative error of the reconstruction of the four modes from the complete interior data is about 0.0018, and from incomplete data is 0.0028. See the Figure 2.5 for reconstructions from complete and incomplete data.

2.4 Concluding Remarks

We presented a new planar conductivity reconstruction method in CDII based on solving the Cauchy problem for the 1-Laplacian with partial data. We show that equipotential lines are characteristics of a corresponding first order quasilinear PDE. In particular this emphasizes the specific (parabolic) character of the 1-Laplacian, namely that the solution on one side of the characteristic does not influence the solution on the other side. This fact was observed previously in [38], where the equipotential lines were shown to be geodesics in an appropriate Riemannian metric.

If $|J|$ is known in the entire domain Ω, then (by the uniqueness of solution in the initial value problem for ODEs,) the method recovers the entire equipotential line originating at Γ. From the weak maximum principle, in order for the characteristics to span the full domain it is necessary that

$$Range(f|_{\Gamma}) = Range(u|_{\partial\Omega}). \tag{2.31}$$

From the strong maximum principle, the maximum occurs on Γ_+ where the normally applied current is negative , while the minimum occurs on Γ_-, where the current is positive. Thus finding the maximum and minimum voltage entails measuring the potential on $\Gamma_{\pm}$. This is problematic in practice since $\Gamma_{\pm}$ are precisely where the electrodes are placed. However, if $\Gamma_{\pm}$ tend to a point (of injection), then the voltage on each of the two arcs of $\partial\Omega \setminus \Gamma\pm$ covers all of the voltage potential inside.

If, as considered in [38], instead of injecting a current, one maintains an almost two-to-one (i.e., each values is taken twice with the exception of the connected maxima and minima) boundary voltage and measures the exiting normal current at an arc Γ satisfying (2.31), then the method here also recovers the conductivity everywhere inside Ω.

CHAPTER 3: STABLE RECONSTRUCTION OF REGULAR 1-HARMONIC MAPS WITH A GIVEN TRACE AT THE BOUNDARY

3.1 Introduction

Let $\Omega \subset \mathbb{R}^2$ be a simply connected, bounded planar domain with piecewise C^1 boundary $\partial\Omega$, $a \in C^{1,1}(\overline{\Omega})$ with $\min_{\overline{\Omega}} a > 0$, and $f \in C^1(\partial\Omega)$. In this chapter we are concerned with the numerical analysis of solutions to the Dirichlet problem for the degenerate elliptic equation of the 1-Laplacian:

$$\nabla \cdot \left(a \frac{\nabla v}{|\nabla v|} \right) = 0, \quad v|_{\partial\Omega} = f. \tag{3.1}$$

Solutions of the 1-Laplacian in (3.1) are called 1-harmonic. The name is motivated by the geometric property that level sets of regular solutions of (3.1) are geodesics in the ambient plane endowed with the metric $g = a^2 I$ [38], (where I denotes the identity metric), thus generalizing the Euclidean case $a \equiv 1$.

We call a *regular solution* of (3.1) a function $u \in Lip(\Omega)$ with

$$\text{essinf}_{\Omega} |\nabla u| > 0.$$

From [39] is known that, if it exists, a regular solution to (3.1) is unique in the class of functions in $W^{1,1}(\Omega)$ with a negligible set of singular points (where the gradient vanishes). However, there are examples of Dirichlet problems for the 1-Laplacian which may not have regular solutions as shown in the introduction of chapter 1.

In this chapter we assume that a regular solution of (3.1) exists, and provide a globally convergent

numerical method to find it. As an application we are able to show conditional stability for the Dirichlet problem nearby the regular solution. To the authors knowledge this is a first stability with respect to the interior data for the Dirichlet problem of the 1-Laplacian.

Throughout this chapter we work under the following

Hypothesis 3.1.1. *The problem (3.1) has a regular solution in* $C^1(\overline{\Omega})$.

Neumann problems associated with the 1-Laplacian were first considered in [24], and Cauchy problems in [38]. The Dirichlet problem for the 1-Laplacian (3.1) was first considered in [40], where level sets of the 1-harmonic maps are shown to be geodesics in a conformal metric, and a locally convergent algorithm (in the sense that a first guess is sufficiently close to the sought solution) was proposed. This local convergence cannot be strengthened based on the length minimizing property alone in a general metric space: In the case of a hemisphere, infinitely many geodesics connect diametral points.

By contrast, in this chapter we propose a globally convergent algorithm in the sense that it is independent on the starting guess. The method of proof relies on the fact that the level sets are characteristics of a first order PDE (see (3.3) below) to solve the two point boundary value problem for each level set by a shooting method. The merit of the work presented here is the global convergence, and its corollary of a local stability result. We show that the length of these characteristics depend continuously on the boundary points and directions. This is a global geometrical property that requires the convexity of the domain, and uses the fact that the Euclidean curvature of the characteristics are a priori bounded. The convergence rate of the algorithm depends on the modulus of continuity of lengths of characteristics with respect to the shooting direction.

The problem (3.1) satisfying Hypothesis 3.1.1 occurs naturally in CDII, where $a(x)$ represents the magnitude of the current density field induced in a body by imposing the voltage f at the boundary.

In Section 3.2 we present our new algorithm which reconstructs the solution to the Dirichlet problem of the 1-Laplacian level set by level set. In Section 3.3 we discuss a generic local stability result that follows from the method. In Section 3.4 we present two numerical experiments to illustrate the feasibility of the algorithm in its application conductivity imaging.

3.2 Reconstruction of The Level Sets of u

We recall first the connection between the level sets of regular solutions of (3.1) and the characteristics of a first order PDE. By Hypothesis 3.1.1 the unknown function θ is well defined in $C^1(\overline{\Omega})$ by

$$\frac{\nabla u(x,y)}{|\nabla u(x,y)|} = \langle \cos\theta(x,y), \sin\theta(x,y) \rangle \,. \tag{3.2}$$

Since u solves problem (3.1), from (3.2) we get that θ is a solution of the first order nonlinear PDE:

$$-\theta_x \sin\theta + \theta_y \cos\theta = -\left(\ln a\right)_x \cos\theta - \left(\ln a\right)_y \sin\theta, \tag{3.3}$$

where the subscripts indicate the partial derivatives.

We solve (3.3) by the method of characteristics starting at a point on the boundary with an initial guess for the "shooting angle". By using the location where it lands on the boundary, the algorithm updates the angle. We prove convergence of the iteration to the level set of u passing through the initial point. This is the content of the two propositions below.

To fix ideas, let $\varphi : [\lambda_-, \lambda_+] \mapsto \Gamma \subset \partial\Omega$, where $\lambda_- = \min_\Omega u$ and $\lambda_+ = \max_\Omega u$, be a piecewise-smooth parametrization of a (maximal) arc of the boundary, on which $f|_\Gamma : \Gamma \to [\lambda_-, \lambda_+]$ is a bijection. Existence of the maximal arc is insured by the almost-two-to-one boundary data.

Let

$$\Theta_\lambda = \{\beta \in (-\pi, \pi] \,|\, \langle -\sin\beta, \cos\beta\rangle \cdot \vec{n}(\varphi(\lambda)) < 0\} \tag{3.4}$$

be the set of angles for directions $\langle -\sin\beta, \cos\beta\rangle$ pointing inside Ω. Here $\vec{n}(\varphi(\lambda))$ is the outward unit normal at $\varphi(\lambda) \in \partial\Omega$.

Throughout this chapter, planar curves $t \to \langle x(t), y(t)\rangle$ are always traced by the parameter t, and we use the dot notations to denote derivatives in t, e.g.,

$$\dot{x}(t) := \frac{dx}{dt}(t), \quad \ddot{x}(t) := \frac{d^2x}{dt^2}(t).$$

We consider the family (indexed in λ) of solutions to the initial value problem, each of which describe a curve originating on the boundary at $\varphi(\lambda)$ in the direction $\langle -\sin\beta, \cos\beta\rangle$.

$$\begin{cases} \dot{x} = -\sin\theta, \\ \dot{y} = \cos\theta, \\ \dot{\theta} = -(\ln a)_x \cos\theta - (\ln a)_y \sin\theta, \\ (x(0), y(0)) = \varphi(\lambda), \quad \theta(0) = \beta \in \Theta_\lambda. \end{cases} \tag{3.5}$$

Since $a \in C^{1,1}(\overline{\Omega})$ is bounded away from zero, the right hand side is Lipschitz continuous and classical arguments in ODE show that there is a unique solution $t \mapsto (x(t, \lambda, \beta), y(t, \lambda, \beta))$ defined on a maximal interval $[0, \tau(\lambda, \beta))$, where

$$\tau(\lambda, \beta) := \sup\{t^* > 0 : (x(t, \lambda, \beta), y(t, \lambda, \beta) \in \Omega,\ 0 < t < t^*\}. \tag{3.6}$$

Since the curves are traced with speed one, then $\tau(s, \beta)$ also represents the length. In general $\tau(s, \beta)$ may not necessarily be finite. We will show in Proposition 3.2.3 below that $\tau(s, \beta)$ is finite

for all $\lambda \in (\lambda_-, \lambda_+)$ and $\beta \in \Theta_\lambda$ as in (3.4). Moreover, in such a case, it follows from its definition (3.6) that $(x(\tau(\lambda,\beta),\lambda,\beta), y(\tau(\lambda,\beta),\lambda,\beta))$ is a boundary point.

The first result shows the connection between the level sets of the unknown solution u of the 1-Laplacian in (3.1), and solutions of the problem (3.5).

Proposition 3.2.1. *Let $(\xi(t),\eta(t)) : [0,T] \mapsto \overline{\Omega}$ be a level curve of u, which solves*

$$\begin{cases} \dot{\xi}(t) = -u_y(\xi,\eta)/|\nabla u(\xi,\eta)| \\ \dot{\eta}(t) = u_x(\xi,\eta)/|\nabla u(\xi,\eta)| \\ (\xi(0),\eta(0)) = \varphi(\lambda^*),\ \lambda^* \in (\lambda_-,\lambda_+), \end{cases}$$

and define $\zeta : [0,T] \mapsto \mathbb{R}$ by

$$\zeta(t) := \mathit{Arg}\left\{ \frac{\nabla u}{|\nabla u|}(\xi(t),\eta(t)) \right\}. \tag{3.7}$$

Then,

(i) the curve $t \mapsto (\xi(t),\eta(t),\zeta(t))$ is a solution of (3.5) with $\beta = \zeta(0)$ and $\lambda = \lambda^*$;

(ii) a solution of (3.5) with a fixed λ and β, which intersects $(\xi(t),\eta(t),\zeta(t))$ at least once, coincides entirely with it in $\overline{\Omega}$.

Proof. Recall that $\theta = \mathrm{Arg}\frac{\nabla u}{|\nabla u|}$ in (3.2) is a solution of (3.3). From its definition in (3.7) along a level curve $t \mapsto (\xi(t),\eta(t))$, we get equality

$$\zeta(t) = \theta(\xi(t),\eta(t)). \tag{3.8}$$

Then

$$\dot{\xi}(t) = -\sin\zeta(t), \text{ and } \dot{\eta}(t) = \cos\zeta(t). \tag{3.9}$$

Now use (3.3), (3.8), and (3.9) to obtain

$$\dot{\zeta}(t) = -\left(\ln a(\xi(t),\eta(t))\right)_{\xi}\cos\zeta(t) - \left(\ln a(\xi(t),\eta(t))\right)_{\eta}\sin\zeta(t),$$

thus proving (i).

To show (ii) let $t \mapsto (x(t,\lambda,\beta), y(t,\lambda,\beta), \theta(t,\lambda,\beta))$ be a solution of (3.5) for fixed λ and β, which intersects $(\xi(t),\eta(t),\zeta(t))$ at $t = t^*$. Since the right hand side of the first three equations in (3.5) is Lipschitz, then by the uniqueness part of solutions to initial value problems in ODE we have that the curve subject to

$$(x(t^*,\lambda,\beta), y(t^*,\lambda,\beta)) = (\xi(t),\eta(t)), \text{ and } \theta(t^*,\lambda,\beta) = \zeta(t^*),$$

is unique. Therefore, the curves $(x(t,\lambda,\beta), y(t,\lambda,\beta), \theta(t,\lambda,\beta))$ and $(\xi(t),\eta(t),\zeta(t))$ coincide everywhere where defined in $\overline{\Omega}$. □

Note that for any fixed boundary point $\varphi(s)$, there is one specific direction $\beta(s)$ which makes the solution of (3.5) be a level curve for u, in particular of finite length. However, when solving for an arbitrary shooting direction angle β, there is no general theory to guarantee the solution is not trapped inside (case in which $\tau(s,\beta) = \infty$). We prove below the finite length property for solutions of (3.5). The proof makes essential use of the curvature bound given by the third equation in (3.5), in conjunction with the fact that Hypothesis 1.1 implies that level sets of u describe global coordinates in $\overline{\Omega}$. The following lemma is key to capturing the effect of the Euclidean curvature of the characteristics on their length.

Lemma 3.2.2. *Let $f \in C^2([0,\infty))$ with $f'(t_0) \geq 0$, $|f''| < K$, and $0 < f(t) < L$. Then,*

$$L > \frac{(f'(t_0))^2}{2K}.$$

Proof. Since $f \in C^2([0,\infty))$, then there exists $t^* \in (t_0, t)$ such that

$$f(t) = f(t_0) + f'(t_0)(t - t_0) + \frac{1}{2}(t - t_0)^2 f''(t^*).$$

Using the bound on the second derivative of f we have that

$$\begin{aligned} |f(t) - f(t_0) - f'(t_0)(t - t_0)| &< \frac{1}{2}(t - t_0)^2 K, \\ f(t) - f(t_0) &> f'(t_0)(t - t_0) - \frac{1}{2}(t - t_0)^2 K. \end{aligned}$$

Now at $t^{**} = \frac{f'(t_0)}{K} + t_0$ and using the inequality, $0 < f(t) < L$, we get that

$$L > f(t^{**}) - f(t_0) > \frac{(f'(t_0))^2}{2K}.$$

□

For the following theorems, for a fixed $\lambda \in (\lambda_-, \lambda_+)$ let

$$\beta_\lambda = \arg \left\{ \frac{\nabla u}{|\nabla u|} (\varphi(\lambda)) \right\},$$

recall the initial value problem (3.5) and the definition of $\tau(\lambda, \beta)$ in (3.6).

Theorem 3.2.3. *Let $\Omega \subset \mathbb{R}^2$ be strictly convex, $a \in C^{1,1}(\overline{\Omega})$, with $\inf_\Omega |\nabla a| > 0$. Then $\tau(\lambda, \beta) < \infty$, for all $\lambda \in (\lambda_-, \lambda_+)$ and $\beta \in \Theta_\lambda$, as in (3.4).*

Proof. For the case when $\beta = \beta_\lambda$, $\tau(\beta_\lambda, \lambda) < \infty$ since all level curves of u have finite length (due to compactness).

Now take an arbitrary $\beta \in \Theta_\lambda$ with $\beta \neq \beta_\lambda$. We consider u along the corresponding solution

$t \mapsto (x(t,\lambda,\beta), y(t,\lambda,\beta), \theta(t,\lambda,\beta))$ of (3.5). By Proposition 1 part (ii) we know that

$$\frac{d}{dt}u(x(t,\lambda,\beta), y(t,\lambda,\beta)) \neq 0.$$

Without loss of generality let us consider the case

$$\frac{d}{dt}u(x(t,\lambda,\beta), y(t,\lambda,\beta)) > 0, \quad 0 \leq t < \tau(\lambda,\beta),$$

and reason by contradiction: assume $\tau(\lambda,\beta) = \infty$.

Since the level sets of u describe general coordinates in $\overline{\Omega}$, with a bounded Jacobian away from zero and infinity, we may assume that level curves of u are straight lines parallel to the x-axis. (For example, the change of coordinates $[0, t(\lambda)] \times [\lambda_-, \lambda_+] \mapsto (x, y) \in \Omega$ defined by solutions of the problem

$$\begin{cases} \dot{x}(t,\lambda) = -u_y(x,y)/|\nabla u(x,y)| \\ \dot{y}(t,\lambda) = u_x(x,y)/|\nabla u(x,y)| \\ (x(0,\lambda), y(0,\lambda)) = \varphi(\lambda) \end{cases}$$

gives a desired diffeomorphism.) In this new coordinates we have $\dot{y}(t) > 0$ for $t \geq 0$. Since $\{(t, y(t)) : 0 \leq t < \tau(\lambda,\beta) = \infty\}$ lies in the compact set $\overline{\Omega}$ with y increasing in t, the limit

$$\lim_{t\to\infty} y(t) =: L \text{ exists.}$$

Then for every $\epsilon > 0$ there is an M_ϵ, such that for all $t > M_\epsilon$

$$|L - y(t)| < \epsilon.$$

Let $K > \max_{\overline{\Omega}} |\nabla \ln a|$, then

$$|\ddot{y}(t)| = |\sin\theta(t)||\dot{\theta}(t)| < K.$$

Consequently, by Lemma 3.2.2 we have that

$$\dot{y}^2(t) < 2K\epsilon, \quad \forall t > M_\epsilon.$$

By choosing $\epsilon < \frac{1}{4K}$ and the arclength parametrization of this curve ($\dot{x}^2 + \dot{y}^2 = 1$) gives the inequality

$$\dot{x}^2(t) > \frac{1}{2}$$

for every $t > M_{\frac{1}{4K}}$. From the Mean Value Theorem one can show that $x(t)$ increases unboundedly thus contradicting the boundedness of Ω. This proves that $\tau(\lambda, \beta)$ must be finite.

□

Theorem 3.2.4. *Assume that Ω is convex. Then the map $\beta \mapsto \tau(\lambda, \beta)$ is continuous at β_λ.*

Proof. For simplicity, we assume first that $\overline{\Omega}$ is a rectangle, say $[0, x_0] \times [0, y_0]$, in the coordinates described by the level sets of u. Or, equivalently, that the level curves of u are parallel to the x-axis. Extend the function a to the open set Ω' such that $\overline{\Omega} \subset \Omega'$, $a \in C^{1,1}(\Omega')$, and the solutions of (3.5) are defined in Ω'. Let $\epsilon > 0$ be given and let $h > 0$ be small enough and, without loss of generality, assume that $\delta := \tau(\lambda, \beta_\lambda + h) - \tau(\lambda, \beta_\lambda) > 0$ (the case when $\delta < 0$ follows similarly). By the stability with respect to t of solutions of initial value problems we have that

$$\|(x(t, \lambda, \beta_\lambda + h), y(t, \lambda, \beta_\lambda + h)) - (x(t, \lambda, \beta_\lambda), y(t, \lambda, \beta_\lambda))\|_{C^1([0, \tau(\lambda, \beta_\lambda)])} < \epsilon. \tag{3.10}$$

We will show that as $\epsilon \to 0$, then

$$\tau(\lambda, \beta_\lambda + h) - \tau(\lambda, \beta_\lambda) \to 0.$$

Observe that

$$\begin{aligned} |(x(0, \lambda, \beta_\lambda + h), y(0, \lambda, \beta_\lambda + h), \theta(0, \lambda, \beta_\lambda + h)) - \\ (x(0, \lambda, \beta_\lambda), y(0, \lambda, \beta_\lambda), \theta(0, \lambda, \beta_\lambda))| \quad < h. \end{aligned}$$

Since $t \mapsto x(t, \lambda, \beta_\lambda + h)$ is twice continuously differentiable, then

$$\begin{aligned} & x(\tau(\lambda, \beta_\lambda + h), \lambda, \beta_\lambda + h) > \\ & x(\tau(\lambda, \beta_\lambda), \lambda, \beta_\lambda + h) + \delta \dot{x}(\tau(\lambda, \beta_\lambda), \lambda, \beta_\lambda + h) - \frac{\delta^2}{2} K, \end{aligned}$$

where $K > \max |\ddot{x}(t, \lambda, \beta)|$. Using the latter inequality and the inequality in (3.10) we get

$$\begin{aligned} & x(\tau(\lambda, \beta_\lambda + h), \lambda, \beta_\lambda + h) > \\ & x(\tau(\lambda, \beta_\lambda), \lambda, \beta_\lambda) - \epsilon + \delta[\dot{x}(\tau(\lambda, \beta_\lambda), \lambda, \beta_\lambda) - \epsilon] - \frac{\delta^2}{2} K \\ & = x_0 - \epsilon + \delta[\dot{x}(\tau(\lambda, \beta_\lambda), \lambda, \beta_\lambda) - \epsilon] - \frac{\delta^2}{2} K. \end{aligned}$$

Since, $x_0 = x(\tau(\lambda, \beta_\lambda + h), \lambda, \beta_\lambda + h)$ and $\dot{x}(\tau(\lambda, \beta_\lambda), \lambda, \beta_\lambda) > 0$, then

$$0 > -\epsilon + \delta[\dot{x}(\tau(\lambda, \beta_\lambda), \lambda, \beta_\lambda) - \epsilon] - \frac{\delta^2}{2} K$$

and

$$\begin{aligned}\delta &< \frac{1}{K}\left[\dot{x}(\tau(\lambda,\beta_\lambda),\lambda,\beta_\lambda) - \epsilon - \sqrt{[\dot{x}(\tau(\lambda,\beta_\lambda),\lambda,\beta_\lambda) - \epsilon]^2 - 2\epsilon K}\right] \\ &= \frac{2\epsilon}{\dot{x}(\tau(\lambda,\beta_\lambda),\lambda,\beta_\lambda) - \epsilon + \sqrt{[\dot{x}(\tau(\lambda,\beta_\lambda),\lambda,\beta_\lambda) - \epsilon]^2 - 2\epsilon K}} \\ &< \frac{2\epsilon}{\dot{x}(\tau(\lambda,\beta_\lambda),\lambda,\beta_\lambda) - \epsilon}.\end{aligned}$$

Thus continuity follows, since, if $\epsilon \to 0$ then, $\tau(\lambda, \beta_\lambda + h) - \tau(\lambda, \beta_\lambda) \to 0$.

□

The continuity of $\tau(\lambda, \beta)$ at β_λ yields the following.

Corollary 3.2.5. *Under the hypotheses of Theorem above, for each $\lambda \in (\lambda_-, \lambda_+)$ consider the map $F_\lambda : \Theta_\lambda \mapsto \mathbb{R}$ defined by*

$$F_\lambda(\beta) := u\left(x(\tau(\lambda,\beta),\lambda,\beta), y(\tau(\lambda,\beta),\lambda,\beta)\right) - \lambda, \tag{3.11}$$

where $(x(\tau(\lambda,\beta),\lambda,\beta), y(\tau(\lambda,\beta),\lambda,\beta)$ is the corresponding solution of (3.5), and Θ_λ is as in (3.4). Then $\beta \mapsto F_\lambda(\beta)$ is a continuous at β_λ.

The algorithm and its convergence rely on the following properties of F.

Proposition 3.2.6. *(i)$F_\lambda(\beta) = 0$ if and only if $\beta = \beta_\lambda$.*

(ii) There exist α and β such that

$$F_\lambda(\alpha) < 0 < F_\lambda(\beta).$$

Proof. First we prove statement (i). Let $\beta \in \Theta_\lambda$ such that

$$F_\lambda(\beta) = 0.$$

Thus, $\lambda = u(x(\tau(s,\beta),s,\beta), y(\tau(s,\beta),s,\beta))$. By Rolle's Theorem $\exists t^* \in (0, \tau(\lambda,\beta))$ such that

$$\frac{d}{dt} u(x(t^*,\lambda,\beta), y(t^*,\lambda,\beta)) = 0.$$

Consequently,

$$\theta(t^*,\lambda,\beta) = \text{Arg}\left\{ \frac{\nabla u}{|\nabla u|}(x(t^*,\lambda,\beta), y(t^*,\lambda,\beta)) \right\}.$$

Therefore, by Proposition 3.2.1 $(x(t,\lambda,\beta), y(t,\lambda,\beta))$ is a level curve and

$$\beta = \beta_\lambda.$$

The converse follows directly from Proposition 3.2.1.

The proof of (ii) is as follows. Let $\alpha, \beta \in \Theta_\lambda$ such that

$$\alpha < \beta_\lambda < \beta. \tag{3.12}$$

Without loss of generality assume that $F_\lambda(\alpha)$, and $F_\lambda(\beta)$ are both negative. Since $|\nabla u| > 0$, the level set $u = \lambda$ splits the domain Ω into two disjoint sets respectively the sub/super level sets. From (3.12) we have, at least for small time $0 < t < \epsilon$, that the curves $(x(t,\lambda,\alpha), y(t,\lambda,\alpha))$ and $(x(t,\lambda,\beta), y(t,\lambda,\beta))$ belong to different partitions. Since $F_\lambda(\alpha)$ and $F_\lambda(\beta)$ have the same sign, the endpoint of the curves belong to the same partition. In particular one of them must have crossed (the divider) the λ-level set of u in $\overline{\Omega}$. Let's say $(x(t,\lambda,\beta), y(t,\lambda,\beta))$ intersects the level curve at $t = t_1$. By the same argument of the proof of statement (i) in this Proposition, there is a $t^* \in (0, t_1)$

such that

$$\frac{d}{dt}u(x(t^*,\lambda,\beta),y(t^*,\lambda,\beta))=0.$$

The latter implies that the curve $(x(t,\lambda,\beta),y(t,\lambda,\beta))$ is a level curve which is a contradiction, since

$$\beta>\beta_\lambda.$$

□

The following algorithm recovers the λ-level set of u, for $\lambda\in(\lambda_-,\lambda_+)$ fixed.

Algorithm: We will recursively define the following sequences. Let $\alpha_1<\alpha_1'\in\Theta_\lambda$ be the angles given by proposition 3.2.6 such that

$$F_\lambda(\alpha_1)<0<F_\lambda(\alpha_1'). \tag{3.13}$$

Consider, for the natural number n, the bisector angle

$$\gamma_n=\frac{\alpha_n+\alpha_n'}{2}.$$

For each member of the sequences (α_n) and (α_n'),

- if $F_\lambda(\gamma_n)\leq 0$, let $\alpha_{n+1}=\gamma_n$ and $\alpha_{n+1}'=\alpha_n'$, or
- if $F_\lambda(\gamma_n)>0$, let $\alpha_{n+1}'=\gamma_n$ and $\alpha_{n+1}=\alpha_n$.

Note the ordering

$$\alpha_1\leq\alpha_n\leq\alpha_{n+1}<\alpha_{n+1}'\leq\alpha_n'\leq\alpha_1'$$

and

$$\alpha'_{n+1} - \alpha_{n+1} = \frac{\alpha'_n - \alpha_n}{2}. \tag{3.14}$$

Consequently,

$$\alpha'_{n+1} - \alpha_{n+1} = \frac{\alpha'_1 - \alpha_1}{2^n}.$$

Therefore, the sequences (α_n) and (α'_n) both converge to the same angle γ. The continuity of F_λ at β_λ and the inequality in (3.13) imply that

$$F_\lambda(\alpha_n) \to F_\lambda(\gamma) = 0 \quad \text{and} \quad F_\lambda(\alpha'_n) \to F_\lambda(\gamma) = 0,$$

and by Proposition 3.2.6

$$\gamma = \beta_\lambda.$$

Proposition 3.2.1 guarantees that the curve $(x(t, \lambda, \gamma), y(t, \lambda, \gamma))$ is the level curve of u corresponding to $u = \lambda$.

Note that it is the modulus of continuity of F which determines the rate of convergence of our algorithm.

3.3 On The Stability of The Method

In this section we discuss a conditional stability result.

An additional differentiation in the first two equations of (3.5) and substitution into the third equation, enables us to eliminate θ. Our method, in fact, solves the family of two point boundary value

problems

$$\begin{cases} \ddot{x} = \dot{y}\left[(\ln a)_x \dot{y} - (\ln a)_y \dot{x}\right] \\ \ddot{y} = -\dot{x}\left[(\ln a)_x \dot{y} - (\ln a)_y \dot{x}\right] \\ (x(0), y(0)) = \varphi(\lambda), \\ (x(L), y(L)) = (x(\tau(\lambda,\beta),\lambda,\beta), y(\tau(\lambda,\beta),\lambda,\beta)). \end{cases} \tag{3.15}$$

In general, a two point boundary value problem may have no solutions, unique solution or infinitely many solutions. However, sufficient conditions for existence, uniqueness and continuous dependence on the data have been long known, see e.g. [20]. In what follows we do not revisit the stability issue of the two point boundary value problem but rather assume that our system (3.15) obeys some sufficient conditions (one such example can be obtained by the reduction of (3.15) to a Fredholm integral system of second type) that yield:

Hypothesis 3.3.1. *For every $\epsilon > 0$ there is a $\delta > 0$ such that if*

$$\|\tilde{a} - a\|_{C^{1,1}(\overline{\Omega})} < \delta \text{ and } \|\tilde{f} - f\|_{C^0(\Gamma)} < \delta,$$

then

$$\max_{t\in[0,L]} (|x(t) - \tilde{x}(t)| + |y(t) - \tilde{y}(t)|) < \epsilon.$$

Let us consider the class $\mathscr{C}$ of pairs $(a, f) \in C^{1,1}(\overline{\Omega}) \times C^1(\Gamma)$, for which the problem (3.1) has a regular solution satisfying Hypotheses 3.1.1 and 3.3.1. Within the class $\mathscr{C}$, our method is conditionally stable in the following sense:

Proposition 3.3.1 (Conditional Stability)**.** *For every $\epsilon > 0$ there is a $\delta > 0$ such that if $(a, f), (\tilde{a}, \tilde{f}) \in \mathscr{C}$ with*

$$\|\tilde{a} - a\|_{C^{1,1}(\overline{\Omega})} < \delta \text{ and } \|\tilde{f} - f\|_{C^0(\Gamma)} < \delta,$$

then

$$\|u - \tilde{u}\|_{C^0(\overline{\Omega})} < \epsilon.$$

Proof. Let $P \in \overline{\Omega}$. Consider the following curves:

- the level curve $[0, L] \ni t \mapsto (x(t), y(t))$ corresponding to $u(P)$, and
- the level curve $[0, L] \ni t \mapsto (x^*(t), y^*(t))$ of $\tilde{u}$ with $(x(0), y(0)) = (x^*(0), y^*(0))$.

For $\epsilon > 0$ and P given, let $P^* \in \{(x^*(t), y^*(t)) : t \in [0, L]\}$ be the closest point to P. From Hypothesis 3.3.1 there is a $0 < \delta < \epsilon/2$ small enough with the property: if

$$\|\tilde{a} - a\|_{C^{1,1}(\overline{\Omega})} < \delta \text{ and } \|\tilde{f} - f\|_{C^0(\Gamma)} < \delta,$$

then

$$\sup_{t\in[0,L]} \sqrt{|x(t) - x^*(t)|^2 + |y(t) - y^*(t)|^2} < \frac{\epsilon}{2L_{\tilde{u}}},$$

where $L_{\tilde{u}}$ is the $\max_{\overline{\Omega}} |\nabla \tilde{u}|$. Consequently, dist$(P, P^*) < \frac{\epsilon}{2L_{\tilde{u}}}$. We estimate

$$\begin{aligned} |u(P) - \tilde{u}(P)| &= |f(x(0), y(0)) - \tilde{u}(P)| \\ &\leq |\tilde{f}(x(0), y(0)) - \tilde{u}(P)| + |f(x(0), y(0)) - \tilde{f}(x(0), y(0))| \\ &\leq \delta + |\tilde{u}(P^*) - \tilde{u}(P)| < \frac{\epsilon}{2} + L_{\tilde{u}}\text{dist}(P^*, P) < \epsilon. \end{aligned}$$

Since P were arbitrary in $\overline{\Omega}$, then

$$\|u - \tilde{u}\|_{C^0(\overline{\Omega})} < \epsilon.$$

□

3.4 Numerical Results

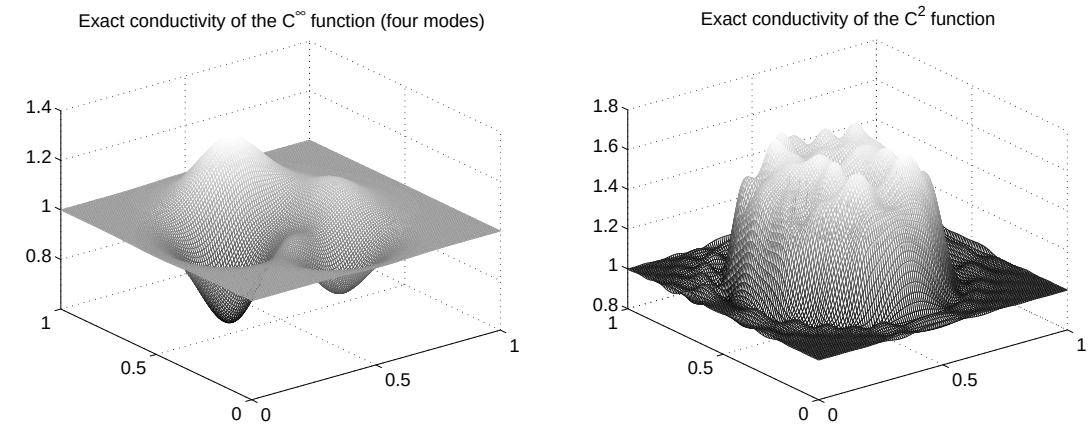

Figure 3.1: The original conductivity distribution maps: the four modes (left) and the cross section of a C^2 approximation of a human brain (right).

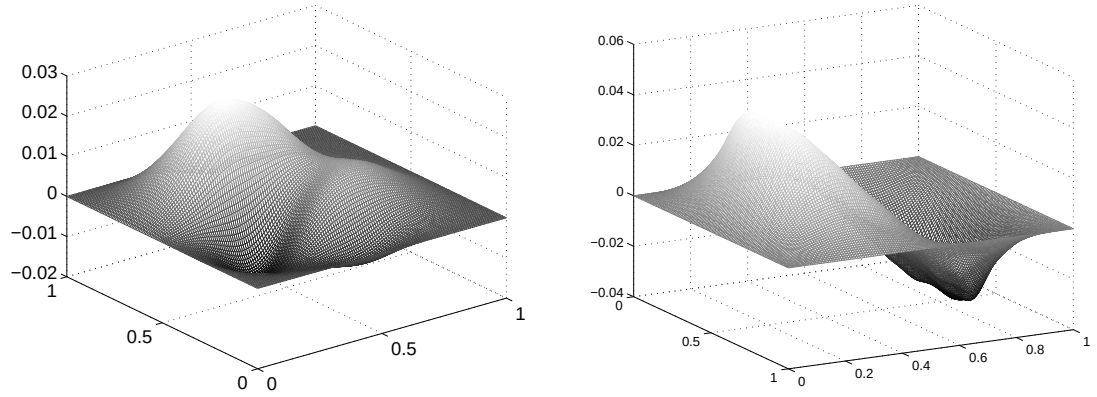

Figure 3.2: The figure illustrates $u(x, y) - y$, where $u(x, y)$ is the solution of (3.16) subject to $f(x, y) = y$ and the conductivities: the C^∞ function (left) and the C^2 function (right).

In this section we present two numerical reconstructions of some conductivities based on the algorithm above. Figure 3.1 illustrates the two conductivities which are to be reconstructed from the

data. Also, figure 3.2 shows the difference of the calculated solution of the conductivity equation

$$\nabla \cdot \sigma \nabla u = 0, \quad u|_{\partial\Omega} = f. \tag{3.16}$$

(for each conductivity) and the harmonic function with the same boundary data.

3.4.1 Data

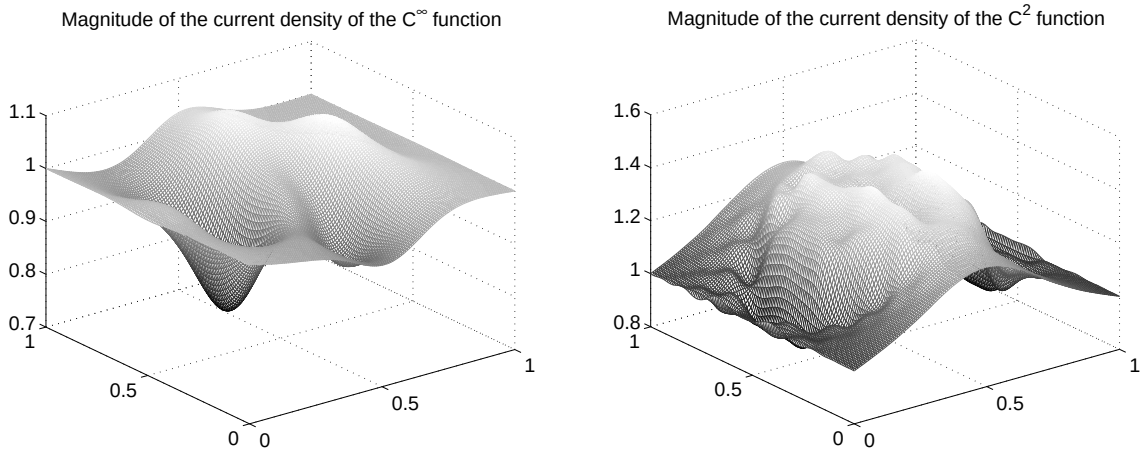

Figure 3.3: Magnitude of the current density of the C^∞ (four modes) (left) and the C^2 function (right) generated over the box $[0,1] \times [0,1]$.

The magnitude of the current density, a, for the numerical experiments is obtained numerically. We solve the Dirichlet problem (3.16) for two different conductivities by using the finite element method in MATLAB's PDE toolbox. The domain Ω is the unit box $[0,1] \times [0,1]$, and the boundary voltage $f(x,y) = y$ is applied at the boundary. The first conductivity map is smoothly defined by the C^∞ (four modes) function described in section 2.3.1 of chapter 2, see the left image in Figure 3.1. The second conductivity is a least square approximation of C^2 B-splines of a piecewise-smooth function given by a CT image of a cross-section of a human brain. This level of smoothness

is needed to meet the theory requirements. The approximating function has the form

$$\sigma(x,y) = \sum_{i=1}^{22}\sum_{j=1}^{18} \alpha_{ij} B(x-x_j)B(y-y_i),$$

and it is shown in Figure 3.1 on the right.

The gradient of the potential ∇u is computed via finite difference. The interior data $a = \sigma|\nabla u|$ is computed in $[0,1] \times [0,1]$, see figure below.

3.4.2 Finding β_λ

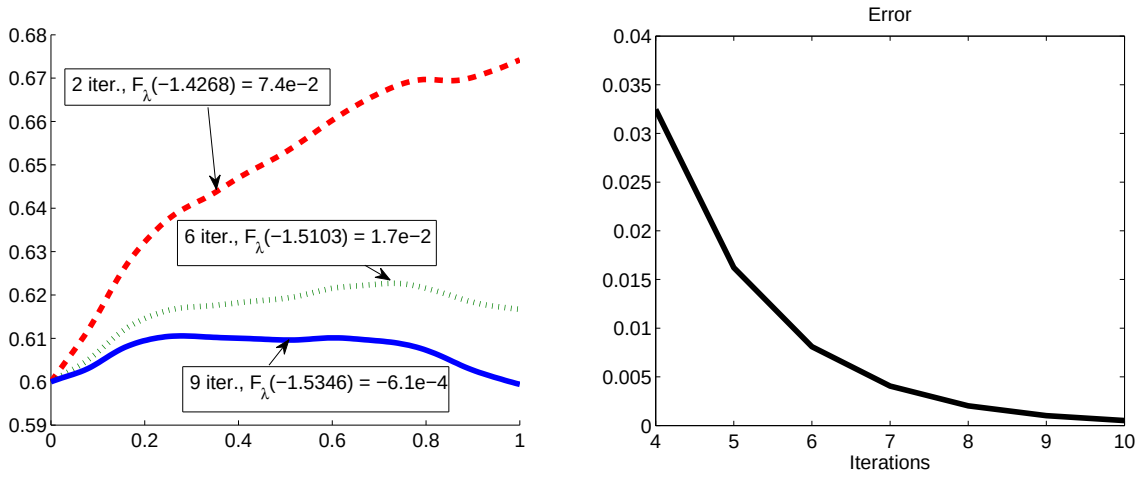

Figure 3.4: The plots in the left box show a few iterations in finding the level curve passing through $(x_1, y_1) = (0, 0.6)$.

The algorithm in section 3.2 finds the root β_λ of the function $F_\lambda(\beta)$ in (3.11), which together with $(x(0,\lambda,\beta_\lambda), y(0,\lambda,\beta_\lambda))$ give the initial condition of a level curve of u which solves (3.5). To find β_λ numerically, we use the boundary points which are joined by the level curve of u corresponding to λ, say (x_1, y_1) and (x_2, y_2). Note that the boundary data is almost-two-to-one and these points are the unique points such that $f(x_1, y_1) = f(x_2, y_2)$.

The method shown here is similar to a bi-section searching algorithm. The novelty is the criterion which ensures convergence. The iterative process is as follows. Assume that $x_1 = 0$ and $y_1 \in (0, 1)$. To initialize the process we solve (3.5) twice: once subject to (x_1, y_1, α_0) and next subject to (x_1, y_1, α_0'), where $\alpha_0, \alpha_0' \in (-\pi, 0)$ are initial guesses such that

$$F_\lambda(\alpha_0) < 0 < F_\lambda(\alpha_0').$$

The next angle is $\gamma_0 = \frac{\alpha_0 + \alpha_0'}{2}$. Solve (3.5) subject to (x_1, y_1, γ_0). If $F_\lambda(\gamma_0) < 0$, then let the next angles $\alpha_1 = \gamma_0$ and $\alpha_1' = \alpha_0'$. Otherwise, let $\alpha_1 = \alpha_0$ and $\alpha_1' = \gamma_0$. Assign the new angle, $\gamma_1 = \frac{\alpha_1 + \alpha_1'}{2}$. Solve (3.5) subject to (x_1, y_1, γ_1). Repeat this scheme n number of times, so that

$$|\beta_\lambda - \gamma_n| < |\alpha_0 - \alpha_0'| \frac{1}{2^n}.$$

The plots in figure 3.4 show a numerical example of the convergence rate of this method for the voltage potential generated with the $\sigma \in C^2$ example.

We can also use the continuity (for $\delta > 0$ small enough, β_λ is close to $\beta_{\lambda+\delta}$) to expedite the convergence rate of the method when from level to level set by using the already calculated values.

In Figure 3.4 the reconstructed level curve passing through $(x_1, y_1) = (0, 0.6)$, which corresponds to the voltage potential generated in brain experiment $\sigma \in C^2$. The initial angles are $\alpha_0 = -\frac{2\pi}{3}$ and $\beta_0 = -\frac{\pi}{10}$. The box on the right shows a plot of the error versus the number of iterations. The error shown is a discrete version of

$$\|(x(t, \lambda, \gamma_i), y(t, \lambda, \gamma_i), \theta(t, \lambda, \gamma_i)) - (x(t, \lambda, \gamma_{i-1}), y(t, \lambda, \gamma_{i-1}), \theta(t, \lambda, \gamma_{i-1}))\|_\infty.$$

The calculated error at the 11-th iteration is $2.5 \cdot 10^{-4}$.

3.4.3 Numerical Experiments

The numerical examples below consider two instances of the 1-Laplacian coming from the inverse conductivity problem with the data described in 3.4.1.

Given the function a in a unit box $[0,1] \times [0,1]$, we solve (3.5) using the adaptive Runge-Kutta-Fehlberg ODE solver for m characteristics subject to the initial conditions of the corresponding level curves of u, the voltage potential, found using the bi-section method in section 3.4.2,

$$x_j(0) = 0, y_j(0) = s_j, \theta_j(0) = \beta_{s_j}, \tag{3.17}$$

where $s_j = \frac{j}{m-1}$, and $j = 0, 2, \ldots, m-1$. Since $f(x,y) = y$, then $\beta_{s_0} = \beta_{s_{m-1}} = -\frac{\pi}{2}$.

The third equation in (3.5) contains the derivative of a in the direction of the unit vector $\eta = \langle \cos\theta, \sin\theta \rangle$:

$$\dot{\theta} = -\partial_\eta \ln a.$$

In order to decrease the error made in differentiating $\ln a$ we use the center difference for the directional derivative:

$$\partial_\eta \ln a(x_j(t_{j_k}), y_j(t_{j_k})) = \frac{1}{2h}\left[\ln a(x_{j+h}^{j_k}, y_{j+h}^{j_k}) - \ln a(x_{j-h}^{j_k}, y_{j-h}^{j_k})\right],$$

where

$$\begin{aligned} x_{j+h}^{j_k} &= x_j(t_{j_k}) + h \cdot \cos\theta_j(t_{j_k}), \\ x_{j-h}^{j_k} &= x_j(t_{j_k}) - h \cdot \cos\theta_j(t_{j_k}), \\ y_{j+h}^{j_k} &= y_j(t_{j_k}) + h \cdot \sin\theta_j(t_{j_k}), \\ y_{j-h}^{j_k} &= y_j(t_{j_k}) - h \cdot \sin\theta_j(t_{j_k}). \end{aligned}$$

In all the numerical experiments the value of $\ln a$ (or a) at a point is interpolated by the bi-quintic piecewise Lagrange polynomials for points away from the boundary, and the bi-cubic or bi-linear interpolation for points near the boundary.

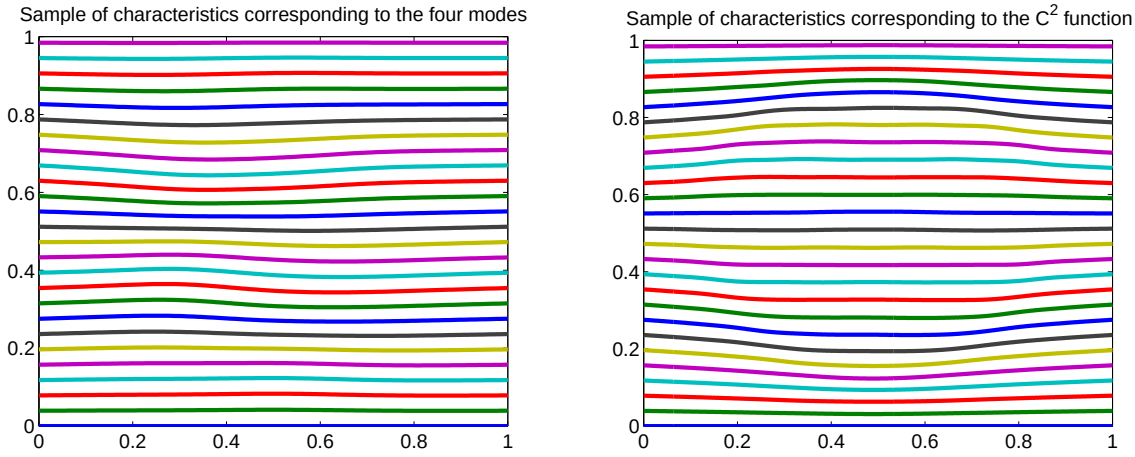

Figure 3.5: The top images show a sample of the characteristics (level curves) of the voltage potential generated by the four modes (left) and the C^2 function (right) reconstructed from the interior data, a, measured in $[0,1] \times [0,1]$.

The characteristics are equipotential lines. The value of the potential along each characteristic is determined by the voltage potential at the boundary. Let

$$\Lambda_j(t) = (x_j(t), y_j(t)),\ j \in \{0, 1, \ldots, m-1\}, t \in [0, \tau_j], \tag{3.18}$$

denote the equipotential line, which solves (3.5) subject to (3.17), and

$$\zeta_i(\xi) = (\hat{x}_i(\xi), \hat{y}_i(\xi)), \xi \in [0, \alpha_i],\ i \in \{0, 1, \ldots, n-1\}, \tag{3.19}$$

denote a smooth non-characteristic curve, which is transversal to each $\Lambda_j, j = 0, 1, \ldots, m-1$. At

the point of intersection we have

$$\begin{cases} 0 = u_x \dot{x_j} + u_y \dot{y_j}, \\ u_\xi = u_x \frac{d\hat{x}_i}{d\xi} + u_y \frac{d\hat{y}_i}{d\xi}, \end{cases} \tag{3.20}$$

and

$$\nabla u = \frac{u_\xi}{\dot{y_j} \frac{d\hat{x}_i}{d\xi} - \dot{x_j} \frac{d\hat{y}_i}{d\xi}} \langle \dot{y_j}, -\dot{x_j} \rangle . \tag{3.21}$$

The non-characteristic curves of (3.19) are obtained by one dimensional interpolation in between points lying on different characteristics. The derivative u_ξ at the node where Λ_j intersects ζ_i, is computed via the Lagrange polynomial interpolation along ζ_i.

In the particular case in which the characteristic curves are graphs, say $|\dot{x_j}| > 0$, $j = 0, 1, \ldots, m-1$, the conductivity is computed on a grid. The first component of each characteristic is regarded as the independent variable x and the second component can be expressed as a function $y_j = \phi_j(x)$, $j = 0, 1, \ldots, m-1$. Thus, by letting $x^k = \frac{k}{n-1}, k = 0, 1, \ldots, n-1$ we approximate the values of $y_j^k = \phi_j(x^k), j = 0, 1, \ldots, m-1, k = 0, 1, \ldots, n-1$ via fifth degree piecewise Lagrange polynomials. Note that for a fixed j, u is constant along the points (x^k, y_j^k), $k = 0, 1, \ldots, n-1$. Then there is a function ψ such that $u_k = \psi(y; x_k)$, for $k = 0, 1, \ldots, n-1$, whose values are known at (x^k, y_j^k). Now, by letting $y^l = \frac{l}{p-1}, l = 0, 1, \ldots, p-1$ we approximate the values $u_k^l = \psi(y^l; x^k)$ via fifth degree piecewise Lagrange polynomials. Therefore, u is approximated on the p by n rectangular grid (x^k, y^l), where $k = 0, 1, \ldots, n-1$, and $l = 0, 1, \ldots, p-1$.

We reconstruct the voltage potential for each conductivity with Gaussian noise added to the data, the magnitude of the current density. In figure 3.6 we show the reconstruction of the difference of the voltage potential and the harmonic solution for the noiseless data. The L_1 relative errors for the reconstructed voltage potentials from noiseless data corresponding to the C^∞ function is 1.2691×10^{-5}, and the C^2 function is 1.4798×10^{-4}. In figure 3.7 we plot the error of the voltage

potential reconstructions from data with various degrees of Gaussian noise.

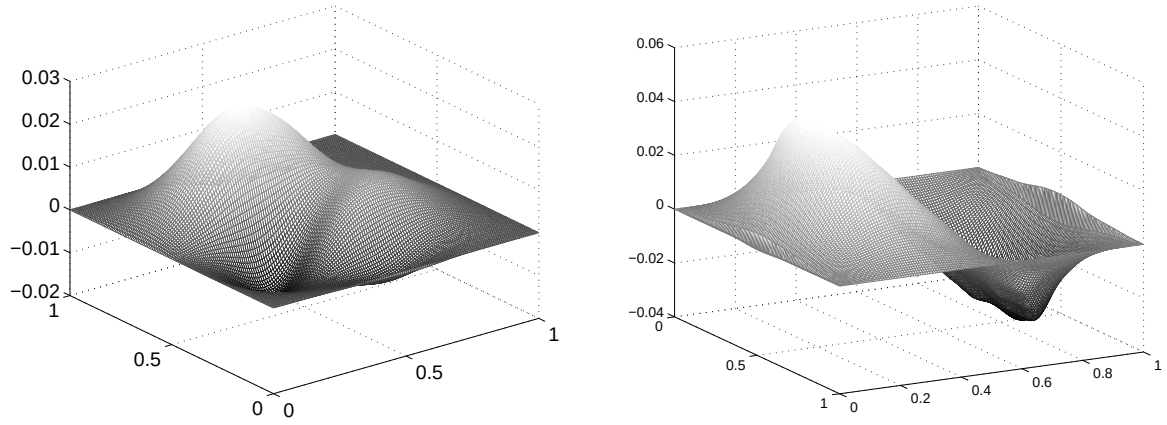

Figure 3.6: The images show the reconstruction of the difference $u(x, y) - y$ for each conductivity from noiseless data: C^∞ function (left) and C^2 function (right).

One recovers the conductivity on the characteristics of u. The gradient of the voltage potential is computed using (3.21). In the specific case in which the equipotential curves are graphs, the conductivity is computed on the rectangular grid from step 2, $(x^k, y^l), k = 0, 1, 2, \ldots, n-1, l = 0, 1, 2, \ldots, p-1$, using the formula

$$\sigma(x^k, y^l) = \frac{a(x^k, y^l)}{|\nabla u|(x^k, y^l)}.$$

The gradient of the voltage potential of the reconstruction of the conductivities shown in figure 3.8 were computed via fintie differences.

3.4.4 Remarks of The Numerical Stability and Applications to Noise Data

Sharp elliptic regularity estimates of Agmon-Douglas-Nirenberg [1] show that we cannot expect stability estimates in the same order of regularity for the 1-Laplacian, due to the degeneracy in

ellipticity. Our Proposition 3.3.1, even in the case of exact boundary data, show a loss of two derivatives in the error estimates of the solution versus the interior data. The numerical experiments below, see Figure 3.7, show better numerical stability behaviour, equivalent to the loss of one derivative in the solution u. In the case of interior data $|\tilde{J}|$ occurring as the magnitude of the current density field of some sufficiently small perturbation in conductivity (in the sense that $\|\sigma - \tilde{\sigma}\|_{C^2(\overline{\Omega})} < \epsilon$ for some small ϵ,) this numerical behavior can be explained using the local stability result in [34]. However, for perturbation in the interior data $|\tilde{J}|$ that are due to measurement errors, (and not coming from a perturbed conductivity), their arguments do not cover the conditional stability in proposition 3.3.1.

3.5 Conclusions

We presented a globally convergent algorithm which solves the Dirichlet problem for the 1-Laplacian in two dimensions by recovering the regular solution (assumed to exist) level set by level set. Such a problem occurs in the inverse hybrid problem of recovering the electrical conductivity of a body when the magnitude of the current density field, obtained by maintaining a fix boundary voltage, is given inside.

The method requires the interior coefficient be of Lipschitz gradient and does not work (in theory) for rougher data. Due to the degeneracy in ellipticity a loss of derivatives in the stability estimates are expected. We show a conditional stability result which estimates the continuous norm of the error in solution with the $C^{1,1}$-norm of error in the data.

Feasibility of the method is numerically illustrated on two examples coming from a hybrid problem in conductivity imaging.

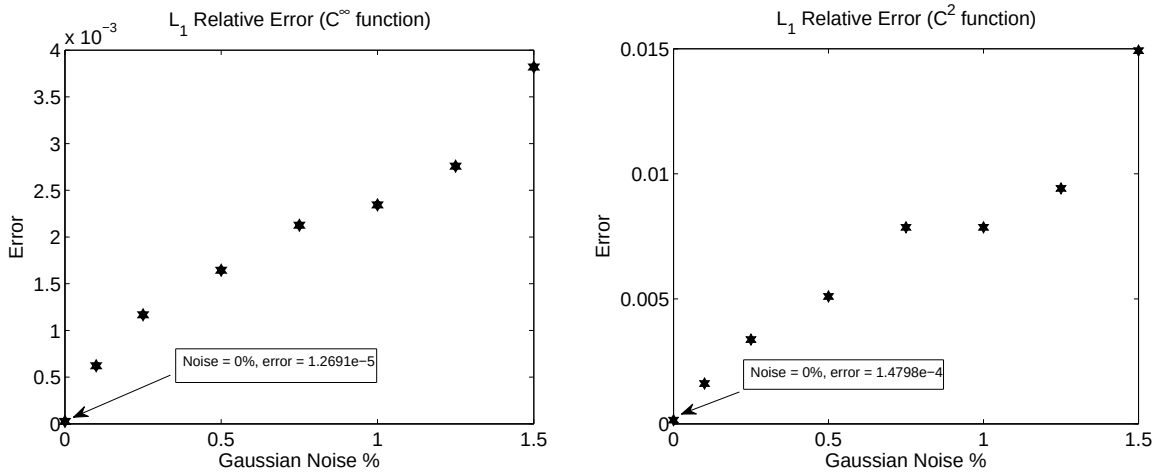

Figure 3.7: L_1 relative error of the voltage potential reconstructed from noisy data for each corresponding conductivity.

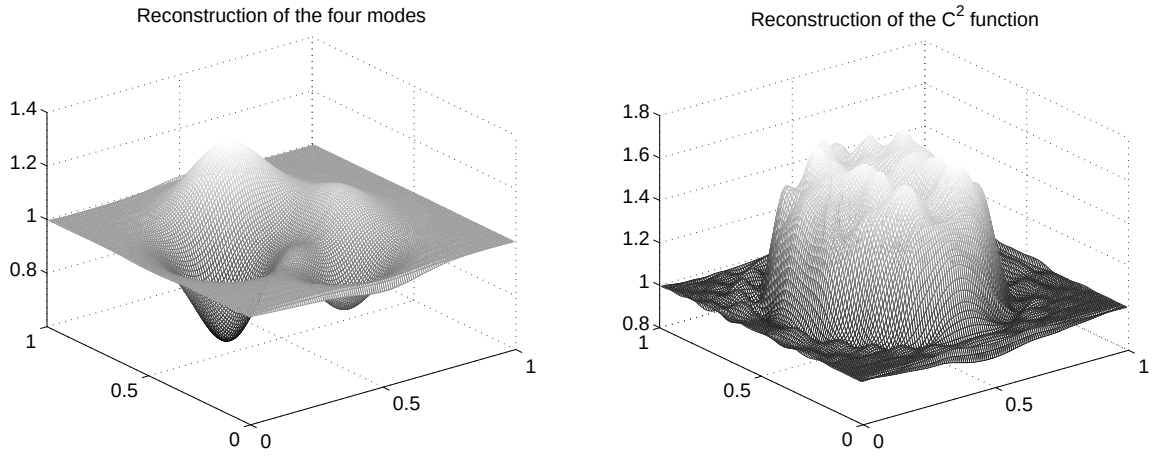

Figure 3.8: The images show the reconstruction of the four modes (left) and the C^2 function (right) reconstructed from the interior data measured in $[0,1] \times [0,1]$. The L_1 relative error for the reconstruction of the four modes and the C^2 function are 0.105% and 0.522%, respectively.

CHAPTER 4: CONDUCTIVITY IMAGING VIA THE COMPLETE ELECTRODE MODEL FOR THE 1-LAPLACIAN

4.1 Introduction

We consider the hybrid inverse problem of reconstructing an isotropic electrical conductivity σ in a connected domain $\Omega \subset \mathbb{R}^d$ from the interior knowledge of the magnitude $|J|$ of the current density generated by one injected current.

Novel from existing works we start from the forward problem of the Complete Electrode Model (CEM) originally introduced in [51] to describe best the physical experiment: Let $e_k \subset \partial\Omega$ denote the surface electrode of impedance z_k through which one injects a net current I_k, $k = 0, ..., N$. The CEM assumes the voltage potential u inside and the constant voltages U_k's on the electrodes distribute according to the boundary value problem

$$\nabla \cdot \sigma \nabla u = 0, \quad \text{in } \Omega, \tag{4.1}$$

$$u + z_l \sigma \frac{\partial u}{\partial \nu} = U_k \quad \text{on } e_k, \quad \text{for } k = 0, ..., N, \tag{4.2}$$

$$\int_{e_k} \sigma \frac{\partial u}{\partial \nu} ds = I_k, \quad \text{for } k = 0, ..., N, \tag{4.3}$$

$$\frac{\partial u}{\partial \nu} = 0, \quad \text{on } \partial\Omega \setminus \bigcup_{k=0}^{N} e_k, \tag{4.4}$$

where ν is the outer unit normal.

If a solution were to exist, an integration of (4.1) over Ω together with (4.3) and (4.4) show that

$$\sum_{k=0}^{N} I_k = 0 \tag{4.5}$$

is necessary. Physically, the zero sum injected current accounts for the absence of sources/sinks of charges.

The constants U_k appearing in (4.2) represent *unknown* voltages on the surface of the electrodes, and the difference from the traces $u|_{e_k}$ of the interior voltage potential governs the flux of the current through the electrode. For conductivities of real part bounded away from zero and infinity, the problem has a unique solution $(u; \langle U_0, ..., U_N \rangle) \in H^1(\Omega) \times \mathbb{C}^{N+1}$ up to an additive constant, as shown in [51].

We assume throughout a real valued coefficient satisfying

$$\epsilon \leq \sigma \leq \epsilon^{-1}, \quad \text{a.e. in } \Omega, \tag{4.6}$$

for some $\epsilon > 0$. Following from (4.6), the set of singular points (where the gradient vanishes) of u coincides with the zeros of J, and

$$\sigma = \frac{|J|}{|\nabla u|}, \tag{4.7}$$

outside the singular set.

In our approach we assume (real valued) positive impedances

$$z_k > 0, \quad k = 0, ..., N. \tag{4.8}$$

Substitution of (4.7) with a replacing $|J|$ into the complete electrode model yields a voltage potential u which satisfies the following boundary value problem for the 1-Laplacian

$$\nabla \cdot a \frac{\nabla u}{|\nabla u|} = 0, \quad \text{in } \Omega, \tag{4.9}$$

subject to

$$u + z_k a\nu \cdot \frac{\nabla u}{|\nabla u|} = U_k, \quad \text{on } e_k, \tag{4.10}$$

$$\int_{e_k} a\nu \cdot \frac{\nabla u}{|\nabla u|} ds = I_k, \quad \text{for } k = 1, ..., N, \tag{4.11}$$

$$\nu \cdot \nabla u = 0, \quad \text{on } \partial\Omega \setminus \bigcup_{k=0}^{N} e_k, \tag{4.12}$$

where ν denotes the unit outer normal at the boundary, and the currents I_k's satisfy (4.5). We refer to the problem (4.9,4.10,4.11, 4.12) and (4.5) as the complete electrode model (CEM) for the 1-Laplacian.

In this chapter we are concerned with finding the electrical conductivity σ given $|J|$ in Ω, the net currents I_k's injected through the electrodes $e_k \subset \Omega$ of known impedances z_k, $k = 0, ..., N$.

In the inverse problem of concern here existence is postulated, and the focus is on the uniqueness and determination of solutions.

In the CEM for the 1-Laplacian we assume $a \in L^2(\Omega)$ with

$$\text{essinf}_{\Omega} a > 0, \tag{4.13}$$

and seek solutions within the class

$$\Sigma_a := \bigcup_{\epsilon>0} \left\{ u \in H^1(\Omega) : \epsilon a \leq |\nabla u| \leq \frac{a}{\epsilon} \right\}, \tag{4.14}$$

which includes the solution coming from the forward CEM problem.

We say that $u \in H^1(\Omega)$ is a *regular weak* solution to the 1-Laplacian equation (4.9) if $u \in \Sigma_a$ and

$$\int_\Omega \frac{a}{|\nabla u|} \nabla u \cdot \nabla \varphi dx = \int_{\partial\Omega} \varphi \frac{a}{|\nabla u|} \frac{\partial u}{\partial \nu} ds, \quad \forall \varphi \in H^1(\Omega). \tag{4.15}$$

As in the forward problem, it is easy to see that addition of one arbitrary constant to u and each of U_k's leaves the problem (4.9, 4.10,4.11) and (4.12) invariant. Without loss of generality, we normalize a constant by imposing the electrode voltages $U = \langle U_0, ..., U_N \rangle$ to lie in the hyperplane

$$\Pi := \{U \in \mathbb{R}^{N+1} : \ U_0 + ... + U_N = 0\}. \tag{4.16}$$

However, the complete electrode model for the 1-Laplacian presents yet another non-uniqueness: Assume that $u : \Omega \to \mathbb{R}$ is a regular weak solution to (4.9, 4.10,4.11) and (4.12). Let $\varphi \in Lip(u(\Omega))$ be a Lipschitz-continuous increasing function. It is easy to verify that

$$v = \varphi \circ u \tag{4.17}$$

is also a regular weak solution of the problem.

Our main result (Theorem 4.4.1) shows that this is the only way the non-uniqueness occurs. As a corollary we show that additional measurements of the voltage potential along a curve joining the electrodes uniquely determines the conductivity; see Theorem 4.4.2. We also propose an iterative algorithm to approximate one such solutions (up to an unknown scaling φ!). Similar to the algorithm in [39] we approximate solutions of the 1-Laplacian by solutions of the 2-Laplacian. An additional measurement of the voltage potential along a curve joining the electrodes identifies the scaling φ, to yield the correct voltage potential solution (of the forward problem). By (4.7) the conductivity σ is recovered. Numerical experiments are performed to illustrate these ideas.

4.2 A Variational Approach to The Complete Electrode Model

In this section we introduce a variational approach to the Complete Electrode Model valid for real valued conductivities (4.8) and positive electrode impedances (4.6). This is an alternate to the Lax-Milgram approach in [51] which has the merit to extend to the degenerate elliptic problem of the 1-Laplacian.

Let $H^1(\Omega)$ be the space of functions which lie in $L^2(\Omega)$ together with their gradients, and Π is the hyperplane in (4.16). We seek weak solutions to (4.1, 4.2, 4.3, 4.4) and (4.5) in the Hilbert space $H^1(\Omega) \times \Pi$, endowed with the product

$$\langle (u, U), (v, V) \rangle := \int_\Omega uv dx + \int_\Omega \nabla u \cdot \nabla v dx + \sum_{k=0}^{N} U_k V_k,$$

and the induced norm

$$\|(u, U)\| := \langle (u, U), (u, U) \rangle^{1/2}. \tag{4.18}$$

The following lower bound is key to establishing existence of the solution to the forward problem.

Lemma 4.2.1.

$$\inf_{H^1(\Omega)\times\Pi} \frac{\int_\Omega |\nabla u|^2 dx + \sum_{k=0}^{N} \int_{e_k} (u - U_k)^2 ds}{\int_\Omega |\nabla u|^2 dx + \int_\Omega u^2 dx + \sum_{k=0}^{N} U_k^2} =: \kappa > 0. \tag{4.19}$$

Proof. We reason by contradiction: Assume the infimum in (4.19) is zero. Without loss of generality (else normalize to 1), there exists a sequence $\{(u_n, U^n)\}$ in the unit sphere of $H^1(\Omega) \times \Pi$, $\|(u_n, U^n)\| = 1$, and such that

$$0 = \lim_{n\to\infty} \int_\Omega |\nabla u_n|^2 dx, \tag{4.20}$$

$$0 = \lim_{n\to\infty} \int_{e_k} (u_n - U_k^n)^2, \quad \text{for } k = 0, ..., N. \tag{4.21}$$

Due to the compactness of the unit sphere in Π and weakly compactness of the unit sphere in $H^1(\Omega)$ there exists some $(u_*, U^*) \in H^1(\Omega) \times \Pi$ with

$$\|(u_*, U^*)\| = 1, \tag{4.22}$$

such that, on a subsequence (denoted the same),

$$u_n \rightharpoonup u_* \quad \text{in } H^1(\Omega), \tag{4.23}$$

$$U^n \to U^* \quad \text{in } \Pi, \quad \text{as } n \to \infty. \tag{4.24}$$

Since the sequence $\{u_n\}$ is bounded in $H^1(\Omega)$, the trace theorem implies that $u_n|_{e_k}$ is (uniformly in n) bounded in $H^{1/2}(e_k)$, hence also in $L^1(e_k)$, for each $k = 0, ..., N$. Using (4.21) and (4.24) in

$$\begin{aligned}\int_{e_k} (u_n - U_k^*)^2 ds = \; & \int_{e_k} (u_n - U_k^n)^2 ds - 2(U_k^n - U_k^*) \int_{e_k} u_n ds \\ & + |e_k|[(U_k^*)^2 - (U_k^n)^2)],\end{aligned}$$

one obtains $u_n|_{e_k} \to U_k^* \quad \text{in } L^2(e_k)$. Since $u_n|_{e_k} \rightharpoonup u_*|_{e_k}$, we conclude that

$$u_*|_{e_k} = U_k^* \quad \text{for each } k = 0, ..., N. \tag{4.25}$$

Now using (4.20) and (4.23)

$$\begin{aligned}0 \leq \; & \int_\Omega |\nabla(u_n - u_*)|^2 dx = \int_\Omega |\nabla u_n|^2 dx - 2 \int_\Omega \nabla u_n \cdot \nabla u_* + \int_\Omega |\nabla u_*|^2 dx \\ & \longrightarrow - \int_\Omega |\nabla u_*|^2 dx, \quad \text{as } n \to \infty,\end{aligned}$$

and, since Ω is connected,

$$u_* \equiv const. \text{ in } \overline{\Omega}. \tag{4.26}$$

From (4.25) and (4.26) we conclude that u_* restricts to each electrode to the same constant, and thus $U_0^* = U_1^* = ... = U_N^* = u_*$. Since $U^* \subset \Pi$, we must have $U^* = \langle 0, ..., 0 \rangle$ and then $u_* \equiv 0$, thus contradicting (4.22).

□

On $H^1(\Omega) \times \Pi$, let us consider the functional

$$F_\sigma(u, U) := \frac{1}{2} \int_{\partial\Omega} \sigma |\nabla u|^2 dx + \frac{1}{2} \sum_{k=0}^{N} \frac{1}{z_k} \int_{e_k} (u - U_k)^2 ds - \sum_{k=0}^{N} I_k U_k. \tag{4.27}$$

Proposition 4.2.2. *For σ satisfying (4.6) let us consider $F_\sigma : H^1(\Omega) \times \Pi \to \mathbb{R}$ defined in (4.27). Then*

(i) F_σ is strictly convex

(ii) F_σ is Gateaux differentiable in $H^1(\Omega) \times \Pi$, and the derivative at (u, U) in the direction (v, V) is given by

$$\langle DF_\sigma(u, U); (v, V) \rangle = \int_\Omega \sigma \nabla u \cdot \nabla v dx + \sum_{k=0}^{N} \frac{1}{z_k} \int_{e_k} (u - U_k)(v - V_k) ds - \sum_{k=0}^{N} I_k V_k. \tag{4.28}$$

(iii) F_σ is coercive, i.e.,

$$F_\sigma(u, U) \geq \frac{c}{2} \|(u, U)\| - \frac{1}{2c} \sum_{k=0}^{N} I_k^2, \tag{4.29}$$

for some constant $c > 0$ dependent on the lower bound ϵ in (4.6), κ in (4.19), and impedances z_k's.

Proof. (i) The functional has two quadratic terms, each strictly convex, and one linear term, hence the sum is strictly convex. (ii) The Gateaux differentiability and the formula (4.28) follow directly from the definition of F_σ.

(iii) Lemma 4.2.1 above shows that

$$F_\sigma(u,U) \geq c\|(u,U)\|^2 - \sum_{k=0}^{N} I_k U_k,$$

where $c = \frac{\kappa}{2}\min\left\{\epsilon, \frac{1}{z_0}, ..., \frac{1}{z_N}\right\}$. By completing the square one obtains

$$\begin{aligned} F_\sigma(u,U) \quad &\geq c\|u\|^2_{H^1(\Omega)} + c\sum_{k=0}^{N}\left(U_k - \tfrac{I_k}{2c}\right)^2 - \tfrac{1}{4c}\sum_{k=0}^{N} I_k^2 \\ &\geq c\|u\|^2_{H^1(\Omega)} + c\sum_{k=0}^{N}\left(\tfrac{1}{2}U_k^2 - \tfrac{I_k^2}{4c^2}\right) - \tfrac{1}{4c}\sum_{k=0}^{N} I_k^2 \\ &\geq \tfrac{c}{2}\|(u,U)\|^2 - \tfrac{1}{2c}\sum_{k=0}^{N} I_k^2 \end{aligned}$$

□

The proposition below is meant to stress the role of the zero-sum injected current condition (4.5) played in the sufficiency part of the proof of existence of solutions the forward CEM problem in [51, Proposition 3.1.]. The result is valid for complex valued conductivity σ and impedances z_k's. Recall the Gateaux derivative of DF_σ in (4.28).

Proposition 4.2.3. *(i) If $(u,U) \in H^1(\Omega)\times\Pi$ is a weak solution to (4.1, 4.2, 4.3) and (4.4), then (4.5) holds and*

$$\langle DF_\sigma(u,U);(v,V)\rangle = 0, \quad \forall\,(v,V)\in H^1(\Omega)\times\Pi. \tag{4.30}$$

(ii) Assume that I_k's satisfy (4.5). If $(u,U)\in H^1(\Omega)\times\Pi$ satisfies (4.30), then it is a weak solution to the forward problem (4.1, 4.2, 4.3) and (4.4).

Proof. (i) Follows from a direct calculation and Green's formula.

(ii) Assume that (4.30) holds.

By choosing $v \in H_0^1(\Omega)$ arbitrary and $V = \overrightarrow{0}$ in (4.30) we get that

$$\int_\Omega \sigma \nabla u \cdot \nabla v dx = 0.$$

Thus $u \in H^1(\Omega)$ is a weak solution of (4.1).

For each fixed $k = 0, 1, ..., N$ keep $V = \overrightarrow{0}$ as above, but choose $v \in H^1(\Omega)$ arbitrary with $v|_{\partial\Omega \setminus e_k} = 0$. A straightforward calculation starting from (4.30) shows that

$$\frac{1}{z_k} \int_{e_k} \left(u - U_k + z_k \sigma \frac{\partial u}{\partial \nu} \right) v ds = 0.$$

Since $v|_{e_k}$ were arbitrary (4.2) follows.

Now choose $V = \overrightarrow{0}$ as above but $v \in H^1(\Omega)$ arbitrary with $v|_{e_k} = 0$ for all $k = 0, ..., N$. It follows from (4.30) that

$$\int_{\partial\Omega} \sigma \frac{\partial u}{\partial \nu} v ds = 0.$$

Since the trace of v is arbitrary off the electrodes (4.4) holds.

Finally, for an arbitrary $V \in \Pi$ choose $v \in H^1(\Omega)$ with the trace $v = V_k$ on each e_k, $k = 0, ..., N$ and $v = 0$ off the electrodes. By using the already established relations (4.1, 4.2, 4.4) and Green's formula in (4.30) we obtain

$$\sum_{k=0}^{N} V_k \left(\int_{e_k} \sigma \frac{\partial u}{\partial \nu} ds - I_k \right) = 0.$$

On the one hand, by introducing the notation $\overrightarrow{\alpha} := \langle \alpha_0, ..., \alpha_N \rangle$ with

$$\alpha_k := \int_{e_k} \sigma \frac{\partial u}{\partial \nu} ds - I_k, \quad k = 0, ..., N,$$

we just showed that $\overrightarrow{\alpha} \perp \Pi$. On the other hand, by using (4.4, 4.5) and (4.1) in the Green's formula, we have

$$\sum_{k=0}^{N} \alpha_k = \int_{\partial\Omega} \sigma \frac{\partial u}{\partial \nu} ds = \int_{\Omega} \nabla \cdot \sigma \nabla u dx = 0,$$

which yields $\overrightarrow{\alpha} \in \Pi$. Therefore $\overrightarrow{\alpha} \in \Pi^{\perp} \cap \Pi = \overrightarrow{0}$, and (4.3) holds.

□

The following result establishes existence and uniqueness of the weak solution to the foward CEM problem; contrast with the proof of Theorem 3.1. in [51].

Theorem 4.2.4. *Let $F_\sigma : H^1(\Omega) \times \Pi \to \mathbb{R}$ be defined in (4.27).*

(i) Then F_σ has a unique minimizer $(u, U) \in H^1(\Omega) \times \Pi$. If, in addition, the injected currents I_k's satisfy (4.5) the minimizer is the weak solution of the problem (4.1, 4.2, 4.3) and (4.4).

(ii) If the problem (4.1, 4.2, 4.3,4.4) has a solution, then it is a minimizer of F_σ in the whole space $H^1(\Omega) \times \Pi$ and hence unique. Moreover, the current I_k's satisfy (4.5).

Proof. (i) Let

$$d = \inf_{H^1(\Omega)\times\Pi} F_\sigma(u, U),$$

and consider a minimizing sequence $\{(u_n, U^n)\}$ in $H^1(\Omega) \times \Pi$,

$$d \leq F_\sigma(u_n, U^n) \leq d + \frac{1}{n}.$$

Since $\inf F_\sigma \geq -\frac{1}{4c}\sum_{k=0}^{N} I_k^2$ we get $d \neq -\infty$. Following (4.29),

$$\lim_{\|(u,U)\|\to\infty} F_\sigma(u,U) = \infty.$$

Thus the minimizing sequence must be bounded, hence weakly compact. In particular, for a subsequence (denoted the same) there is some $(u_*, U^*) \in H^1(\Omega) \times \Pi$, such that

$$u_n \rightharpoonup u_* \text{ in } H^1(\Omega), \quad \text{and } U_n \to U^* \text{ in } \Pi, \text{ as } n \to \infty. \tag{4.31}$$

On the other hand since F_σ is convex, and Gateaux differentiable at (u_*, U^*) in the direction $(u_n - u_*, U^n - U^*)$, we have

$$F_\sigma(u_n, U^n) \geq F_\sigma(u_*, U^*) + \langle DF_\sigma(u_*, U^*); (u_n - u_*, U^n - U^*)\rangle.$$

We take the limit with $n \to \infty$. The weak convergence in (4.31) yields

$$\langle DF_\sigma(u_*, U^*), (u_n - u_*, U^n - U^*)\rangle \to 0.$$

Thus $d \geq F_\sigma(u_*, U^*) \geq d$ which shows that (u_*, U^*) is a global minimizer. Strict convexity implies its uniqueness. At the minimum (u_*, U^*) the Euler-Lagrange equations (4.30) are satisfied. An application of Proposition (4.2.3) part (ii) shows that (u_*, U^*) is a weak solution to the forward problem.

(ii) By Proposition 4.2.3 part (i) shows that (u_*, U^*) solves the Euler-Lagrange equations, and due to the convexity it is a minimizer of F_σ. Due to the strict convexity of the functional the minimizer is unique, hence the weak solution is unique. □

4.3 A variational approach for the complete electrodes model for the 1-Laplacian

We consider the complete electrode model for the 1-Laplacian in (4.9, 4.10,4.11, 4.12) and I_k's satisfying (4.5).

Recall the assumption (4.13) on $a \in L^2(\Omega)$ and the class Σ_a of regular weak solutions in (4.14). From (4.13) we see that any $u \in \Sigma_a$ satisfies

$$\epsilon \leq \frac{a}{|\nabla u|} \leq \frac{1}{\epsilon}, \tag{4.32}$$

for some $\epsilon > 0$.

We introduce the functional $G_a : H^1(\Omega) \times \Pi \to \mathbb{R}$, defined by

$$G_a(u, U) = \int_\Omega a|\nabla u| dx + \frac{1}{2} \sum_{k=0}^{N} \frac{1}{z_k} \int_{e_k} (u - U_k)^2 - \sum_{k=0}^{N} I_k U_k. \tag{4.33}$$

Proposition 4.3.1. *Let $(u, U) \in \Sigma_a \times \Pi$. Then G_a is Gateaux differentiable at (u, U) and satisfies*

$$\langle DG_a(u, U); (v, V)\rangle = \langle DF_{\frac{a}{|\nabla u|}}(u, U); (v, V)\rangle, \text{ for all } (v, V) \in H^1(\Omega) \times \Pi, \tag{4.34}$$

where the derivative in the right hand side is given by (4.28) with $\sigma = a/|\nabla u|$.

Proof. The Gateaux differentiability and the identity (4.34) follow from a direct direct calculation and the estimate below: Let $v \in H^1(\Omega)$ be arbitrary, then

$$\begin{aligned} \frac{1}{t} \int_\Omega a(|\nabla(u + tv)| - |\nabla u|) dx = \quad & \int_\Omega a \frac{2\nabla u \cdot \nabla v}{|\nabla(u+tv)|+|\nabla u|} dx \\ & + t \int_\Omega a \frac{|\nabla v|^2}{|\nabla(u+tv)|+|\nabla u|} dx. \end{aligned}$$

Since

$$\frac{a}{|\nabla(u+tv)|+|\nabla u|} \leq \frac{a}{|\nabla u|} \leq \frac{1}{\epsilon},$$

both integrands above are in $L^1(\Omega)$ and the Lebesgue dominated convergence yields

$$\lim_{t\to 0}\frac{1}{t}\int_\Omega a(|\nabla(u+tv)|-|\nabla u|)dx = \int_\Omega \frac{a}{|\nabla u|}\nabla u\cdot\nabla v dx.$$

□

The following result connects minimizers of the functional G_a with the *regular weak solutions* of the 1-Laplacian.

Proposition 4.3.2. *Let* $(u,U)\in\Sigma_a\times\Pi$.

(i) If (u,U) *is a global minimizer of* $G_a : H^1(\Omega)\times\Pi\to\mathbb{R}$*, then it is a regular solution to CEM for the 1-Laplacian.*

(ii) Conversely, if (u,U) *is a regular weak solution to CEM for the 1-Laplacian then it is global minimizer of* G_a*.*

Proof. (i) If (u,U) is global minimizer with $u\in\Sigma_a$, then the Gateaux derivative

$$\langle DG_a(u,U);(v,V)\rangle = 0, \text{ for all } (v,V)\in H^1(\Omega)\times\Pi,$$

and the differential identity (4.34) yields

$$\langle DF_{\frac{a}{|\nabla u|}}(u,U);(v,V)\rangle = 0, \text{ for all } (v,V)\in H^1(\Omega)\times\Pi.$$

Various choices of (v,V) as in the proof of [51, Proposition 3.1.] shows the (u,U) solves (4.1, 4.2,

4.3, 4.4) with $\sigma = a/|\nabla u|$, in other words it solves CEM for the 1-Laplacian.

(ii) Since G_a is convex and differentiable at $(u, U)) \in \Sigma_a \times \Pi$, then, for any $(v, V) \in H^1(\Omega) \times \Pi$,

$$G_a(v, V) \geq G_a(u, U) + \langle DG_a(u, U); (v - u, V - U)\rangle. \tag{4.35}$$

If $(u, U) \in \Sigma_a \times \Pi$ is a weak solution of the 1-Laplacian, then

$$\langle DG_a(u, U); (v, V)\rangle = 0, \text{ for all } (v, V) \in H^1(\Omega) \times \Pi,$$

so that the second term in the right hand side of (4.35) vanishes showing that (u, U) is global minimizer. □

We note here that the proposition above does not prove existence of solutions to the CEM for the 1-Laplacian. The problem is that the functional G_a is not coercive in the $H^1(\Omega) \times \Pi$ but merely in $W^{1,1}(\Omega) \times \Pi$, which is a non-reflexive Banach space. In particular, bounded sequences are not weak-star-compact, and the argument in the proof of Theorem 4.2.4 breaks down. However, if a is the magnitude $|J|$ of the corresponding current density field and identity then the identity (4.34) also postulate the existence of the regular weak solutions to CEM for 1-Laplacian.

4.4 Characterization of Non-Uniqueness in The Complete Electrode Model for The 1-Laplacian and Applications

In this section we state and prove our main result and its consequences to the conductivity imaging problem.

Theorem 4.4.1. *Let $a \in L^2(\Omega)$ satisfy (4.13), and $(u, U), (v, V) \in \Sigma_a \times \Pi$ be two regular weak solutions to (4.9,4.10, 4.11,4.12) and (4.5). In addition, assume that $u, v \in C^1(\Omega) \cap C(\overline{\Omega})$, then*

there exists $\varphi \in C^1(u(\Omega))$*, with* $\varphi'(t) > 0$*, such that*

$$v = \varphi \circ u. \tag{4.36}$$

Moreover, for each $k = 0, ..., N$ *and* $t \in v(e_k)$ *(the range of* v *on the electrode),*

$$\varphi(t) = t + (U_k - V_k). \tag{4.37}$$

Proof. Since each term in G_a is convex, for any $0 \leq \lambda \leq 1$,

$$G_a[\lambda(u, U) + (1 - \lambda)(v, V)] \leq \lambda G_a(u, U) + (1 - \lambda)G_a(v, V).$$

Proposition 4.3.2 part (ii) yields that both (u, U) and (v, V) are global minimizers of G_a, so that the above inequality holds with equality. Moreover, the linear part cancels to yield

$$\int_\Omega a\left(\lambda|\nabla u| + (1 - \lambda)|\nabla v| - |\lambda\nabla u + (1 - \lambda)\nabla v|\right) dx = 0, \tag{4.38}$$

$$\int_{e_k} \left[\lambda(u - U_k)^2 + (1 - \lambda)(v - V_k)^2 - (\lambda(u - U_k) + (1 - \lambda)(v - V_k))^2\right] ds = 0, \tag{4.39}$$

for all $0 \leq \lambda \leq 1$, and $k = 0, ..., N$. The non-negativity of the integrand in (4.39) and strict convexity of quadratics yield for each $k = 0, ..., N$ that

$$u|_{e_k} - U_k = v|_{e_k} - V_k, \text{ a.e. on } e_k. \tag{4.40}$$

The non-negativity of the integrand in (4.38) imply that a.e. in Ω

$$(\lambda|\nabla u| + (1 - \lambda)|\nabla v|)^2 = |\lambda\nabla u + (1 - \lambda)\nabla v|^2$$

or

$$\nabla u \cdot \nabla v = |\nabla u| \cdot |\nabla v|. \tag{4.41}$$

Since both gradients are continuous and bounded away from zero, they must be parallel i.e.,

$$\nabla u = \mu \nabla v, \tag{4.42}$$

for some $\mu \in C(\Omega)$ with $\inf_\Omega \mu > 0$.

Since $u, v \in \Sigma_a \cap C^1(\Omega)$ with a essentially positive as in (4.13), then $\inf |\nabla u| > 0$ and $\inf |\nabla v| > 0$. By the implicit function theorem, their level sets are C^1-smooth surfaces. A differentiation in the direction tangential to the level sets and (4.42) yield that u and v are constant on each other level sets, in particular they share the same set of level sets. For each $t \in v(\Omega)$ let $L_t := \{x \in \Omega : v(x) = t\}$ denote the t-level set of v, and define

$$\varphi(t) := u|_{L_t} \tag{4.43}$$

Since L_t is also a level set for u, the function φ is well defined by (4.43) on the range $v(\Omega)$ of v, and the relation 4.36 follows.

Moreover, since $u \in C^1(\Omega)$ then u is differentiable in any direction, in particular in the direction of ∇u (which does not vanish), and therefore φ is differentiable. From $\nabla u(x) = \varphi'(v(x))\nabla v(s)$ and (4.42) we get $\varphi'(v(x)) = \mu(x)$, for all $x \in \Omega$, thus $\varphi' > 0$. By combining (4.40) with (4.36), for each $t \in v(e_k)$ we obtain (4.37) □

In order to determine the conductivity uniquely we must show $\varphi' \equiv 1$. In practice this can be done by additional measurements on a curve joining the electrodes. For simplicity we formulate the result for two electrodes through which we inject (respectively extract) the current in a three

dimensional body.

Theorem 4.4.2 (Unique determination)**.** *Let $\Omega \subset \mathbb{R}^3$ have connected Lipschitz boundary. Assume $\sigma, \tilde{\sigma} \in C^{1,\alpha}(\Omega)$ are unknown, for $0 < \alpha < 1$. Let $e_k \subset \partial\Omega$, $k = 0, 1$ be two electrodes, and $\Gamma \subset \partial\Omega$ be a simple curve joining the electrodes such that $\partial\Omega \setminus (e_0 \cup e_1)$ is simply connected (as a surface). Let $u, \tilde{u}$ be solutions to (4.1), subject to (4.2, 4.3, 4.4) corresponding to σ, respectively $\tilde{\sigma}$, and $N = 1$. Assume that*

$$\begin{aligned} \sigma|\nabla u| &= \tilde{\sigma}|\nabla \tilde{u}|, \text{ in } \Omega, \\ \inf_\Omega \sigma|\nabla u| &> 0, \\ u|_\Gamma &= \tilde{u}|_\Gamma + C, \end{aligned} \tag{4.44}$$

for some constant C. Then

$$\begin{aligned} u &= \tilde{u} + C \text{ in } \Omega, \\ \sigma &= \tilde{\sigma} \text{ in } \Omega. \end{aligned}$$

Proof. The reasoning in the proof of [39, Theorem 1.3.], which shows that each connected component Σ_t of a level set $\{x \in \Omega : \tilde{u}(x) = t\}$ reaches the boundary $\partial\Omega$ also extends to the CEM boundary conditions: Indeed, arguing by contradiction, assume $\Sigma_t \bigcap \partial\Omega = \emptyset$. Then $\partial\Omega \bigcup \Sigma_t$ is a compact manifold with two connected components. By Alexander duality theorem applied to $\partial\Omega \bigcup \Sigma_t$ (see, e.g. Theorem 27.10 in [19],) $R^3 \setminus (\partial\Omega \bigcup \Sigma_t)$ is partitioned into three open connected components: $(R^3 \setminus \overline{\Omega}) \bigcup O_1 \bigcup O_2$. Since $\Sigma_t \subset \Omega$ we have $O_1 \bigcup O_2 = \Omega \setminus \Sigma_t$ and then $\partial O_i \subset \partial\Omega \bigcup \Sigma_t$ for $i = 1, 2$. At least one of the ∂O_1 or ∂O_2 is in Σ_t. Assume not, i.e. for each $i = 1, 2$, $\partial O_i \bigcap \partial\Omega \neq \emptyset$. Since $\partial\Omega$ is connected (by assumption), we have that $O_1 \bigcup O_2 \bigcup \partial\Omega$ is connected which implies $O_1 \bigcup O_2 \bigcup (R^3 \setminus \Omega)$ is also connected. By applying once again Alexander's duality theorem for $\Sigma_t \subset R^3$, we have that $R^3 \setminus \Sigma_t$ has exactly two open connected components, one of which is

unbounded: $R^3 \setminus \Sigma_t = O_\infty \bigcup O_0$. Since $O_1 \bigcup O_2 \bigcup (R^3 \setminus \Omega)$ is connected and unbounded, we have $O_1 \bigcup O_2 \bigcup (R^3 \setminus \Omega) \subset O_\infty$, which leaves $O_0 \subset R^3 \setminus (O_1 \bigcup O_2 \bigcup (R^3 \setminus \Omega)) \subset \Sigma_t$. This is impossible since O_0 is open and Σ_t is a hypersurface. Thus O_1 or O_2 or both have the boundary in Σ_t. To fix ideas, consider $\partial O_1 \subset \Sigma_t$. But then $\tilde{u} \equiv t$ in O_1, for otherwise the new map

$$\tilde{u}_1(x) = \begin{cases} \tilde{u}(x), & x \in \Omega \setminus O_1, \\ t, & x \in \overline{O_1}, \end{cases}$$

is in $H^1(\Omega) \bigcap C(\overline{\Omega})$ (since O_1 is an extension domain as ∂O_1 has a unit normal everywhere) and would decrease the functional G_a in (4.33); in contradiction with the minimality of $\tilde{u}$. Therefore $\tilde{u} \equiv t$ in O_1, and $|\nabla \tilde{u}| \equiv 0$ in O_1. Again we reached a contradiction. These contradictions followed from the assumption that $\Sigma_t \bigcap \partial\Omega = \emptyset$. We conclude that each (connected component) of an arbitrary level set must reach the boundary $\partial\Omega$.

We show next that each level set must meet $\Gamma \cup e_0 \cup e_1$, and argue again by contradiction: Assume that we have a level set Σ_t such that its trace $L_t := \Sigma_t \cap \partial\Omega$ lies entirely in the simple connected surface $\partial\Omega \setminus (\Gamma \cup e_0 \cup e_1)$. Off the electrodes the equation (4.4) yields Σ_t intersects $\partial\Omega$ orthogonally, in particular the intersection L_t is an immersed C^1-smooth curve lying in the simple connected surface $\partial\Omega \setminus (\Gamma \cup e_0 \cup e_1)$. We note first that L_t cannot have an end point in $\partial\Omega \setminus (\Gamma \cup e_0 \cup e_1)$, since at such a point the gradient $\nabla\tilde{u}$ must vanish. Since the curve is a compact submanifold it must a closed curve. (So far L_t may have self intersections, at which points the tangents must be parallel, otherwise would be a singular point for $\tilde{u}$.) By Jordan's theorem the two dimensional surface $\partial\Omega \setminus (\Gamma \cup e_0 \cup e_1)$ is separated by L_t into at least two connected components (accounting possible self-intersections), at least one of which, say O with boundary entirely contained in L_t. Consider $\tilde{u}$ restricted to $\overline{O}$. Then either $\tilde{u}(x) \geq t$ or $\leq t$ for all $x \in \overline{O}$, and thus $\tilde{u}$ would have an extremum in O, and thus $\nabla\tilde{u}$ vanishes there. However, O lies within the boundary region (off the electrodes) where the normal derivative vanishes, and by the (Hopf's) strong maxim principle its

gradient cannot vanish in this region of the boundary. This contradiction shows that each level set must at least meet one of the electrodes or the curve Γ, in particular the range of $\tilde{u}$ on $\Gamma \cup e_0 \cup e_1$ is the same as its range on $\overline{\Omega}$.

By applying the characterization in Theorem 4.4.1 we have that

$$u(x) = \varphi \circ \tilde{u}(x), \quad \text{in } \Omega,$$

and, for t a value in the range $\tilde{u}(e_k)$, $k = 0, 1$, we have

$$\varphi(t) = t + (U_k - V_k).$$

For $t \in \tilde{u}(\Gamma)$ a voltage on Γ, by (4.36) we have that

$$\varphi(t) = t + C.$$

Since $\tilde{u}$ is continuous on $\overline{\Omega}$, we must have

$$U_0 - V_0 = U_1 - V_1 = C.$$

Since the range of $\tilde{u}$ on $\Gamma \cup e_0 \cup e_1$ is the same as the range on $\overline{\Omega}$, we conclude that

$$\varphi(t) = t + C,$$

for all $t \in \tilde{u}(\overline{\Omega})$ which, together with (4.36) shows (4.45) in $\overline{\Omega}$. In particular, $\nabla u = \nabla \tilde{u}$ and, by (4.44), $\sigma = \tilde{\sigma}$ in Ω.

□

4.5 A Minimization Algorithm for The Weighted Gradient Functional with CEM Boundary Constraints

In this section we propose an iterative algorithm which minimizes the functional G_a in (4.33). It is the analogue of an algorithm in [39] adapted to the CEM boundary conditions.

Recall the class Σ_a in (4.14) and the hyperplane Π in (4.16). The key property exploited by the algorithm is contained in the following lemma.

Lemma 4.5.1. *Assume that $v \in \Sigma_a$. Consider the CEM in (4.1, 4.2, 4.3) and (4.4) for the conductivity $\sigma = a/|\nabla v|$, and let $(u, U) \in H^1(\Omega) \times \Pi$ be its solution as guaranteed by Theorem 4.2.4. Then*

$$G_a(u, U) \leq G_a(v, V), \quad \textit{for all } V \in \Pi. \tag{4.45}$$

Moreover, if the equality holds then $(u, U) = (v, V)$.

Proof. Let $V \in \Pi$ be arbitrary. Since (u, U) is a global minimizer of F_σ as in (4.27) with $\sigma = a/|\nabla v|$ as shown in Theorem 4.2.4, we estimate

$$\begin{aligned} G_a(v, V) &= \int_\Omega a|\nabla v|dx + \tfrac{1}{2}\sum_{k=0}^{N}\left[\tfrac{1}{z_k}\int_{e_k}(v - V_k)^2 ds - 2I_k V_k\right] \\ &= \tfrac{1}{2}\int_\Omega a|\nabla v|dx + F_{\frac{a}{|\nabla v|}}(v, V) \\ &\geq \tfrac{1}{2}\int_\Omega a|\nabla v|dx + F_{\frac{a}{|\nabla v|}}(u, U). \end{aligned} \tag{4.46}$$

Since

$$\begin{aligned}\int_\Omega a|\nabla u|dx &= \int_\Omega \left[\tfrac{a}{|\nabla v|}\right]^{\frac{1}{2}} |\nabla v| \left[\tfrac{a}{|\nabla v|}\right]^{\frac{1}{2}} |\nabla u|dx \\ &\leq \left(\int_\Omega \tfrac{a}{|\nabla v|}|\nabla v|^2 dx\right)^{\frac{1}{2}} \left(\int_\Omega \tfrac{a}{|\nabla v|}|\nabla u|^2 dx\right)^{\frac{1}{2}} \\ &\leq \tfrac{1}{2}\int_\Omega a|\nabla v|dx + \tfrac{1}{2}\int_\Omega \tfrac{a}{|\nabla v|}|\nabla u|^2 dx,\end{aligned}$$

we also obtain

$$\begin{aligned}G_a(u,U) &= \int_\Omega a|\nabla u|dx + \tfrac{1}{2}\sum_{k=0}^N \left[\tfrac{1}{z_k}\int_{e_k}(u-U_k)^2 ds - 2I_k U_k\right] \\ &\leq \tfrac{1}{2}\int_\Omega a|\nabla v|dx + \tfrac{1}{2}\int_\Omega \tfrac{a}{|\nabla v|}|\nabla u|^2 dx + \tfrac{1}{2}\sum_{k=0}^N \left[\tfrac{1}{z_k}\int_{e_k}(u-U_k)^2 ds - 2I_k U_k\right] \\ &= \tfrac{1}{2}\int_\Omega a|\nabla v|dx + F_{\frac{a}{|\nabla v|}}(u,U). \qquad (4.47)\end{aligned}$$

From (4.46) and (4.47) we conclude (4.45). Moreover, if the equality holds in (4.45) then equality holds in (4.46), and thus

$$F_{a/|\nabla v|}(u,U) = F_{a/|\nabla v|}(v,V). \qquad (4.48)$$

Since (u,U) is a solution to the forward problem (for $\sigma = a/|\nabla v|$) it is also a global minimizers of $F_{a/|\nabla v|}$ over $H^1(\Omega)\times\Pi$. But (4.48) shows that (v,V) is also a global minimizer for $F_{a/|\nabla v|}$. Now the uniqueness of the global minimizers in Theorem 4.2.4 (for $\sigma = a/|\nabla v|$) yields $(u,U) = (v,V)$.

□

We give next a posteriori conditions which ensures the algorithm to converge to a minimizer.

4.6 A minimization algorithm for conductivity imaging

Let $|J|$ be satisfying (4.13), the impedances $z_k > 0$, $k = 0, ..., N$, and the injected current I_k satisfy (4.5). Assume that the unknown conductivity satisfy

$$\epsilon < \sigma < \epsilon^{-1},$$

for some known $\epsilon > 0$.

Let $\delta > 0$ measure a desired error to be used in the stopping criteria.

- Step 1: Solve (4.1, 4.2, 4.3) and (4.4) for $\sigma = |J|$, and let u_0 be its unique solution, and define
$$\sigma_1 := \min\left\{\max\left\{\frac{|J|}{|\nabla u_0|}, \epsilon\right\}, \frac{1}{\epsilon}\right\};$$
- Step 2: For σ_n given: Solve (4.1, 4.2, 4.3) and (4.4) for the unique solution u_n;
- Step 3: If
$$\|\nabla u_n - \nabla u_{n-1}\|_{C(\overline{\Omega})} > \delta \frac{\epsilon}{\text{essinf}|J|},$$
then define
$$\sigma_{n+1} := \min\left\{\max\left\{\frac{|J|}{|\nabla u_n|}, \epsilon\right\}, \frac{1}{\epsilon}\right\}$$
and repeat Step 2;
- Else STOP.

4.7 Numerical Implementations

We illustrate the theoretical results in a numerical simulation in two dimensions. Given a current pattern $I \in \Pi$ and a set of surface electrodes e_k with impedance $z_k > 0$ for $k = 0, 1, \ldots, N$, the minimization algorithm in the previous section involves solving the Complete Electrode Model problem (4.1, 4.2, 4.3) and (4.4) at each iteration for a certain conductivity map, say σ, see section 4.6. In this paper we approximate the solution to the CEM on an uniform triangulation of a unit box, $[0, 1] \times [0, 1]$, as shown in figure 4.1, in a finite-dimensional space spanned by the set of planes

$$P := \bigcup_{l=1}^{2(\sqrt{m}-1)^2} T_l,$$

where m is the number of grid points (we assume m is a squared number) in the triangulated unit box and T_l is the set of planes supported in the l-th triangle, Δ_l for $l = 1, 2, \ldots, 2(\sqrt{m} - 1)^2$. For l odd

$$T_l = \left\{ 1 - \frac{1}{h}(x - x_{k_l}) - \frac{1}{h}(y - y_{k_l}), \frac{1}{h}(x - x_{k_l}), \frac{1}{h}(y - y_{k_l}) \right\},$$

for $(x, y) \in \Delta_l$, where (x_{k_l}, y_{k_l}) corresponds to the location of the southwest grid point of the square in which Δ_l is inscribed, and h is the length of the side of the square. The planes supported by even numbered triangles is given by

$$T_l = \left\{ 1 + \frac{1}{h}(x - x_{r_l}) + \frac{1}{h}(y - y_{r_l}), -\frac{1}{h}(y - y_{r_l}), -\frac{1}{h}(x - x_{r_l}) \right\}$$

for $(x, y) \in \Delta_l$, where (x_{r_l}, y_{r_l}) corresponds to the location of the northeast grid point of the square in which Δ_l is inscribed, and h is the length of the side of the square. In figure 4.1, the triangle Δ_{11} lies in a square whose southwest grid point position is (x_7, y_7) and the northeast grid point location is (x_{12}, y_{12}).

To obtain an approximate solution to the forward problem (4.1, 4.2, 4.3, 4.4) and (4.5) we look in

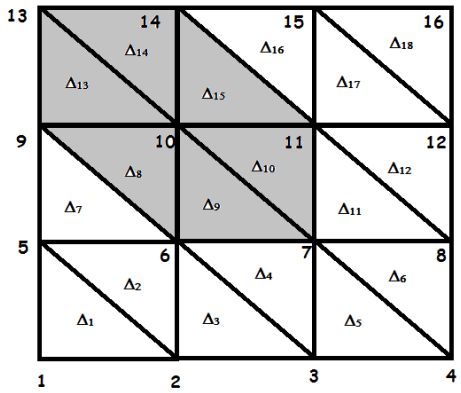

Figure 4.1: The uniform triangulated unit box with 16 nodes or grid points and 18 triangles. The shaded triangles are adjacent to the 10-th node. Notice that the corner nodes, 1, 4, 13 and 16, have only one or two adjacent triangles.

the space of functions of the form

$$u_p(x,y) = \sum_{j=1}^{m} u_j \psi_j(x,y), \tag{4.49}$$

where ψ_j is the sum of the all planes in P adjacent to the j-th node in the unit box, see figure 4.1. Consequently from proposition 4.2.2, substituting (4.49) into (4.28), and by selecting $v = \psi_j$, for $j = 1, \ldots, m$, and $V \equiv \vec{0}$, we get the system of equations

$$\int_\Omega \sigma \nabla u_p \cdot \nabla \psi_j dxdy + \sum_{k=0}^{N} \frac{1}{z_k} \int_{e_k} (u_p - U_k)\psi_j ds = 0, \quad \forall j = 1, \ldots, m \tag{4.50}$$

coupled with the equations (now by setting $v \equiv 0$ and $V \neq \vec{0}$)

$$-\sum_{k=0}^{N} \frac{1}{z_k} \int_{e_k} (u_p - U_k) V_k^j ds = \sum_{k=0}^{N} I_k V_k^j, \quad \forall j = 0, \ldots N-1, \tag{4.51}$$

where $V_k^j = 1$ whenever $k = j$ for $k = 0, \ldots, N-1$ and $V_N^j = -1$ for every $j = 0, \ldots N-1$ (Note that forming V in this fashion is equivalent to choosing the j-th vector for the j-th equation in (4.51) from the set

$$\left\{ \begin{bmatrix} 1 \\ 0 \\ 0 \\ \vdots \\ 0 \\ -1 \end{bmatrix}, \begin{bmatrix} 0 \\ 1 \\ 0 \\ \vdots \\ 0 \\ -1 \end{bmatrix}, \cdots, \begin{bmatrix} 0 \\ 0 \\ \vdots \\ 0 \\ 1 \\ -1 \end{bmatrix} \right\},$$

for $j = 0, 1, \ldots, N-1$. This set forms a basis for the space Π.), and

$$U_N = -\sum_{k=0}^{N-1} U_k.$$

The values of $\{u_1, u_2, \ldots, u_m, U_0, U_1, \ldots, U_{N-1}\}$ are obtained by solving the linear system

$$\begin{bmatrix} \Lambda & \Psi \\ \Psi^T & \Upsilon \end{bmatrix} \begin{bmatrix} u_1 \\ u_2 \\ \vdots \\ u_m \\ U_0 \\ U_1 \\ \vdots \\ U_{N-1} \end{bmatrix} = \begin{bmatrix} 0 \\ 0 \\ \vdots \\ 0 \\ I_0 - I_N \\ I_1 - I_N \\ \vdots \\ I_{N-1} - I_N \end{bmatrix}, \tag{4.52}$$

where the entries of Λ,

$$\Lambda(i,j) = \int_{\Omega} \sigma \nabla \psi_j \cdot \nabla \psi_i dx dy + \sum_{k=0}^{N} \frac{1}{z_k} \int_{e_k} \psi_j \psi_i ds, \quad \forall\, i,j = 1,2,\ldots,m,$$

the entries of Ψ,

$$\Psi(i,k) = \frac{1}{z_N} \int_{e_N} \psi_i ds - \frac{1}{z_k} \int_{e_k} \psi_i ds, \quad \forall\, i = 1,2,\ldots,m,\ k = 0,\ldots,N-1,$$

and

$$\Upsilon = \begin{bmatrix} \frac{|e_0|}{z_0} + \frac{|e_N|}{z_N} & \frac{|e_1|}{z_1} & \cdots & \frac{|e_{N-1}|}{z_{N-1}} \\ \frac{|e_0|}{z_0} & \frac{|e_1|}{z_1} + \frac{|e_N|}{z_N} & \cdots & \frac{|e_{N-1}|}{z_{N-1}} \\ \vdots & \vdots & \ddots & \vdots \\ \frac{|e_0|}{z_0} & \cdots & \frac{|e_{N-2}|}{z_{N-2}} & \frac{|e_{N-1}|}{z_{N-1}} + \frac{|e_N|}{z_N} \end{bmatrix}.$$

For a numerical scheme to solve the Complete Electrode Morel in three dimensions see [53].

4.7.1 An Illustration of Non-Uniqueness

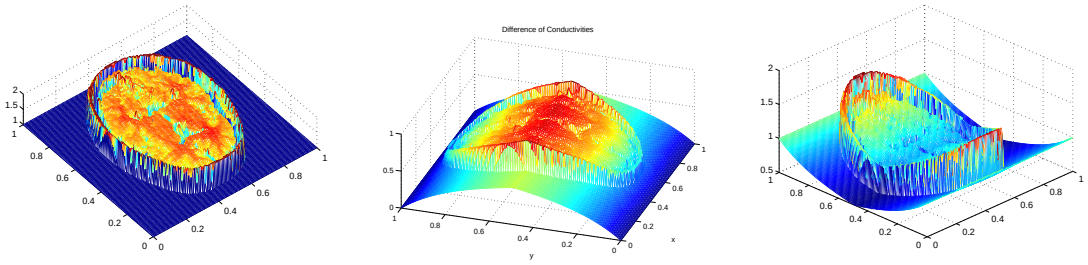

Figure 4.2: The left figure is the conductivity map of a brain σ_u and the figure on the right is the scaled conductivity of the brain $\sigma_v = \frac{\sigma_u}{\varphi(u)}$, see section 4.7.1. The figure in the center displays the absolute difference between the adjacent conductivities. The L_2 difference between σ_u and σ_u is 27.24.

Next we demonstrate the characterization of non-uniqueness in the Complete Electrode Model for the 1-Laplacian with a numerical example. Let σ_u be the planar conductivity map of a brain shown in figure 4.2 and the scaled version, $\sigma_v = \frac{\sigma_u}{\varphi(u)}$ where

$$\frac{d}{dt}\varphi(t) := \begin{cases} 2 - 2|t|, & |t| < \frac{1}{2} \\ 1, & |t| \geq \frac{1}{2} \end{cases}$$

with $\varphi\left(-\frac{1}{2}\right) = -\frac{1}{2}$, and u is the solution to the forward problem (4.1, 4.2, 4.3, 4.4) and (4.5) approximated by solving the linear system (4.52) with σ_u, $-I_0 = 1.2079 = I_1$, $z_0 = z_1 = 10^{-3}$, $e_0 = \{(x, y) \in [0, 1] \times [0, 1] : y = 0\}$ and $e_1 = \{(x, y) \in [0, 1] \times [0, 1] : y = 1\}$. Similarly, using the same currents and the same electrodes with the conductivity σ_v, we obtain another solution v. We compare the respective magnitudes of the current density generated by u and v both computed using (4.7) in figure 4.3. The L_2 norm of the difference of the magnitudes of the current density yielded by u and v is in the order of 10^{-3}.

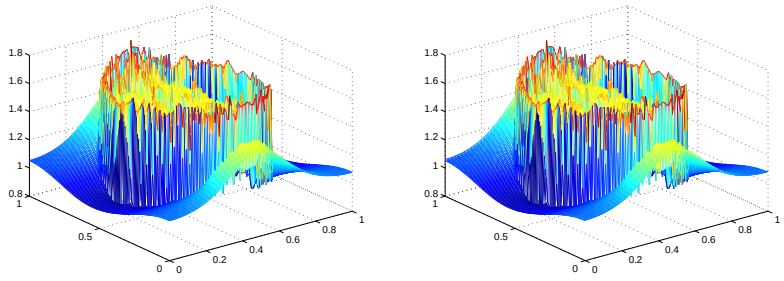

Figure 4.3: The left figure is the magnitude of the current density induced by the brain σ_u and the voltage potential u and the figure on the right is the magnitude of the current density generated by the scaled version of the brain σ_v and the voltage potential v displayed in figure 4.2. The functions are almost identical.

4.7.2 *Numerical Reconstruction of a Planar Torso*

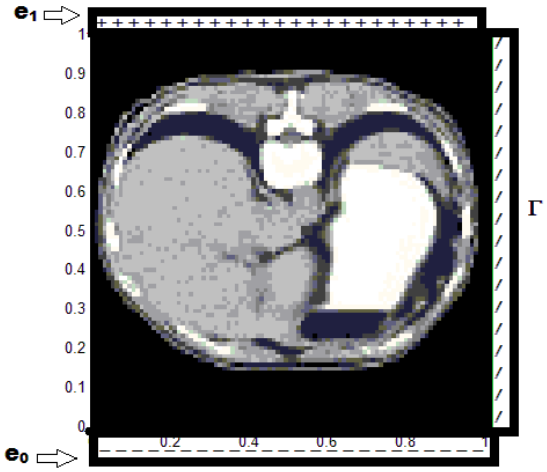

Figure 4.4: The planar conductivity map of a torso on a unit box. The electrodes e_0 and e_1 are indicated on the bottom and the top of the figure, respectively. In the numerical experiment to follow, the voltage potential is measured on Γ which is the right side of the unit box connecting the electrodes e_0 and e_1.

Here we reconstruct the planar conductivity of a torso on the unit box $[0,1] \times [0,1]$ (the exact conductivity is shown in figure 4.4) using simulated measurements via the minimization algorithm described in section 4.6.

The magnitude of the current density (see figure 4.6), $|J|$, is obtained by solving the forward problem (4.1, 4.2, 4.3, 4.4) and (4.5) with the conductivity of a torso in figure 4.4. The currents $-I_0 = 3\ mA = I_1$ are injected on the electrodes

$$e_0 = \{(x,y) \in [0,1] \times [0,1] :\ y = 0\} \quad \text{and} \quad e_1 = \{(x,y) \in [0,1] \times [0,1] :\ y = 1\}$$

with impedances $z_0 = z_1 = 8.3\ m\Omega \cdot m^2$, respectively. The values of the exact conductivity map of

the torso ranges from 1.0 S/m to 1.8 S/m. To obtain the scaling function φ, the voltage potential is measured on $\Gamma = \{(x, y) \in [0, 1] \times [0, 1] : x = 1\}$, displayed in figure 4.5.

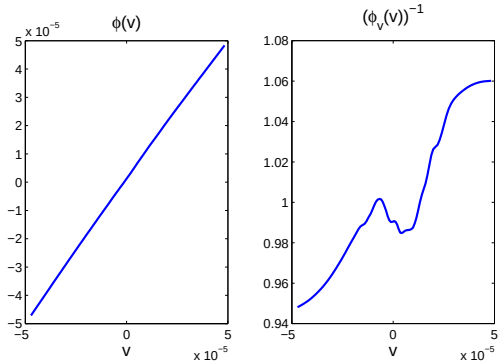

Figure 4.5: The voltage potential measured on Γ as a function of the equipotential curves of v, corresponding to the numerical experiment for reconstructing the planar torso, is shown in the left figure and the reciprocal of its derivative is shown on the right.

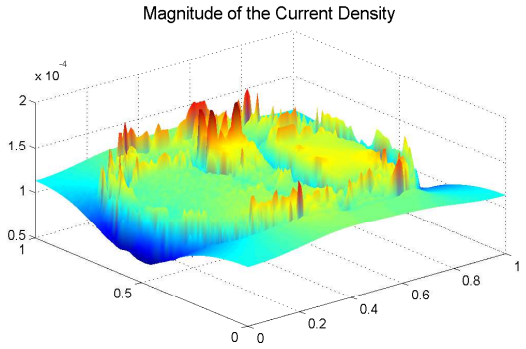

Figure 4.6: The simulated magnitude of the current density, $|J|$, corresponding to the numerical experiment for reconstructing the planar torso, is shown above.

Then, using only the currents I_0 and I_1, the impedances z_0 and z_1, and the magnitude of the current density $|J|$ we solve the inverse problem (4.9, 4.10, 4.11, 4.12) and (4.5) via the minimization algorithm in section 4.6 and obtain a minimizer, v. The corresponding conductivity $\sigma_v = \frac{|J|}{|\nabla v|}$ is

displayed in figure 4.7. The set stopping criteria for this experiment $\delta = 10^{-7}$ is attained with 320 iterations. The solution is v is computed on a 90×90 grid of points.

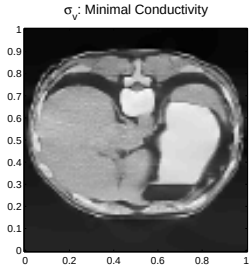

Figure 4.7: The conductivity obtained by solving the inverse problem (4.9, 4.10, 4.11, 4.12) and (4.5) via the minimization algorithm in section 4.6.

The reconstructed conductivity of a torso, σ_u, is directly obtained using the voltage $u\,|_\Gamma = \varphi(v)$ and the conductivity σ_v by the scaling $\sigma_u = \frac{\sigma_v}{\varphi_v(v)}$, per theorem 4.4.2. See figure 4.8 for the image of the reconstructed conductivity σ_u. The L_2 error of the reconstruction is 0.04.

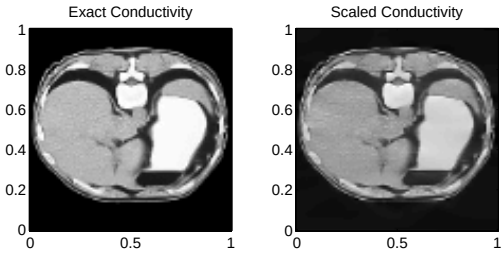

Figure 4.8: The exact conductivity (left) versus the reconstructed conductivity of a torso (right), σ_u, obtained by scaling the conductivity, σ_v, by the reciprocal of the derivative of the function $\varphi(v)$.

4.8 Conclusions

In this chapter we considered reconstructing the electrical conductivity by solving the 1-Laplacian subject to the boundary conditions of the Complete Electrode Model and characterized the non-uniqueness of this problem. CEM is a more accurate model for modeling the voltage distribution in a conductive body by injecting currents through a set of electrodes.

Different from the previous work on the CEM in [51] we solved the forward problem using a variational approach for real valued voltage potentials by considering positive real value impedances, also known as ideal impedances.

Through the variational approach we characterize the non-uniqueness of the inverse problem by introducing the functional G_a whose Gateaux derivative coincides with the Gateaux derivative of the functional F_σ corresponding to the forward problem. This way we are able to establish a relation between the forward and the inverse problem. Moreover, we show the necessary measurements needed to obtain a unique conductivity from solving the 1-Laplacian with the CEM.

APPENDIX A: LEVEL SETS ON THE PLANE

Lemma A.0.1. *Let $\Omega \subset \mathbb{R}^2$ be an open bounded set with $\partial\Omega$ a rectifiable curve, and*

$$u \in C^1(\Omega) \cap C^0(\overline{\Omega})$$

with

$$|\nabla u| > 0, \quad \forall (x, y) \in \Omega.$$

Then, for $\lambda \in$ Range$\{u\}$, the level set

$$\Sigma_\lambda = \left\{(x, y) \in \overline{\Omega} : u(x, y) = \lambda\right\},$$

is compact and it is a finite collection of rectifiable curves.

Proof. Clearly, Σ_λ is compact. Let the point $P = (x, y) \in \Sigma_\lambda \cap \Omega$, then by hypothesis, either $u_y(P) > 0$ or $u_x(P) > 0$. Thus, by the Implicit Function Theorem (IFT), there exist a number $r_P > 0$, a ball $\mathcal{B}(P; r_P)$, and a graph G_P such that

$$G_P = \mathcal{B}(P; r_P) \cap \Sigma_\lambda \cap \Omega,$$

and $P \in G_P$. Since, P was arbitrarily picked from $\Sigma_\lambda \cap \Omega$, then every point in $\Sigma_\lambda \cap \Omega$ is contained in a graph which is also contained in Σ_λ. Note that by the IFT, G_P is described by a continuously differentiable function, say $g_P : I_P \mapsto \mathbb{R}$, where I_P is an open interval. Let $K_P \subset I_P$ be a closed interval, then, since g'_P is continuous, the length of the curve described by g_P restricted to K_P is finite, i.e.

$$\int_{K_P} \sqrt{1 + (g'_P(\alpha))^2} d\alpha < \infty.$$

Thus, by slightly shrinking the interval I_P and the ball $\mathcal{B}(P; r_P)$ the length of each graph, G_P, is

finite. Moreover, G_P is open. Let

$$\mathcal{A} = \bigcup_{P \in \Sigma_\lambda \cap \Omega} G_P,$$

so that $\mathcal{A}$ is an open covering of $\Sigma_\lambda \cap \Omega$. Since $\Sigma_\lambda \cap \partial\Omega$ is a compact rectifiable curve, then it has a finite covering, say $\mathcal{S}$. Hence, $\mathcal{S} \cup \mathcal{A}$ covers Σ_λ, since Σ_λ is compact, it is covered by a finite collection of rectifiable curves.

□

Lemma A.0.2. *Let $\Omega \subset \mathbb{R}^2$ be a bounded simply connected open set with $\partial\Omega$ a rectifiable curve, and*

$$u \in C^{1,1}(\Omega) \cap C^0(\partial\Omega) : \bar{\Omega} \mapsto \mathbb{R}$$

with

$$|\nabla u| > 0, \quad \forall x \in \Omega,$$

and $u(x_0, y_0) = \lambda$ where $(x_0, y_0) \in \Omega$. Then the initial value problem

$$\begin{cases} \dot{x}(t) = -\frac{u_y(x,y)}{|\nabla u(x,y)|} \\ \dot{y}(t) = \frac{u_x(x,y)}{|\nabla u(x,y)|} \\ (x(0), y(0)) = (x_0, y_0) \end{cases} \tag{A.1}$$

has the following properties:

i) there exist a unique solution $x(t), y(t) \in C^0([T_-, T_+]) \cap C^1(T_-, T_+)$ which solves (A.1) in the interval (T_-, T_+) and is contained in $\bar{\Omega} \times [T_-, T_+]$, where T_- and T_+ are finite, $T_- < 0 < T_+$, and

$$(x(T_-), y(T_-)) \neq (x(T_+), y(T_+)) \in \partial\Omega.$$

ii)

$$u(x(t), y(t)) = \lambda, \quad \forall t \in [T_-, T_+].$$

iii) The curve traced by $(x(t), y(t)), t \in [T_-, T_+]$ *is simply connected.*

Proof. Since ∇u is continuous then (A.1) has solutions $x(t), y(t) \in C^1(I)$ for some interval I. By hypothesis we have that

$$\dot{x}(t)u_x(x(t), y(t)) + \dot{y}(t)u_y(x(t), y(t)) = 0, \quad \forall t \in I.$$

Therefore,

$$u(x(t), y(t)) = \lambda, \quad \forall t \in I.$$

First, I will show that there is a unique solution to (A.1) defined over $[0, T_+]$ such that $(x(T_+), y(T_+)) \in \partial\Omega$. Indeed, by hypothesis we have that $|\nabla u|$ is Lipschitz on the product domain $\mathbb{R} \times \Omega$, then, by continuation, (A.1) has a unique solution $x(t)$ and $y(t)$ which is defined for $0 \leq t < T_+$, where either of the following three cases occur:

1) $T_+ = \infty$,

2) if $T_+ < \infty$, then either

$$\lim_{t \to T_+} \sqrt{x^2(t) + y^2(t)} = \infty, \tag{A.2}$$

3) or $(x(t), y(t))$ approaches a point $(X_+, Y_+) \in \partial\Omega$, as $t \to T_+$.

Observe that if $T_+ = \infty$, then the length of the curve $\{(x(t), y(t)) : t \geq 0\}$ is unbounded since

$$\lim_{t \to \infty} \int_0^t \sqrt{\dot{x}^2(s) + \dot{y}^2(s)} ds = \lim_{t \to \infty} t = \infty.$$

But, the level set $\{(x,y) \in \Omega : u(x,y) = \lambda\}$ contains all of the points $(x(t), y(t))$, and, since $|\nabla u| > 0, \forall (x,y) \in \Omega$, by Lemma A.0.1 its length is finite. Thus by contradiction $T_+ < \infty$. The limit in (A.2) is a contradiction since Ω is a bounded set. Therefore, we are left with the third and only possible case. There is a sequence $t_k \in [0, T_+)$ such that $t_k \to T_+$ as $k \to \infty$, and $(x_k, y_k) = (x(t_k), y(t_k))$ such that

$$\lim_{k\to\infty} (x_k, y_k) = (X_+, Y_+), .$$

Using the continuity and the boundedness of the solutions $x(t), y(t)$ in $[0, T_+)$ we can define

$$x(T_+) = X_+, \quad y(T_+) = Y_+.$$

so that $x(t), y(t)$ are continuous functions on $[0, T_+]$. By the continuity of u in $\bar{\Omega}$, then $u(x(T_+), y(T_+)) = \lambda$. If we make a change of variables $t = -\tau$ in (A.1) and using the same justifications as above we conclude that the pair of functions $x(t), y(t) \in C^0([T_-, T_+]) \cap C^1(T_-, T_+)$ solve (A.1) uniquely in (T_-, T_+) and $u(x(t), y(t)) = \lambda$ for every $t \in [T_-, T_+]$.

Suppose that

$$(x(t_1), y(t_1)) = (x(t_2), y(t_2)), \quad t_1 < t_2 \in [T_-, T_+].$$

Let γ be the closed curve traced by $(x(t), y(t)), t \in [t_1, t_2]$ and let Γ be the closure of the region enclosed by γ. Since, Ω is simply connected, then $\Gamma \subset \bar{\Omega}$. Also, Γ is compact and $u|_\gamma = \lambda$. Therefore, by continuity, u achieves a minimum or maximum value in the compact set Γ. Since u is not constant in Γ ($|\nabla u| \neq 0$) and $u|_{\partial\Gamma} = \lambda$, we are left with $|\nabla u| = 0$ at some points in the interior of Γ where u is max or min. This contradicts the hypothesis. Therefore,

$$(x(t_1), y(t_1)) \neq (x(t_2), y(t_2)),$$

in particular

$$(x(T_-), y(T_-)) \neq (x(T_+), y(T_+)),$$

Moreover, the curve traced by

$$(x(t), y(t)), \quad t \in [T_-, T_+]$$

is simply connected.

□

Theorem A.0.3. *Let $\Omega \subset \mathbb{R}^2$ be a simply connected open bounded set, and let*

$$u \in C^{1,1}(\Omega) \cap C^0(\bar{\Omega}) : \bar{\Omega} \mapsto \mathbb{R}, \quad u|_{\partial\Omega} = f,$$

where f is almost two-to-one, and

$$|\nabla u| > 0, \quad \forall (x, y) \in \Omega.$$

Then, for any pair of points $(x_0, y_0), (x_1, y_1) \in \partial\Omega$ such that

$$f(x_0, y_0) = f(x_1, y_1)$$

there is a unique simply connected curve $\gamma_0 \subset \bar{\Omega}$ joining (x_0, y_0) and (x_1, y_1), and

$$u|_{\gamma_0} = f(x_0, y_0) = f(x_1, y_1).$$

Proof. Let $(x_0, y_0) \in \Omega$, and $u(x_0, y_0) = \lambda$. Then by Lemma A.0.2, there is a simply connected curve, say γ_0, which is traced by $(x(t), y(t)), t \in [T_-, T_+]$, where $x(t), y(t)$ are a pair of continuous

functions which satisfy (A.1) uniquely in (T_-, T_+), $(x(0), y(0)) = (x_0, y_0)$, $(x(T_-), y(T_-)) \neq (x(T_+), y(T_+)) \in \partial\Omega$, and $u|_{\gamma_0} = \lambda$. $\square$

APPENDIX B: ON THE STABILITY OF A FAMILY OF ODE'S

Let $\vec{u}, \vec{x} : I \times J \mapsto \mathbb{R}^3, I = [0, a], J = [s_-, s_+]$, and $F, G \in C^{1,1}(\overline{\Omega} \times \mathbb{R}; \mathbb{R}^3)$ such that

$$\begin{cases} \vec{u}_t(t,s) = F(\vec{u}(t,s)) \\ \vec{u}(0,s) = f(s) \in C^1(J) \end{cases} \tag{B.1}$$

and

$$\begin{cases} \vec{x}_t(t,s) = G(\vec{x}(t,s)) \\ \vec{x}(0,s) = g(s) \in C^1(J). \end{cases} \tag{B.2}$$

Theorem B.0.4. *For any $\epsilon > 0$, there exist $\delta > 0$ such that if*

$$\|F - G\|_{C^{1,1}(\overline{\Omega})} \leq \delta \tag{B.3}$$

$$\|f - g\|_{C^1(J)} \leq \delta, \tag{B.4}$$

then

$$\|\vec{u} - \vec{x}\|_{C^1(I \times J)} \leq \epsilon. \tag{B.5}$$

The proof of the previous theorem is shown later in this chapter. The following Fiber Contraction Theorem is only stated.

Theorem B.0.5. Fiber Contraction Theorem I *Let (X, d) and (Y, ρ) be complete metric spaces and*

$$T : X \times Y \mapsto X \times Y$$

such that

$$(i) \quad T(x,y) = (T_1(x), T_2(x,y)) \in X \times Y,$$

$$(ii) \quad T_1 : X \mapsto X, \quad \textit{is a } \lambda\textit{-contraction},$$

$$(iii) \quad \rho(T_2(x,y), T_2(x,\tilde{y})) \leq \lambda \rho(y, \tilde{y}), \quad \forall x \in X,$$

then T has a unique fixed point $(x^*, y^*) \in X \times Y$ such that

$$T(x^*, y^*) = (x^*, y^*)$$

and for every $(x_0, y_0) \in X \times Y$

$$T^n(x_0, y_0) \xrightarrow{d\times\rho} (x^*, y^*).$$

Theorem B.0.6. Fiber Contraction Theorem II *Let $\tilde{T}, T : X \times Y \mapsto X \times Y$ as in Theorem B.0.5 with*

$$\begin{aligned}
&(i) \quad d(T_1 x, \tilde{T}_1 x) \leq \eta, \quad \forall x \in X, \\
&(ii) \quad \rho(T_2(x, y), \tilde{T}_2(x, y)) \leq \eta, and \\
&(iii) \quad \rho(T_2(x, y), T_2(\tilde{x}, y)) \leq C_y d(x, \tilde{x}),
\end{aligned}$$

then

$$d(x^*, \tilde{x}^*) \leq \frac{\eta}{1 - \lambda}$$

and

$$\rho(y^*, \tilde{y}^*) \leq \frac{\eta}{1 - \lambda} \left(C_{\tilde{y}^*} + \frac{C_{y*}}{1 - \lambda} \right),$$

where (x^*, y^*) and $(\tilde{x}^*, \tilde{y}^*)$ are fixed points for T and $\tilde{T}$, respectively.

Proof. Observe that by using (i) and the contraction property of $\tilde{T}_1$

$$\begin{aligned}
d(x^*, \tilde{x}^*) &= d(T_1 x^*, \tilde{T}_1 \tilde{x}^*) \leq d(T_1 x^*, \tilde{T}_1 x^*) + d(\tilde{T}_1 x^*, \tilde{T}_1 \tilde{x}^*) \\
&\leq \eta + \lambda d(x^*, \tilde{x}^*),
\end{aligned}$$

it follows that

$$d(x^*, \tilde{x}^*) \leq \frac{\eta}{1-\lambda}. \tag{B.6}$$

Now,

$$\begin{aligned}
\rho(y^*, \tilde{y}^*) &= \rho(T_2(x^*, y^*), \tilde{T}_2(\tilde{x}^*, \tilde{y}^*)) \\
&\leq \rho(T_2(x^*, y^*), T_2(\tilde{x}^*, \tilde{y}^*)) + \rho(\tilde{T}_2(\tilde{x}^*, \tilde{y}^*), T_2(\tilde{x}^*, \tilde{y}^*)) \\
&\leq \rho(T_2(x^*, y^*), T_2(\tilde{x}^*, y^*)) + \rho(T_2(\tilde{x}^*, \tilde{y}^*), T_2(\tilde{x}^*, y^*)) + \eta \\
&\leq C_{y^*} d(x^*, \tilde{x}^*) + \lambda \rho(y^*, \tilde{y}^*) + \eta \\
&\leq C_{y^*} \frac{\eta}{1-\lambda} + \lambda \rho(y^*, \tilde{y}^*) + \eta,
\end{aligned}$$

by using (ii), (iii), the contraction property of T_2 and the inequality in (B.6). Thus,

$$\rho(y^*, \tilde{y}^*) \leq \frac{\eta}{1-\lambda} \left(1 + \frac{C_{y^*}}{1-\lambda}\right).$$

□

Define the map

$$T = (T_1, T_2) : X \times Y \mapsto X \times Y \tag{B.7}$$

corresponding to problem (B.1) as

$$\begin{aligned}
T_1 \vec{u} &= \int_0^t F(\vec{u}(\xi, s)) d\xi + \vec{f}(s), \\
T_2(\vec{u}, \vec{v}) &= \int_0^t \nabla_{\vec{u}} F(\vec{u}(\xi, s)) \cdot \vec{v}(\xi, s) d\xi + \frac{d}{ds} \vec{f}(s).
\end{aligned}$$

where

$$\begin{aligned} X &= \overline{B(\vec{f};R)} = \left\{ \vec{u} \in C(I \times J; \mathbb{R}^3); \max_{t\in I, s\in J} \left| \vec{u}(t,s) - \vec{f}(s) \right| \leq R \right\}, \qquad \text{(B.8)} \\ Y &= \left\{ \vec{v} \in C\left(I \times J; \mathbb{R}^3\right); \max_{t\in I, s\in J} |\vec{v}(t,s)| \leq N \right\}, \qquad \text{(B.9)} \\ N &\geq \max_{s\in J} \left| \frac{d}{ds} f(s) \right| \end{aligned}$$

with the metrics

$$d(\vec{u},\vec{v}) = \rho(\vec{u},\vec{v}) = \|\vec{u} - \vec{v}\|_\mu.$$

Note that

$$T(\vec{u},\vec{v}) = \langle T_1\vec{u}, T_2(\vec{u},\vec{v})\rangle.$$

Recall Bielecki's norm

$$\|\vec{u}\|_\mu = \sup_{I\times J} |\vec{u}(t,s)| e^{-\mu t}, \quad \mu > 0.$$

Proposition B.0.7. *$T_1 : \overline{B(\vec{f};R)} \mapsto \overline{B(\vec{f};R)}$ and it is a contraction in $\|\cdot\|_\mu$ for the positive numbers R and μ prescribed later in the proof below.*

Proof. Observe that

$$\left| T_1\vec{u}(t,s) - \vec{f}(s) \right| = \left| \int_0^t F(u(\xi,s))d\xi \right| \leq Ma$$

where

$$M = \max_{\vec{\zeta}\in\overline{\Omega}\times\mathbb{R}} \|F(\vec{\zeta})\|_{C^{1,1}(\overline{\Omega}\times\mathbb{R})}. \qquad \text{(B.10)}$$

By letting $R = Ma$ we get that

$$T_1 : \overline{B(\vec{f};R)} \mapsto \overline{B(\vec{f};R)}.$$

To prove the contraction property of T_1, let $\vec{u}, \tilde{\vec{u}} \in \overline{B(\vec{f}; R)}$, then

$$\begin{aligned}\left|T_1\vec{u}(t,s) - T_1\tilde{\vec{u}}\right| &\leq \int_0^t \left|F(\vec{u}(\xi,s) - F(\tilde{\vec{u}}(\xi,s))\right| e^{-\mu\xi+\mu\xi} d\xi \\ &\leq M\int_0^t |\vec{u}(\xi,s) - \tilde{u}(\xi,s)| e^{-\mu\xi+\mu\xi} d\xi \\ &\leq M\|\vec{u} - \tilde{\vec{u}}\|_\mu \frac{e^{\mu t}}{\mu},\end{aligned}$$

thus

$$\left\|T_1\vec{u}(t,s) - T_1\tilde{\vec{u}}\right\|_\mu \leq \frac{M}{\mu}\|\vec{u} - \tilde{\vec{u}}\|_\mu.$$

By picking $\mu > M$ the proof is completed. □

Remark B.0.8. *The contraction mapping theorem guarantees the existence and uniqueness of $\vec{u}^* \in X$ such that*

$$T_1\vec{u}^* = \vec{u}^*.$$

Proposition B.0.9. *$T_2 : X \times Y \mapsto X \times Y$ is a contraction on the fiber in $\|\cdot\|_\mu$ with μ and M as in the proof of proposition B.0.7.*

Proof. Let $\vec{u} \in X$ and $\vec{v}, \tilde{\vec{v}} \in Y$, consequently, we have that

$$\begin{aligned}\left|T_2(\vec{u}(t,s), \vec{v}(t,s)) - T_2(\vec{u}(t,s), \tilde{\vec{v}}(t,s))\right| &\leq \int_0^t \left|\nabla_{\vec{u}} F(\vec{u}(\xi,s)) \cdot (\vec{v}(\xi,s) - \tilde{\vec{v}}(\xi,s))\right| d\xi \\ &\leq \int_0^t M|\vec{v}(\xi,s) - \tilde{\vec{v}}(\xi,s)| e^{\mu\xi-\mu\xi} d\xi.\end{aligned}$$

Therefore,

$$\left\|T_2(\vec{u}(t,s), \vec{v}(t,s)) - T_2(\vec{u}(t,s), \tilde{\vec{v}}(t,s))\right\|_\mu \leq \frac{M}{\mu}\|\vec{v} - \tilde{\vec{v}}\|_\mu$$

□

Let $(\vec{u}_0, \vec{v}_0) \in X \times Y$. Define the recurrance relation

$$(\vec{u}_n, \vec{v}_n) = T(\vec{u}_{n-1}, \vec{v}_{n-1}), \quad n \in \mathbb{N}.$$

Then, by Theorem B.0.5 there is a unique point $(\vec{u}^*, \vec{v}^*) \in X \times Y$ such that

$$\begin{aligned} (\vec{u}_n, \vec{v}_n) &\to (\vec{u}^*, \vec{v}^*), \quad \text{and} \\ T(\vec{u}^*, \vec{v}^*) &= (\vec{u}^*, \vec{v}^*). \end{aligned}$$

Proposition B.0.10.

$$\vec{u}^* \in C^1(I \times J; \mathbb{R}^3).$$

Proof. Choose $\vec{u}_0(t,s) = \vec{f}(s)$ and $\vec{v}_0(t,s) = \frac{d}{ds}\vec{f}(s)$. Then, $\vec{v}_0(t,s) = \frac{\partial}{\partial s}\vec{u}_0(t,s)$ and

$$\begin{aligned} \vec{u}_1(t,s) = T_1\vec{u}_0 &= \int_0^t F(\vec{u}_0(\xi,s))d\xi + \vec{f}(s), \\ \frac{\partial}{\partial s}\vec{u}_1(t,s) &= \int_0^t \nabla_{\vec{u}} F(\vec{u}_0(\xi,s)) \cdot \frac{\partial}{\partial s}\vec{u}_0(\xi,s)d\xi + \frac{d}{ds}\vec{f}(s) = \vec{v}_1(t,s). \end{aligned}$$

To prove by induction that $\vec{v}_n = \frac{\partial}{\partial s}\vec{u}_n$ for every n, assume that

$$\vec{v}_{n-1}(t,s) = \frac{\partial}{\partial s}\vec{u}_{n-1}(t,s).$$

Now,

$$\begin{aligned} \vec{u}_n &= \int_0^t F(\vec{u}_{n-1}(\xi,s))d\xi + \vec{f}(s), \\ \frac{\partial}{\partial s}\vec{u}_n(t,s) &= \int_0^t \nabla_{\vec{u}} F(\vec{u}_{n-1}(\xi,s)) \cdot \frac{\partial}{\partial s}\vec{u}_{n-1}(\xi,s)d\xi + \frac{d}{ds}\vec{f}(s) \\ &= \int_0^t \nabla_{\vec{u}} F(\vec{u}_{n-1}(\xi,s)) \cdot \vec{v}_{n-1}(\xi,s)d\xi + \frac{d}{ds}\vec{f}(s) = \vec{v}_n(t,s). \end{aligned}$$

Thus,

$$\begin{cases} \vec{u}_n(t,s) \to \vec{u}^* \in X \\ \frac{\partial}{\partial s}\vec{u}_n(t,s) = \vec{v}_n(t,s) \to \vec{v}^*(t,s) \in Y \end{cases}$$

implies $\vec{u}^*$ is differentiable and by Weierstrass Theorem

$$\frac{\partial}{\partial s}\vec{u}^*(t,s) = \vec{v}^*(t,s).$$

□

The proof of Theorem B.0.4 is as follows.

Proof. Let $\epsilon > 0$ and let $\tilde{T} : X \times Y \mapsto X \times Y$ be the map corresponding to problem (B.2) defined as

$$\begin{aligned} \tilde{T}_1\vec{x} &= \int_0^t G(\vec{x}(\xi,s))d\xi + \vec{g}(s), \\ \tilde{T}_2(\vec{x},\vec{y}) &= \int_0^t \nabla_{\vec{x}} G(\vec{x}(\xi,s)) \cdot \vec{y}(\xi,s)d\xi + \frac{d}{ds}\vec{g}(s), \end{aligned}$$

$T : X \times Y \mapsto X \times Y$ be the map defined in (B.7) with the complete metric spaces (X,d) and (Y,ρ) defined in (B.8) and (B.9), respectively. By the Propositions B.0.7 and B.0.9 we have that $\tilde{T}_1$ is a contraction and $\tilde{T}_2$ is a contraction on the fiber. Consequently, by Theorem B.0.5 there exist a unique pair $(\vec{x}^*,\vec{y}^*) \in X \times Y$ such that

$$\tilde{T}(\vec{x}^*,\vec{y}^*) = (\vec{x}^*,\vec{y}^*).$$

Let $\delta > 0$ be the number in the inequalities (B.3) and (B.4), and let $(\vec{x},\vec{y}), (\vec{u},\vec{v}) \in X \times Y$. Then,

$$
\begin{aligned}
\left\| T_1\vec{x}(t,s) - \tilde{T}_1\vec{x}(t,s) \right\|_\mu &\leq \int_0^t \left\| F(\vec{x}(\xi,s)) - G(\vec{x}(\xi,s)) \right\|_\mu d\xi + \left\| f(s) - g(s) \right\|_\mu \\
&\leq \delta(a+1), \\
\left\| T_2(\vec{x}(t,s), \vec{y}(t,s)) \right. &- \left. \tilde{T}_2(\vec{x}(t,s), \vec{y}(t,s)) \right\|_\mu \\
&\leq \int_0^t \left\| \nabla_{\vec{x}} F(\vec{x}(\xi,s)) - \nabla_{\vec{x}} G(\vec{x}(\xi,s)) \right\|_\mu \left\| \vec{y}(\xi,s) \right\|_\mu d\xi \\
&+ \left\| \frac{d}{ds} f(s) - \frac{d}{ds} g(s) \right\|_\mu \\
&\leq \delta\left[aN+1\right], \\
\left\| T_2(\vec{x}(t,s), \vec{y}(t,s)) \right. &- \left. T_2(\vec{u}(t,s), \vec{y}(t,s)) \right\|_\mu \\
&\leq \int_0^t \left\| \nabla_{\vec{x}} F(\vec{x}(\xi,s)) - \nabla_{\vec{x}} F(\vec{u}(\xi,s)) \right\|_\mu \left\| \vec{y}(\xi,s) \right\|_\mu d\xi \\
&\leq aMN \|\vec{x} - \vec{u}\|_\mu.
\end{aligned}
$$

Let $(\vec{x}^*, \vec{y}^*), (\vec{u}^*, \vec{v}^*)$ be the fixed points of T and $\tilde{T}$, respectively. Therefore by Theorem B.0.6,

$$
\|\vec{u}^* - \vec{x}^*\|_\mu \leq \frac{\delta\eta\mu}{\mu - M}
$$

and

$$
\|\vec{v}^* - \vec{y}^*\|_\mu \leq \frac{\delta\eta\mu}{\mu - M}\left(1 + \frac{aMN\mu}{\mu - M}\right)
$$

where

$$
\eta = \max\left\{aN+1,\ aMN\right\}.
$$

By picking

$$
\delta \leq \epsilon \cdot \min\left\{ \frac{\mu - M}{\eta\mu\left(1 + \frac{aMN\mu}{\mu - M}\right)},\ \frac{\mu - M}{\eta\mu} \right\}
$$

we get

$$\|\vec{u}^* - \vec{x}^*\|_\mu \leq \epsilon, \quad \|\vec{v}^* - \vec{y}^*\|_\mu \leq \epsilon. \tag{B.11}$$

By proposition B.0.10 we have that

$$\vec{v}^*(t,s) = \frac{\partial}{\partial s}\vec{u}^*(t,s), \quad \vec{y}^*(t,s) = \frac{\partial}{\partial s}\vec{x}^*(t,s).$$

Therefore,

$$\|\vec{u}^* - \vec{x}^*\|_{C^1(I\times J)} \leq \epsilon.$$

□

REFERENCES

[1] S. AGMON, DOUGLIS A., AND NIRENBERG L, *Estimates near the boundary for solutions of elliptic partial differential equations satisfying general boundary conditions.* I. Comm. Pure Appl. Math. **12**(1959) 623-727. II. Comm. Pure Appl. Math. **17**(1964) 35-92.

[2] G. ALESSANDRINI, *An identification problem for an elliptic equation in two variables*, Annali di matematica pura ed applicata, **145** (1986), pp. 265–295.

[3] G. ALESSANDRINI AND R. MAGNANINI, *The index of isolated critical points and solutions of elliptic equations in the plane*, Ann. Suola Norm. Sup. Pisa Cl. Sci. (4), **94** (1992), pp. 567–589.

[4] G. ALESSANDRINI AND R. MAGNANINI, *Elliptic equations in divergent form, geometric critical points of solutions, and Stekloff eigenfunctions*, SIAM J. Math. Anal., **35** (1994), pp. 1259–1268.

[5] H. AMMARI, An Introduction to Mathematics of Emerging Biomedical Imaging, Math.& Applications, Vol. 62, Springer-Verlag, Berlin, 2008.

[6] H. AMMARI, Y. CAPDEBOSCQ, H. KANG, AND A. KOZHEMIAK, *Mathematical models and reconstruction methods in magneto-acouostic imaging*, European J. Appl. Math., **20**(2009), pp. 303–317.

[7] H. AMMARI, E. BONNETIER, Y. CAPDEBOSCQ, M. TANTER, AND M. FINK, *Electrical Impedance Tomography by Elastic Deformation*, SIAM J. Appl. Math., **68** (2008), pp.1557–1573.

[8] H. AMMARI AND H. KANG, *Multi-Scale and Multi-Physics Biomedical Imaging Modalities*, in Handbook of Mathematical Methods in Imaging, ed. O. Scherzer, Springer, New York, to appear.

[9] P. M. ANSELON AND P. J. LAURENT, *A general method for construction of interpolating and smoothing spline-function*, Numer. Math., **12** (1968).

[10] L. BERS, F. JOHN, AND M. SCHECHTER, *Partial Differential Equation*, John Wiley & Sons, New York, 1957.

[11] N. ZHANG, *Electrical impedance tomography based on current density imaging*, Thesis: University of Toronto, Canada, 1992.

[12] F. Monard and G. Bal *Inverse diffusion problems with redundant internal information*, Inverse Probl. Imaging **6** (2012), no. 2, 289313.

[13] C. DE BOOR, *Bicubic spline interpolation*, J. Math. Phis., **41** (1962).

[14] E. BOMBIERI, E. DE GIORGI AND E. GIUSTI, *Minimal Cones and the Bernstein Problem*, Inventiones Math. **7** (1969), pp. 243–268.

[15] B. GEBAUER AND O. SCHERZER, *Impedance-acoustic tomography*, SIAM J. Appl. Math., **69** (2008), pp. 565–576.

[16] M. G. CRANDALL, H. ISHII, AND P. -L. LIONS, *Users guide to viscosity solutions of second order partial differential equations*, Bull. Amer. Math. Soc. **27**(1992), 167

[17] M. G. CRANDALL, H. ISHII, AND P. -L. LIONS, *Users guide to viscosity solutions of second order partial differential equations*, Bull. Amer. Math. Soc. 27(1992), 167.

[18] D. GILBARG AND N. S. TRUDINGER, *Elliptic Partial Differential Equations*, 2nd ed., Springer-Verlag, NY, 2001.

[19] J. M. GREENBERG AND J. R. HARPER 1981 *Algebraic Topology* (Benjamin - Cummings)

[20] H. B. KELLER, *Numerical methods for two-point boundary value problems*, Dover Publications Inc., New York, 1992.

[21] P. KUCHMENT, *Mathematics of hybrid imaging: A brief review*, in The Mathematical Legacy of Leon Ehrenpreis, I. Sabadini and D. Struppa, eds., Springer-Verlag, 2012.

[22] P. Kuchment and D. Steinhauer, *Stabilizing inverse problems by internal data*, Inverse Problems **28**(2012), no. 8, 084007

[23] S. KIM, O. KWON, J. K. SEO, AND J. R. YOON, *On a nonlinear partial differential equation arising in magnetic resonance electrical impedance tomography*, SIAM J. Math. Anal., **34** (2002), pp. 511–526.

[24] S. KIM, O. KWON, J. K. SEO, AND J. R. YOON, *On a nonlinear partial differential equation arising in magnetic resonance electrical impedance tomography*, SIAM J. Math. Anal., **34** (2002), pp. 511–526.

[25] E. J. WOO AND J. K. SEO, *Magnetic resonance electrical impedance tomography (MREIT) for high resolution conductivity imaging*, Physiol. Meas., **29** (2008), pp. R1-R26.

[26] X. LI, Y. XU AND B. HE, *Imaging Electrical Impedance from Acoustic Measurements by Means of Magnetoacoustic Tomography with Magnetic Induction (MAT-MI)*, IEEE Transactions on Biomedical Engineering, 54(2007), pp. 323?330.

[27] O. KWON, E. J. WOO, J. R. YOON, AND J. K. SEO, *Magnetic resonance electric impedance tomography (MREIT): Simulation study of J-substitution algorithm*, IEEE Trans. Biomed. Eng., **49** (2002), pp. 160–167

[28] O. KWON, J. Y LEE, AND J. R. YOON, *Equipotential line method for magnetic resonance electrical impedance tomography*, Inverse Problems. **18** (2002), pp. 1089-1100

[29] J. Y. LEE *A reconstruction formula and uniqueness of conductivity in MREIT using two internal current distributions*, Inverse Problems, **20** (2004), pp. 847–858

[30] J. J. LIU, J. K. SEO, M. SINI AND E. J. WOO, *On th conductivity imaging by MREIT: available resolution and noisy effect*, J. Phys.: Conf. Ser. **73** (2007), 012015 (20pp).

[31] J. J. LIU, J. K. SEO, M. SINI AND E. J. WOO, *On the convergence of the harmonic Bz Algorithm in Magnetic Resonance Imaging*, SIAM J. Appl. Math. **67** (2007), 1259–1282.

[32] Q. MA AND B. HE, *Investigation on magnetoacoustic signal generation with magnetic induction and application to electrical conductivity reconstruction*, Phys. Med. Biol., **52** (2007), pp. 5085–5099.

[33] J. M. MAZÓN, J. D. ROSSI, S. S. DE LEÓN, *Functions of least gradient and 1-Harmonic functions*, 2014, Indiana Univ. Math. J., to appear

[34] C. Montalto and P. Stefanov, *Stability of coupled-physics inverse problems with one internal measurement*, Inverse Problems **29**(2013), 125004 doi:10.1088/0266-5611/29/12/125004

[35] A. MORADIFAM, A. NACHMAN, AND A. TIMONOV, *A convergent algorithm for the hybrid problem of reconstructing conductivity from minimal interior data*, Inverse Problems **28** (2012), no. 8, 084003, 23 pp.

[36] A. Moradifam, A. Nachman, and A. Tamasan, *Conductivity imaging from one interior measurement in the presence of perfectly conducting and insulating inclusions*, SIAM J. Math. Anal. 44 (2012), no. 6, 39693990.

[37] A. MORADIFAM, A. NACHMAN, AND A. TAMASAN, *Uniqueness of minimizers of weighted least gradient problems arising in conductivity imaging*, arXiv:1404.5992 [math.AP]

[38] A. NACHMAN, A. TAMASAN, AND A. TIMONOV, *Conductivity imaging with a single measurement of boundary and interior data*, Inverse Problems, **23** (2007), pp. 2551–2563.

[39] A. NACHMAN, A. TAMASAN, AND A. TIMONOV, *Recovering the conductivity from a single measurement of interior data*, Inverse Problems, **25** (2009) 035014 (16pp).

[40] A. NACHMAN, A. TAMASAN, AND A. TIMONOV, *Reconstruction of planar conductivities in subdomains from incomplete data*, SIAM J. Appl. Math. **70**(2010), 3342 –3362.

[41] A. NACHMAN, A. TAMASAN, AND A. TIMONOV, *Current density impedance imaging* in Tomography and inverse transport theory, 135149, Contemp. Math. **559**, AMS, Providence, RI, 2011

[42] M. Z. NASHED AND A. TAMASAN, *Structural stability in a minimization problem and applications to conductivity imaging*, Inverse Probl. Imaging, **5** (2010), 219–236.

[43] J. O. NIEMINEN, K.C.J. ZEVENHOVEN, P.T. VESANEN, Y.-C. HSU, AND R.J. ILMONIEMI, *Current density imaging using ultra low field MRI with adiabatic pulses*, Magnetic Resonance Imaging **32**(2014), 54–59.

[44] G. C. SCOTT, M. L. JOY, R. L. ARMSTRONG, AND R. M. HENKELMAN, *Measurement of nonuniform current density by magnetic resonance*, IEEE Trans. Med. Imag., **10** (1991), pp. 362–374

[45] P. STERNBERG AND W. P. ZIEMER, *Generalized motion by curvature with a Dirichlet condition*, J. Differ. Eq., **114** (1994), pp. 580–600.

[46] A. TAMASAN AND J. VERAS, *Conductivity imaging by the method of characteristics in the 1-Laplacian*, Inverse Problems **28** (2012), no. 8, 084006, 13 pp.

[47] A. TAMASAN, A. TIMONOV AND J. VERAS, *Stable reconstruction of regular 1-Harmonic maps with a given trace at the boundary*, Applicable Analysis: An International Journal, DOI: 10.1080/00036811.2014.918260.

[48] M. W. HIRSH, C. C. PUGH, *Stable manifolds for hyperbolic sets*, Proc. Symp. Pure Math., **14**(1970), 133-163.

[49] M. J. JOY, A. I. NACHMAN, K. F. HASANOV, R. S. YOON, AND A. W. MA, *A new approach to Current Density Impedance Imaging (CDII)*, Proceedings ISMRM, No. 356, Kyoto, Japan, 2004.

[50] A. MORADIFAM, A. I. NACHMAN, AND A. TIMONOV, *A convergent algorithm for the hybrid problem of reconstructing conductivity from minimal interior data*, Inverse Problems **28** (2012) 084003 (23pp).

[51] E. SOMERSALO, M. CHENEY, AND D. ISAACSON, *Existence and uniqueness for electrode models for electric current computed tomography*, SIAM J. APPL. MATH., **52 (4)**, pp 1023-1040, 1992.

[52] A. TAMASAN AND J. VERAS, *Conductivity imaging by the method of characteristics in the 1-Laplacian*, Inverse Problems **28**(2012), 084006 (13pp)

[53] P. VAUHKONEN, M. VAUHKNOEN, T. SAVOLAINEN, AND J. KAIPIO, *Three-Dimensional Electrical Impedance Tomography Based on The Complete Electrode Model*, IEEE Trans. on Biomedical Engineering **46 (9)**, pp 1150-1160, 1999

[54] J. VERAS, A. TAMASAN AND A. TIMONOV, *Stable reconstruction of regular 1-Harmonic maps with a given trace at the boundary*, Applicable Analysis (2014), doi:10.1080/00036811.2014.918260